Bridge Factors Factual Report Attachment 73 – FHWA Assessment of Bridge Design and Performance

Miami, FL

HWY18MH009

(91 pages)

Florida International University Pedestrian Bridge Collapse Investigation: Assessment of Bridge Design and Performance

Prepared for:

National Transportation Safety Board
NTSB Accident ID: HWY18MH009

Prepared jointly by:

Reggie Holt, P.E.
Federal Highway Administration
Office of Bridges and Structures
1200 New Jersey Avenue, SE
Washington, DC 20590

Benjamin Graybeal, Ph.D., P.E.
Federal Highway Administration
Office of Infrastructure Research
6300 Georgetown Pike
McLean, VA 22101

September 12, 2019

TABLE OF CONTENTS

1 BACKGROUND

1.1 COLLAPSE OVERVIEW

The Florida International University (FIU) Pedestrian Bridge in Miami, Florida was designed to be a two-span, single plane concrete truss bridge complimented architecturally with a central pylon and steel pipe stays. The bridge had a total length of 273 feet with main span of 174 feet and back span of 99 feet. The main span crossed SW 8th Street (US 41) and the back span crossed the Tamiami Canal. On Thursday, March 15, 2018, about 1:47 p.m. eastern daylight time, the 174-foot main span of this partially constructed bridge collapsed onto SW 8th Street resulting in the tragic loss of 6 lives.

1.2 FEDERAL HIGHWAY ADMINISTRATION (FHWA) ROLE

The FIU Pedestrian Bridge collapse investigation was led by the National Transportation Safety Board (NTSB). The Federal Highway Administration (FHWA) supported NTSB in its investigation by providing resources and expertise to evaluate the bridge design and construction processes. Additionally, FHWA conducted numerous tests on and examinations of the physical evidence, including concrete and steel samples, as well as construction equipment associated with the collapsed structure. The FHWA team consisted of personnel from the Office of Bridges and Structures, the Turner-Fairbank Highway Research Center, the Resource Center, and the Florida Division Office.

1.3 REPORT PURPOSE

This report focuses on the findings from FHWA's review and assessment of the superstructure final design calculations and the Released for Construction bridge plans. The superstructure final design calculations, referred to herein as the FIGG Design, were signed and checked by Licensed Professional Engineers employed by FIGG Bridge Engineers. The Released for Construction Plans, herein referred to as the FIGG Plans, were sealed and signed by a Professional Engineer with FIGG Bridge Engineers. In addition, pre- and post-collapse evidence along with material examinations are used to correlate findings between the design assessment and observed bridge performance. This report is based on evidence and information available to the NTSB which was then made available to FHWA.

Sections in this report will focus on the design and performance of the northernmost nodal region of the 174-foot-long main span. Nodal regions are located at any part of the bridge in which truss members are connected to either the bridge canopy or deck. The failure of this specific nodal region was the triggering event for the collapse.

2 FIU PEDESTRIAN BRIDGE OVERVIEW

2.1 BRIDGE TYPE AND LAYOUT

The Florida International University (FIU) Pedestrian Bridge in Miami, Florida was designed to be a two-span, single plane concrete truss containing longitudinal, transverse, and truss member post-tensioning. This truss structure was complimented architecturally with a central pylon and steel pipe stays. The bridge had a total length of 273 feet with a main span of 174 feet and back span of 99 feet. The main span crossed SW 8th Street (US 41) and the back span crossed the Tamiami Canal. Figure 1 shows an artistic rendering of the proposed structure with annotations to assist the reader in identifying key aspects.

The superstructure had a 31'-8" wide concrete walkway containing longitudinal and transverse post-tensioning which acted as the truss bottom chord and a 16'-0" wide canopy containing longitudinal post-tensioning which acted as the truss top chord. Truss members were aligned along the longitudinal centerline of the cross-section. Truss member cross sections measured 1'-9" wide in the transverse direction and ranged from 2'-0" to 3'-0" deep in the perpendicular direction. Figure 2 shows a vertical cross sectional cut through the superstructure, and figure 3 shows an artistic rendering of a cut away section of the completed bridge. The main span included 12 truss members with truss members numbered 3, 5, 6, 7, 8, and 10 being permanently post-tensioned via internal post-tensioning rods. Members 2 and 11 were temporarily post-tensioned, again via internal post-tensioning rods, to address temporary construction conditions. The numbering for each main-span truss member is shown in figure 4. Blisters were located on the top of the canopy to accommodate the truss member post-tensioning anchorages and provide a connection platform for the steel pipe stays.

The deck/walkway cross-section was thickened to form deck diaphragms at the end bent and pier locations. These diaphragms are approximately 4-feet deep by 20-feet wide and centrally located in the bridge cross-section. The primary purpose of the diaphragms is to transfer the weight of the main span to the supporting end bents and pier. The diaphragm at End Bent 1 was 3'-6" thick, while the diaphragm at Pier 2 was 2'-0" thick.

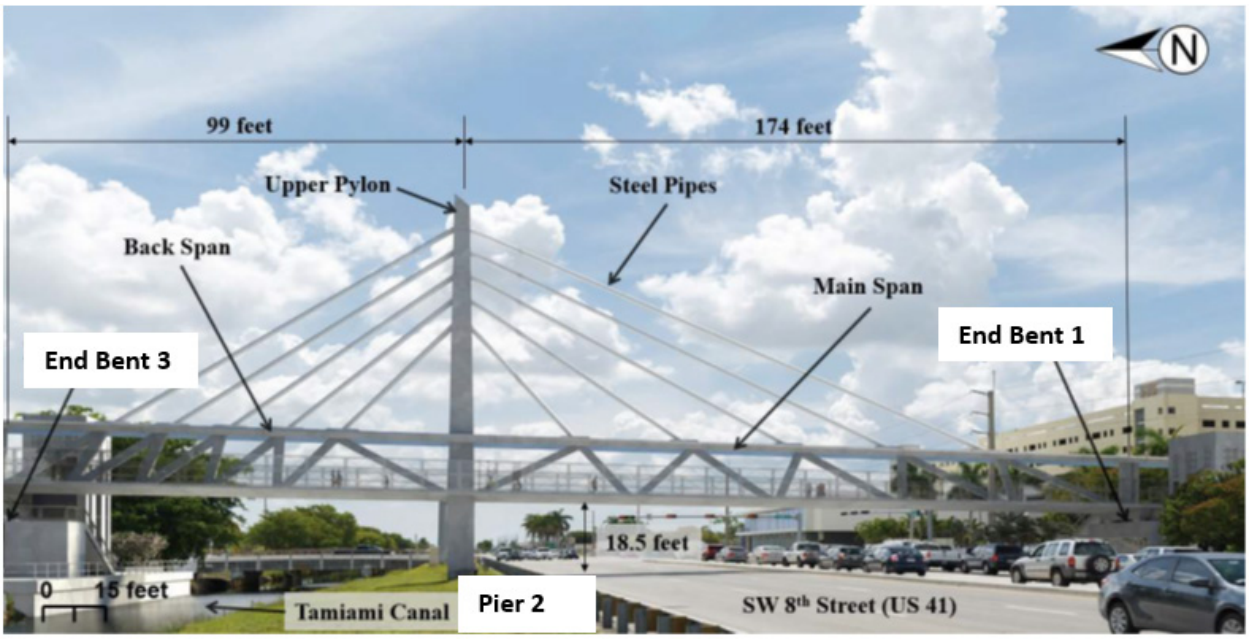

Figure 1. Rendering of completed bridge.

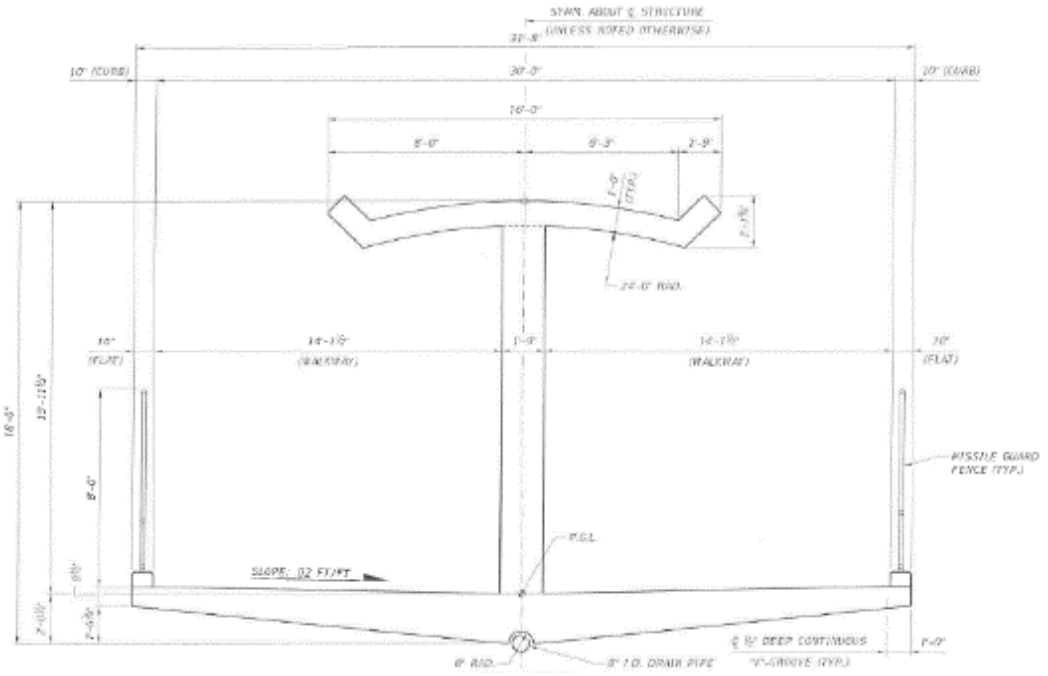

Figure 2. Bridge cross section.

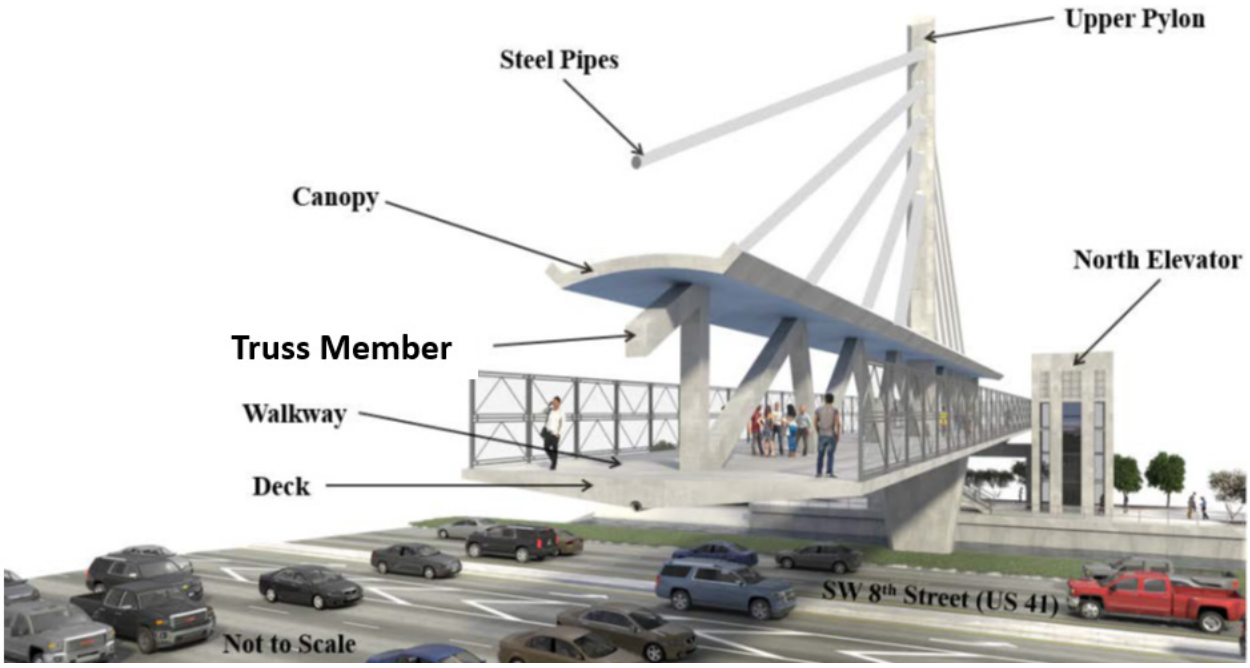

Figure 3. Rendering of cut-away section of completed bridge.

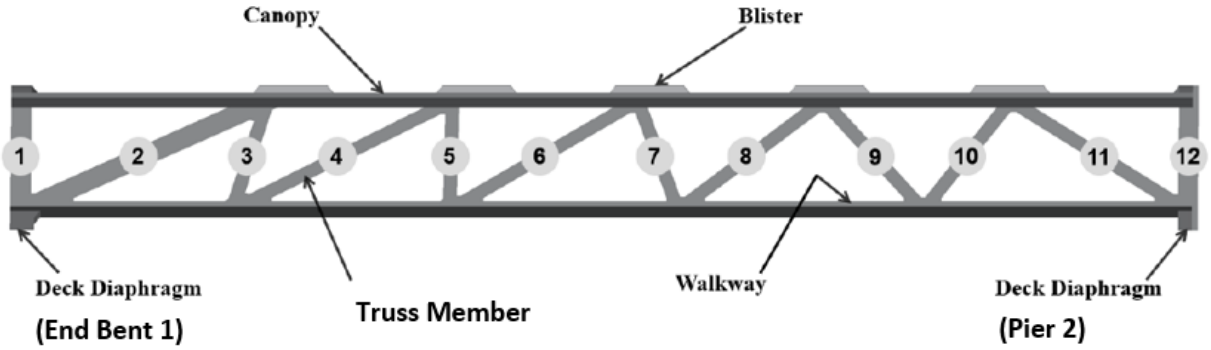

Figure 4. Main span nomenclature and truss element identification numbering.

2.2 STAGED CONSTRUCTION

Eight construction stages were prescribed for the construction of the FIU pedestrian bridge in the FIGG Plans. However, for purposes of this report only four of the most significant construction stages will be described. These stages are also illustrated in figure 5. These 4 stages include:

- Stage 1 – Construct bridge substructure elements (End Bent 1, Pier 2, and End Bent 3). Fabricate main-span truss in casting yard adjacent to SW 8th Street including the temporary post-tensioning of members 2 and 11.

- Stage 2 – Transport main span from casting yard to final position supported under the bridge deck at approximately the member 3-4 nodal point and the member 9-10 nodal point. Place main span so it is simply supported on End Bent 1 and Pier 2. Detension truss members 2 and 11.
- Stage 3 – Construct back span, supported on Pier 2 and End Bent 3. *This stage was not initiated due to the collapse of the bridge.*
- Stage 4 – Monolithically connect main span, back span, and Pier 2. Construct upper pylon and install steel pipe stays. *This stage was not initiated due to the collapse of the bridge.*

2.3 BRIDGE AT TIME OF COLLAPSE

The main span truss had permanent post-tensioning running longitudinally for the full-length of the span within the deck and canopy, and transverse post-tensioning in the deck. Truss members numbered 3, 5, 6, 7, 8 and 10 were permanently post-tensioned as well. All of this permanent post-tensioning was installed during Stage 1 prior to transport of the truss. Truss members numbers 2 and 11 were temporarily post-tensioned prior to transport of the truss, then were detensioned within hours after placement of the truss on the permanent supports (end of Stage 2). The bridge collapse occurred approximately 5 days after the completion of Stage 2.

Two post-Stage 2 remedial measures were taken that were not included in the planned construction stages. These remedial measures were implemented to address observed distress in the nodal region connecting truss members 11 and 12 to the deck (located above Pier 2). These remedial measures included:

1. Placement of additional shim between the underside of the deck diaphragm and the top of Pier 2 within the truss member 12 footprint, with shim installation occurring on March 13, 2018. This is further discussed in Section 3.7 and shown in Figure 16.

2. Retensioning the post-tensioning rods in truss member 11, with re-tensioning occurring on March 15, 2018. This is further discussed in Section 3.8.

The collapse occurred immediately after the re-tensioning of the member 11 post-tensioning rods. Construction Stages 3 and 4 were never performed due to the collapse.

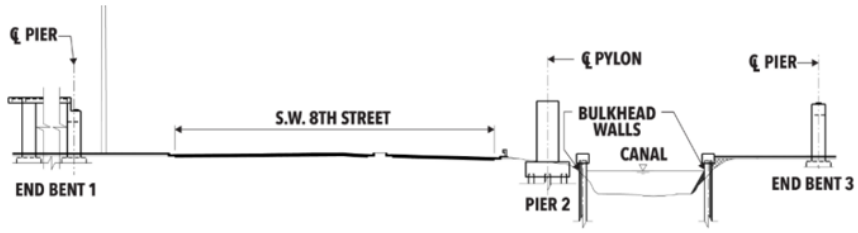

Stage 1

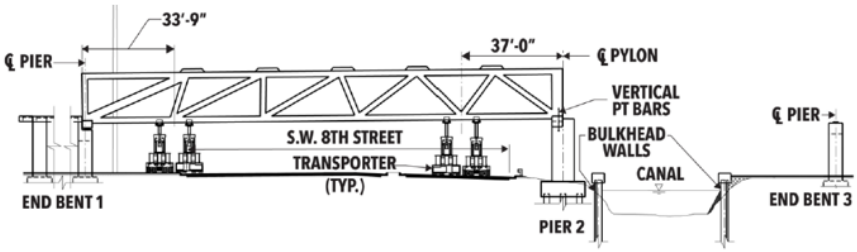

Stage 2

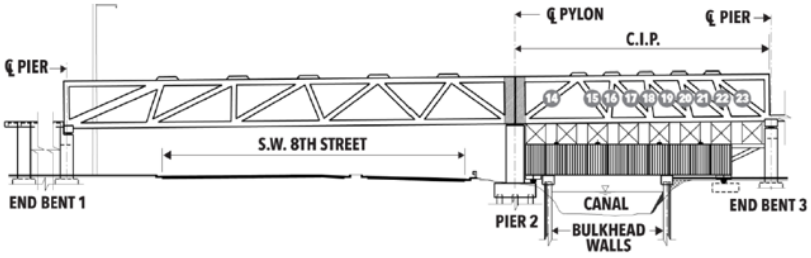

Stage 3

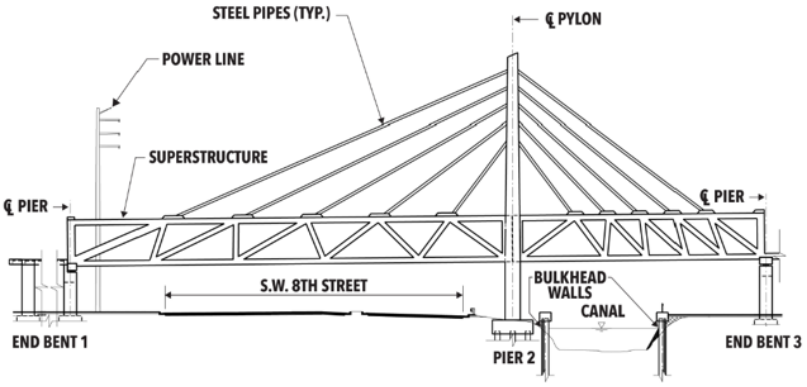

Stage 4

Figure 5. Bridge construction stages.

3 PROGRESSION TO BRIDGE COLLAPSE

The collapse of the FIU pedestrian bridge was preceded by a series of events and documented observations which demonstrated and communicated the distress that the structure was experiencing. Documentation, whether captured contemporaneously in response to an event, separately in association with a wholly different topic, or post-collapse as part of the investigation, allows for the creation of a timeline that chronicles the performance of the structure from early in construction through the March 15, 2018 collapse.

The following chronological description provides insight into local structural performance observations and the meaning thereof within the context of the overall bridge. Most of the discussion will focus on the truss member 11 and 12 nodal region where significant distress was observed prior to the collapse and from which the collapse initiated. Similar but lesser distress was observed in the truss member 1 and 2 nodal region during the weeks leading up to the collapse. This nodal region did not progress to failure and thus it is not the focus of this report. The truss member 11 and 12 nodal region is illustrated in Figure 6, wherein members, faces, and directions are identified to allow the reader to better grasp critical aspects of the following narrative.

A timeline of key events in the construction of the bridge is provided in Figure 7.

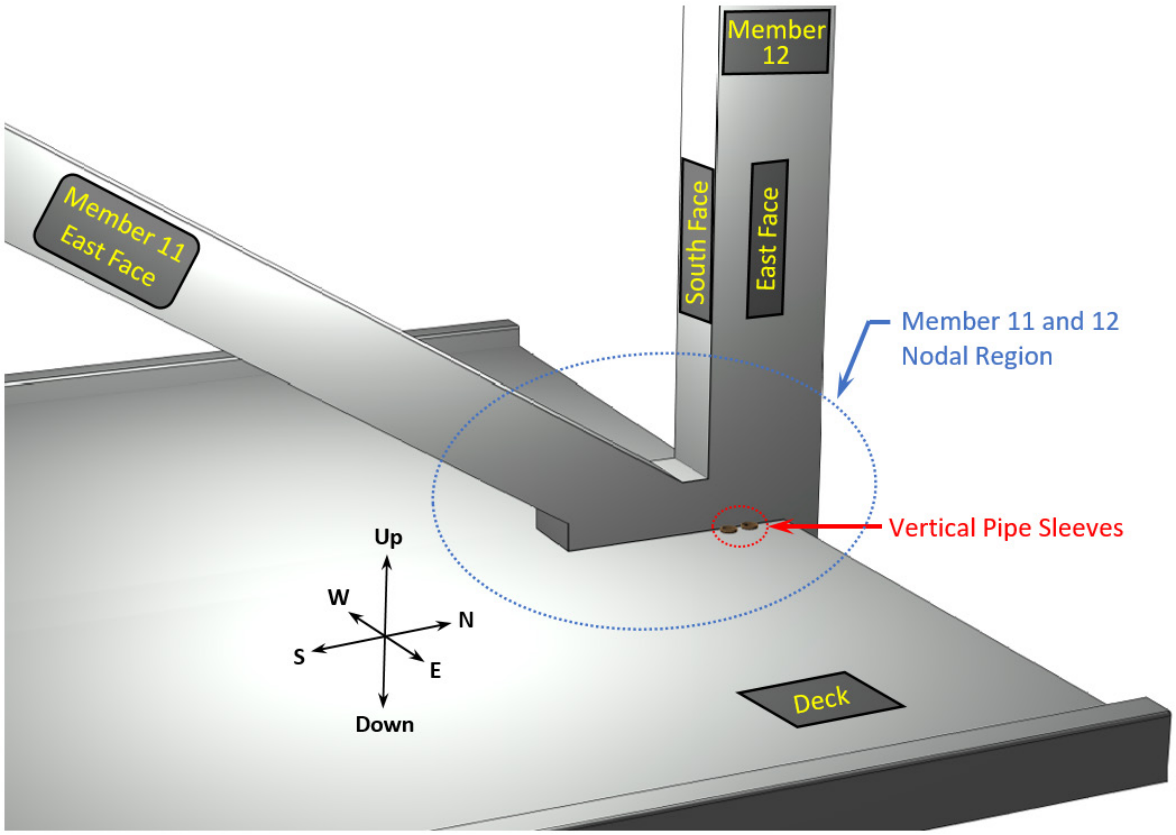

Figure 6. Illustration of the member 11 and 12 nodal region.

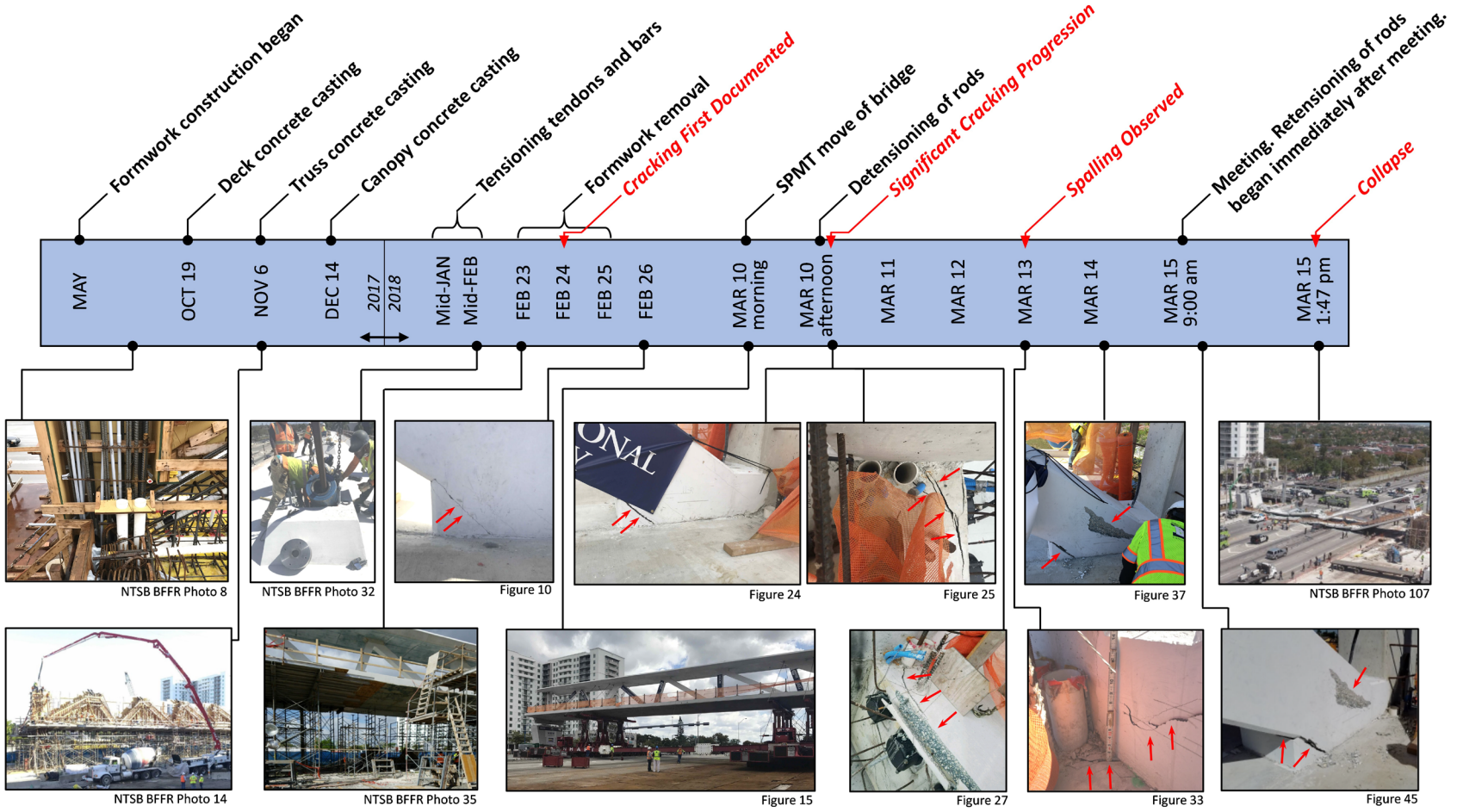

Notes:
- NTSB BFFR Photo # = National Transportation Safety Board Bridge Factors Factual Report Photo #
- Figure # = Image from Figure # in this report

Figure 7. Illustrated timeline identifying key events during the construction of the bridge.

3.1 PRECURSOR EVENTS

Prior to the timeline discussed herein, a series of relevant events occurred. Important events, including the completion of the FIGG Design and the selection of methods of construction, are discussed elsewhere and will not be discussed in this section of the report. This chapter focuses on the construction and erection of the bridge.

3.2 DETAILING AND CONSTRUCTION OF THE TRUSS MEMBER 11 AND 12 NODAL REGION

The realization of a reinforced concrete structure involves the determination of the process to fill the formwork with concrete and also the delineation of every item that will be contained within the concrete structure. Aside from the properties of the steel reinforcement and the concrete, two specific aspects of this realization process are of particular importance to the structural performance of this nodal region. The first is the concrete placement process and the associated cold joints that are defined and created. The second is the specific location of non-structural elements within the concrete.

The casting process for the superstructure of the bridge included three distinct concrete pours. The first was for the deck of the bridge, the second was for the diagonal and vertical truss members, and the third was for the canopy of the structure. These pours were completed sequentially with significant time allotted between pours to allow for development of the mechanical properties of the concrete from earlier pours. The truss member 11 and 12 nodal region includes portions of the first two of these concrete pours. A cold joint, where freshly placed concrete was cast against and expected to bond to previously placed concrete, existed at the horizontal plane where truss members 11 and 12 connected to the deck. Figure 8 shows this region of interest.

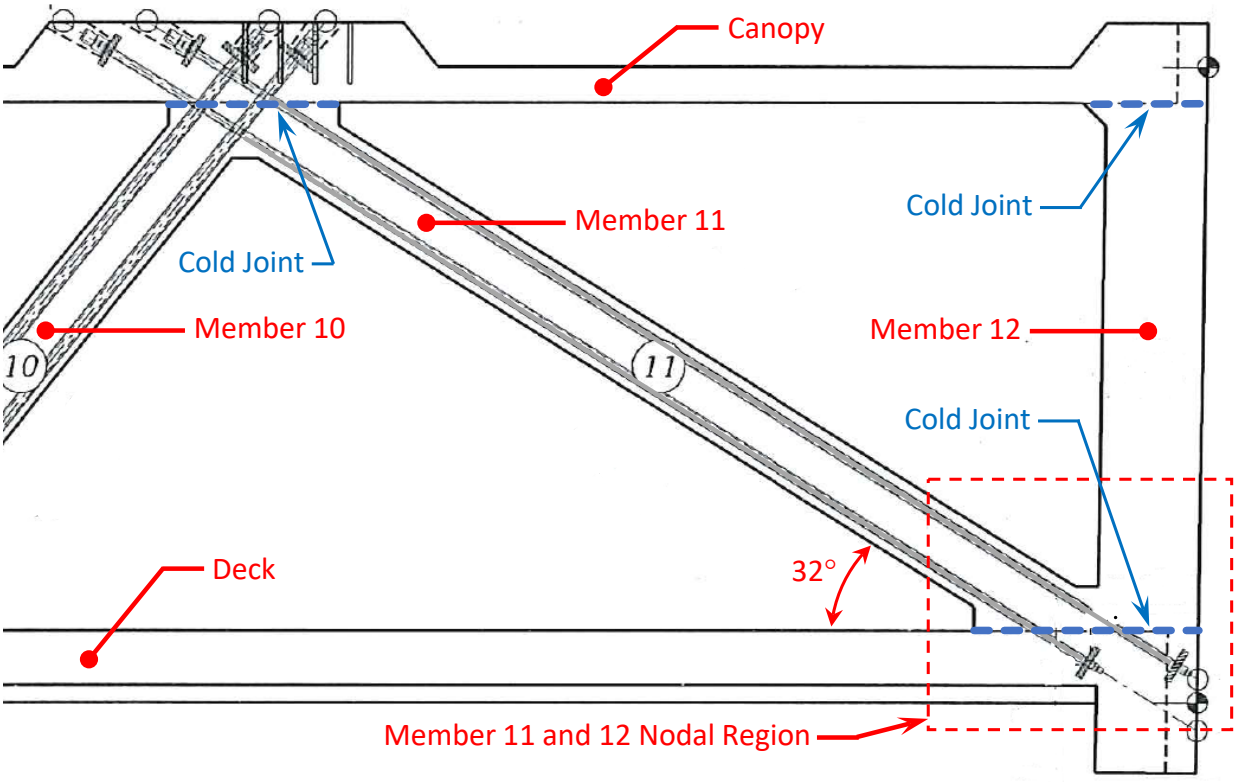

Figure 8. Elevation view of a vertical cross section through the longitudinal centerline of the member 11 and 12 nodal region.

As this was a simple span structure and a single plane truss, there were no alternate load paths that bypassed this nodal region. The cold joint at the base of truss members 11 and 12 is in a location that would be subjected to significant shear and axial stresses.

A separate factual report[a] provides extensive documentation of the cold joint under discussion here. There is significant evidence that the construction process that was used to complete the concrete deck pour that constitutes the deck-side surface of this cold joint did not include intentional surface roughening[b] of the concrete under truss members 11 and 12. Assuming that the hardened cold joint surface from the first pour had been cleaned, the second placement of concrete would have had the ability to chemically bond to the first pour across the cold joint creating a cohesive resistance to shearing forces. However, the concrete resistance to shearing action along this cold joint plane would have been contingent upon this chemical bond and

[a] Graybeal and Haber, "NTSB Accident ID: HWY18MH009, Concrete Interface Under Members 11 and 12" Turner-Fairbank Highway Research Center Factual Report, Federal Highway Administration, February 2019.
[b] Intentionally roughened concrete is described as a "clean concrete surface, free of laitance, with surface intentionally roughened to an amplitude of 0.25 in." in Article 5.8.4.3 of *AASHTO LRFD Bridge Design Specification, 7th Ed*.

could not have relied upon enhanced interlocked concrete planes that occur when fresh concrete is consolidated against an intentionally roughened interface of hardened concrete.

This structure included various hollow pipes, some of which passed through the member 11 and 12 nodal region. Given that these pipes are composed of non-structural plastic, they effectively act as voids within the mass of the concrete. These voided areas exhibit a lower stiffness and are less able to resist applied loads than monolithic regions. If these pipes pass through a critical region of the structure, the concrete surrounding the pipes will be subjected to higher stresses. Also, if not considered in design, the voids may cause an overstress and the unanticipated redirection of an assumed load path. Figure 55, presented in a later chapter, shows the truss member 11 and 12 nodal region in July 2017 as the steel reinforcement and non-structural elements were being installed in the formwork. The deck is in the bottom right of the photo; truss member 12 is in the center of the photo extending toward the top. Note the two vertical white plastic pipes, referred to as vertical pipe sleeves, toward the foreground of the vertical column reinforcement in truss member 12. Two matching pipes also existed on the opposite side of truss member 12. These four, 4.5-inch-diameter pipes perforate the pair of vertical, critical shear planes in the deck immediately east and west of truss members 12.[c,d] A fifth large pipe, this one a plastic drain pipe, ran in a north-south orientation through the diaphragm immediately under truss member 12. This 8.625-inch diameter pipe is visible in Figure 29. All five non-structural pipes are visible bordering the failure planes evident in the post-collapse photos shown in Figure 48 and Figure 49, demonstrating their importance to the behavior of the nodal region.

3.3 Cracking Under Truss Member 11 after Formwork Removal

The construction of the bridge main span included the casting of the superstructure concrete, the curing of all placed concrete, and the application of the post-tensioning in the deck, canopy, and truss members. The main-span was cast above ground level and supported by temporary falsework. After the concrete was sufficiently cured, the formwork containing the concrete and falsework providing continuous support along the length of the span was sequentially removed. As removal progressed, the dead load (i.e., self-weight) of the structure was progressively transferred to the internal structural load carrying elements and to the external temporary supports at each end of the main-span until the bridge was self-supporting.

During the removal of the span-supporting formwork, a noteworthy event occurred. On Saturday, February 24, 2018, the construction personnel working on and around the structure reported hearing a loud, distinct, concrete cracking sound that came from the structure. Construction activities were briefly halted and the structure was inspected. A crack was found

[c] These vertical pipes provided a conduit through which vertical post-tensioning rods and #11 reinforcing bars could pass.

[d] Navigational directions in report sections 3.2, 3.3, and 3.4 refer to the orientation of the bridge at the time of collapse, not to the orientation of the bridge during casting or SPMT movement.

in the truss member 11 and 12 nodal region near and at the truss member 11 intersection with the deck. Photographs of this crack were captured during (Figure 9 and Figure 10) and soon after (Figure 11 and Figure 12) formwork release.[e] A similar crack was found in the member 1 and 2 nodal region at the opposite end of the bridge span.[f]

The crack in the truss member 11 and 12 nodal region began at the reentrant corner between the south face of truss member 11 and the deck. It largely followed the location of the cold joint between truss member 11 and the deck. The southernmost portion of the crack deviated from the cold joint, instead following the projection of the south face of truss member 11 through the chamfer that closed the reentrant corner between the south face of truss member 11 and the deck. This specific path of the southernmost portion of this crack is of significance in that this path allowed the crack to bypass 21 percent of the reinforcing steel area that was, per the FIGG Design and FIGG Plans, intended to offer interface shear resistance at the base of truss member 11. Per the construction plans, eight #7 reinforcing bars and two #6 reinforcing bars were to cross the cold joint under truss member 11. Although all ten bars were present in the structure, because of the detailing specified on the FIGG Plans, the southernmost two #7 bars were not anchored above the crack. Thus, those two bars were not engaged by the crack and could not offer resistance to the northward thrusting shear demand of the upper portion of the node. Figure 14 provides an illustration showing the size and location of the ten legs of these reinforcing bars. These bars are also shown later in the report in Figure 57.

Finding:

The FIGG Plans called for a detailing scheme wherein the southernmost two reinforcing bars were not anchored on both sides of the critical horizontal shear plan at the base of member 11. This detailing scheme resulted in less reinforcing steel than expected participating in resisting the critical interface shear demand.

The timing and location of this crack leads to the conclusion that the application of the dead load to the bridge stressed this nodal region in a way that surpassed the strength of the concrete. The cohesive strength of the concrete at the cold joint and the tensile strength of the bulk concrete in the chamfer were the primary load resisting mechanisms at the location where this crack occurred. The loss of cohesion along the non-intentionally roughened cold joint, combined with the opening of a tensile crack in the chamfer, resulted in a change in the anticipated load path across the cold joint. In this case, the large northward thrusting shear demand parallel to the interface under truss member 11 would have ceased to be partially carried by the cohesive and tensile resistance of the concrete along the now-cracked plane.

[e] Directional arrows in Figure 9, Figure 10, Figure 11, and Figure 12 show the orientation of the bridge at the time of collapse, not at the time when the photo was captured.

[f] Views of the crack in the member 1 and 2 nodal region are shown in NTSB Bridge Factors Factual Report Photos 44 and 45.

Remaining resistance mechanisms would have been a combination of 1) the reinforcing bars crossing the interface, 2) the frictional resistance generated by the clamping force on the interface, and 3) the flexural and shear resistance afforded by the member 12 connection to the deck. Effectively, the centroid of the horizontal shear load resisting mechanism shifted northward upon the occurrence of this crack during formwork removal.

Additionally, note that the photograph shown in Figure 13 was captured on March 8, 2018 during the timeframe between the formwork removal and the initiation of the self-propelled modular transporter (SPMT) transport of the bridge.[g] The photo was captured by the company that operated the SPMTs. The identified cracking, in the deck on the west face of member 12, extends from the vertical pipe sleeves toward the north end of the bridge. This cracking demonstrates that the distress in the member 11 and 12 nodal region extended across the nodal region prior to the SPMT transport and all subsequent construction actions.

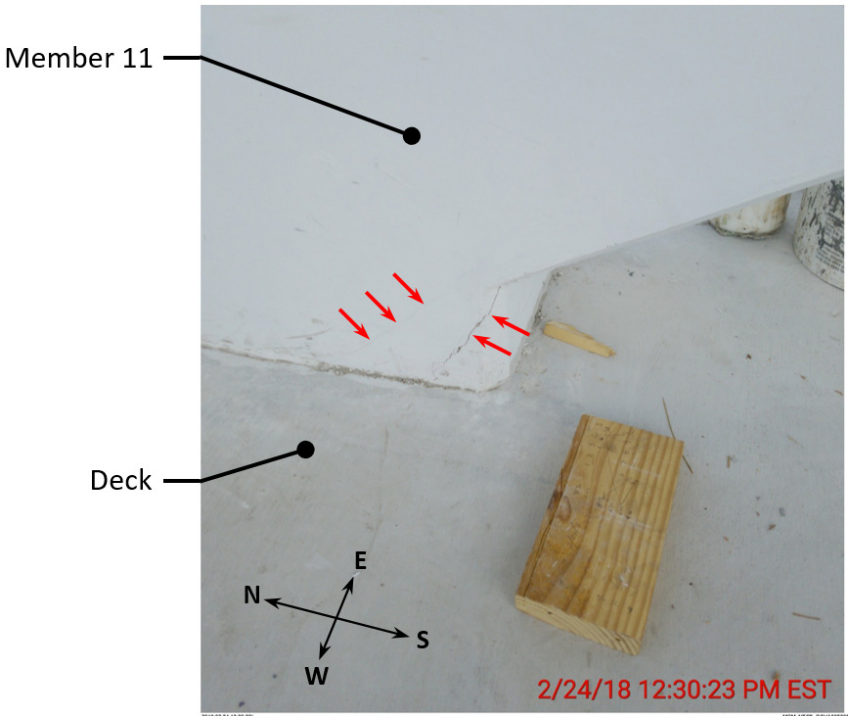

Figure 9. Photograph showing cracking at southwest corner of truss member 11 near where it met the deck. Captured on February 24, 2018 at 12:30 p.m. Corresponds to Bridge Factors Factual Report Photo 39.

[g] Directional arrows in Figure 13 show the orientation of the bridge at the time of collapse, not at the time when the photo was captured.

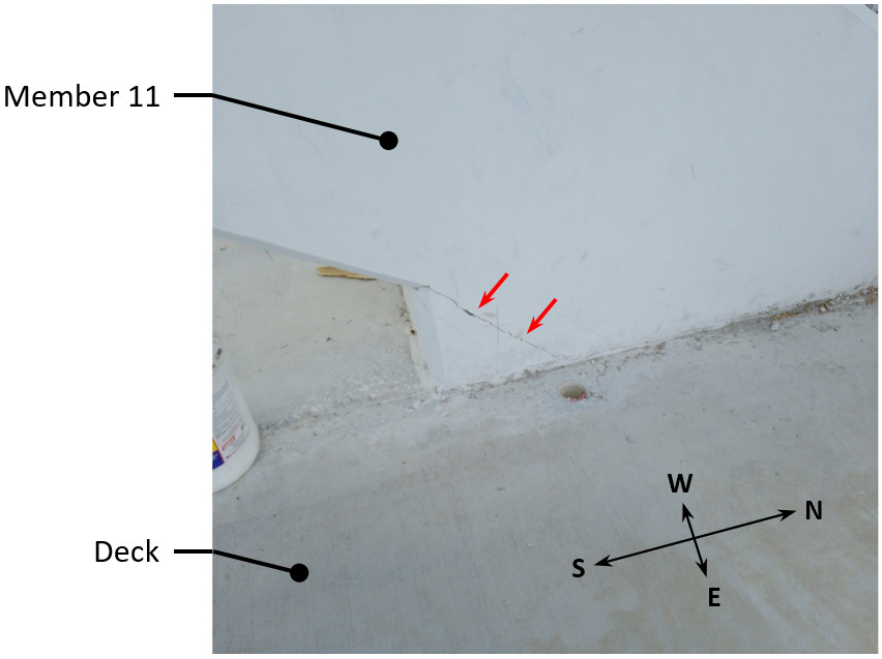

Figure 10. Photograph showing cracking at southeast corner of truss member 11 near where it met the deck. Captured on February 24, 2018 at 12:29 p.m. Corresponds to Bridge Factors Factual Report Photo 38.

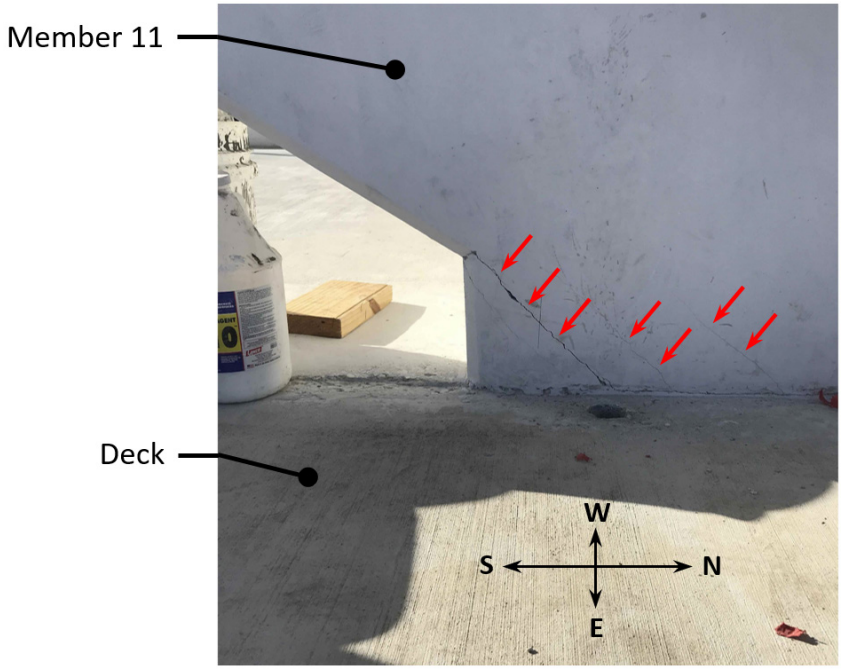

Figure 11. Photograph showing cracking at southeast corner of truss member 11 near where it met the deck. Captured on February 26, 2018 at 8:38 a.m. Corresponds to Bridge Factors Factual Report Photo 42.

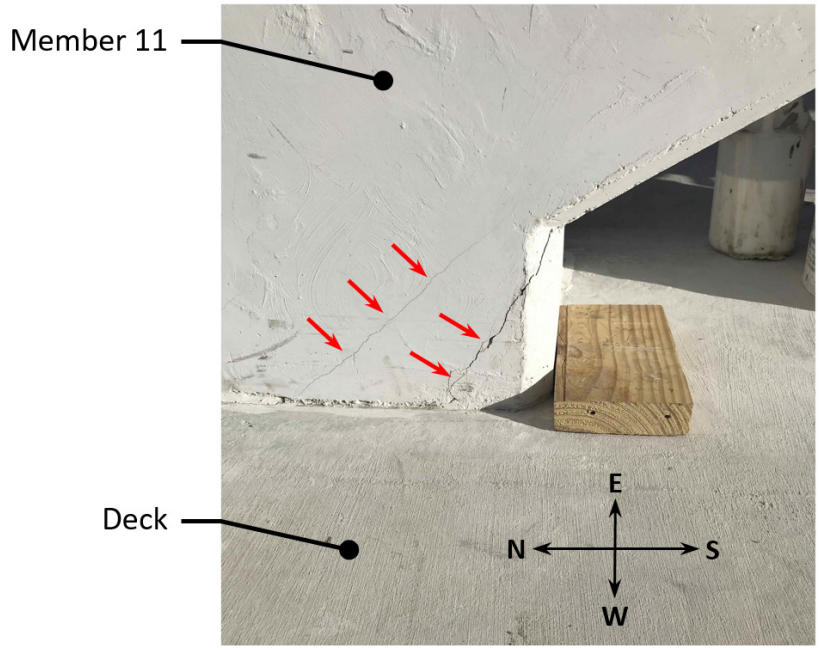

Figure 12. Photograph showing cracking at southwest corner of truss member 11 near where it met the deck. Captured on February 26, 2018 at 8:38 a.m. Corresponds to Bridge Factors Factual Report Photo 43.

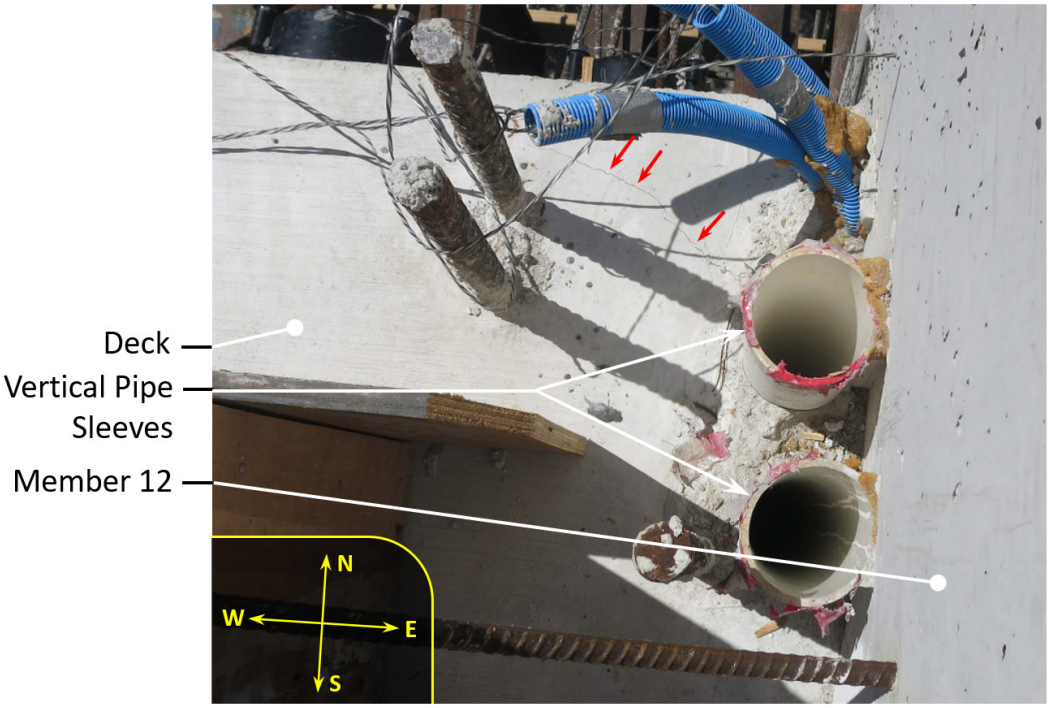

Figure 13. Photograph showing the deck on the west side of member 12 prior to SPMT transport. Captured on March 8, 2018. Corresponds to Bridge Factors Photographs – FIGG Bridge Engineers, Inc. Photo Submission FCA 10-9.

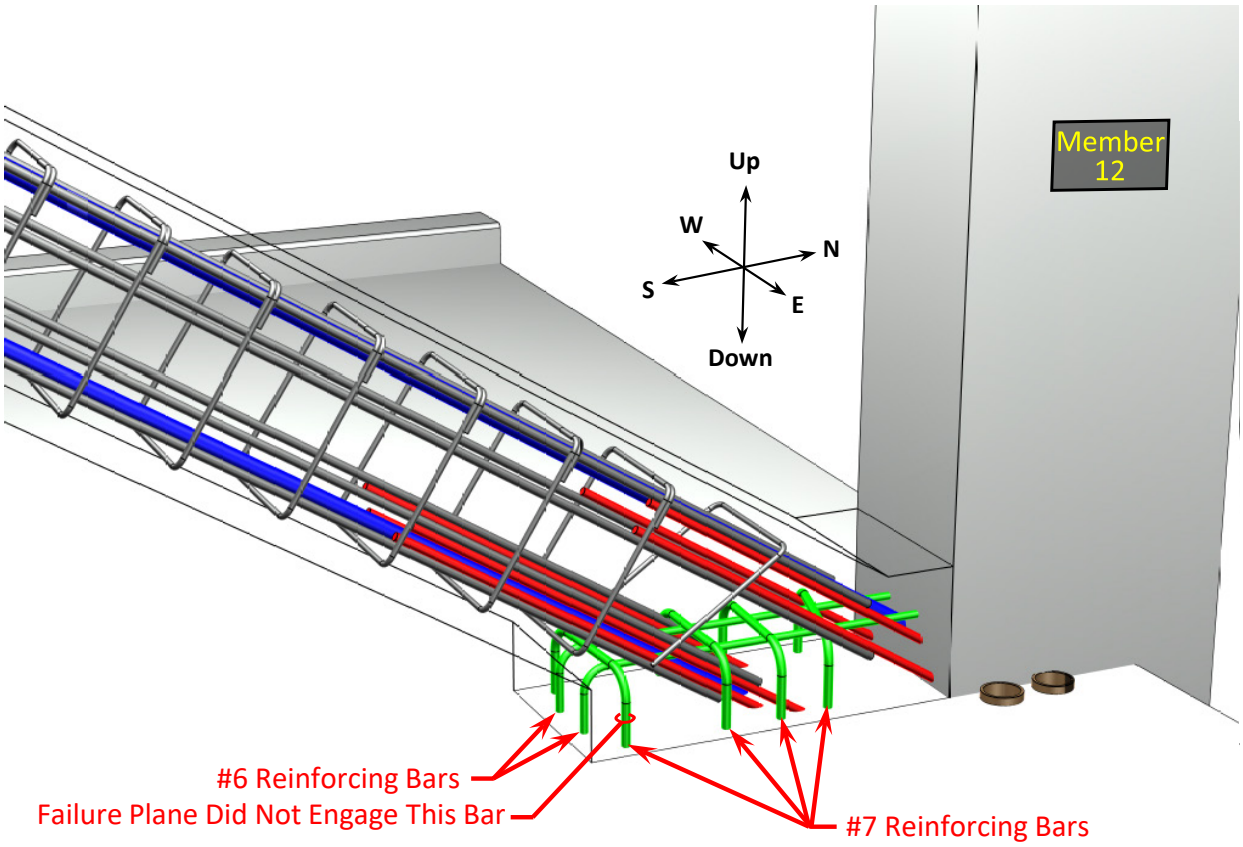

Figure 14. Illustration showing the steel reinforcing bars passing from the deck into the base of truss member 11.

3.4 SPMT Pick-up, Transport, and Set-Down of Bridge Main Span

The construction process for the main span of this bridge included near-site construction followed by heavy lift transport to the permanent installation site. The transport was provided by self-propelled modular transporters (SPMT) that lifted the bridge, carried it a short distance, then set it onto its permanent support piers. The proposed and executed transport process included lifting the bridge from support points that were shifted one nodal location toward midspan at each end of the bridge. A photograph of the transport process is shown in Figure 15.

This transport scheme, with support points that differed from both the original fabrication support points and the support points after the placement of the main span onto the piers, resulted in a significant change in the demand resisted by critical elements within the structure. Of note, during transport the cantilevered region at the north end of the bridge included the truss member 11 and 12 nodal region. In this cantilevered configuration, the dead load effects on this region were effectively reversed such that the shear demand on the horizontal shear plane under truss member 11 changed from a northward to a southward thrust. Once the

bridge was set down on its permanent support piers, the shear demand reverted to its original orientation.

Although apparently not intentionally roughened, the upper and lower concrete surfaces at this plane would have offered some interlocking resistance due to their matched profiles. The SPMT transport process imposed one cycle of reverse shear demand on a critical plane at the cold joint. Given the crack that had already formed on this horizontal shear plane during formwork release, the single reversal cycle on the previously cracked plane would have likely decreased the interlock. Thus, once the bridge had been placed on the permanent support piers, the centroid of the shear resisting mechanisms under truss members 11 and 12 would likely have shifted farther to the north.

Figure 15. Photograph showing SPMT transport of the bridge.

3.5 SETTING OF BRIDGE SPAN ON PIER 2 SHIM STACKS

During the initial main span fabrication, the bearing support configuration supplied by the falsework on the north end of the bridge consisted of full-width support under the end diaphragm. This configuration allowed truss member forces to flow directly into the continuous support beneath the truss line. This support configuration changed as the bridge was moved to its permanent support piers. For the pier at the north end of the bridge, four discrete shim stacks were used. Two of these shim stacks were located toward the east side of the diaphragm and two were located toward the west side. No shim stacks were located directly beneath the truss line when the SPMTs lowered the bridge to its final position. Figure 16 provides an illustration showing the shim stack configuration after the SPMT transport. The inner east side shim stack under the north diaphragm can be seen in the photograph in Figure 32.

This new bearing configuration served to increase the shear demand on the north-south oriented vertical shear planes in the deck immediately east and west of the truss member 11 and 12 intersection with the deck. There are two notable details pertaining to these shear

planes. First, the shear planes are perforated by vertically-oriented plastic pipe sleeves that pass upward through the diaphragm and end adjacent to the east and west sides of truss member 12 where it meets the deck. These voids reduce the amount of concrete available to resist the demand placed on the nodal region by truss members 11 and 12. Second, the transverse post-tensioning tendons in the deck, which provide a clamping force on these vertical shear planes, were detailed and installed such that the northernmost post-tensioning point was located 49-inches south of the north end of the bridge. (See Figure 44.) This location is at the center of the plane where truss member 11 meets the deck, placing it well south of the vertical shear planes under discussion here. Thus, the clamping force from the transverse post-tensioning was less effective at the northernmost extent of the span where large shear forces were being generated by the dead load of the structure.

A photograph of the cracking observed in the chamfer of truss member 11 at the deck was captured immediately after the SPMT transport. This photograph, shown in Figure 17, was captured prior to the initiation of the detensioning operation.[h] The photos in Figure 18 and Figure 19 were also captured after the SPMT transport and before the detensioning operation; however, the specific time is unknown. Figure 18 shows that cracks in members 11 and 12, and a crack at the north end of the deck near the east face of member 12, were present and relatively narrow. Figure 19, although somewhat out of focus, shows the crack in the deck on the west side of member 12 that was previously observed in Figure 13. The cracks in Figure 18 and Figure 19 are significantly narrower and less extensive than those observed on the same day at approximately 3:16 p.m. after the detensioning of member 11. The 3:16 p.m. photographs are shown in Figure 25 and Figure 26 and are discussed in the next section.

[h] A photograph showing west side of member 2 at the deck after SPMT transport was also captured on March 10, 2018 at 12:29 p.m. This photograph can be found in the NTSB Bridge Factors Factual Report and is listed as “FIGG Bridge Engineers, Inc. Photo Submission FCA-S6”.

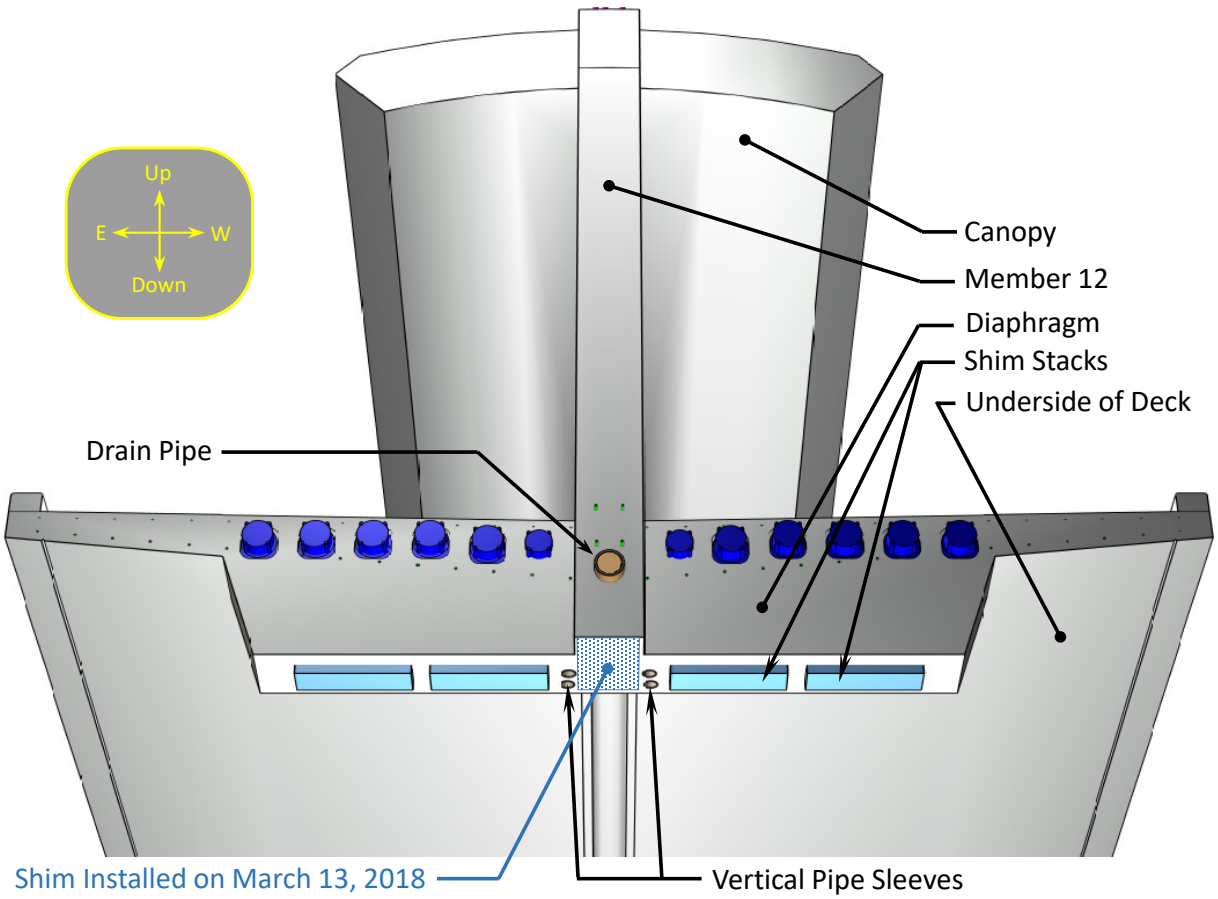

Figure 16. Illustration showing the post-SPMT transport support locations on the underside of the north diaphragm.

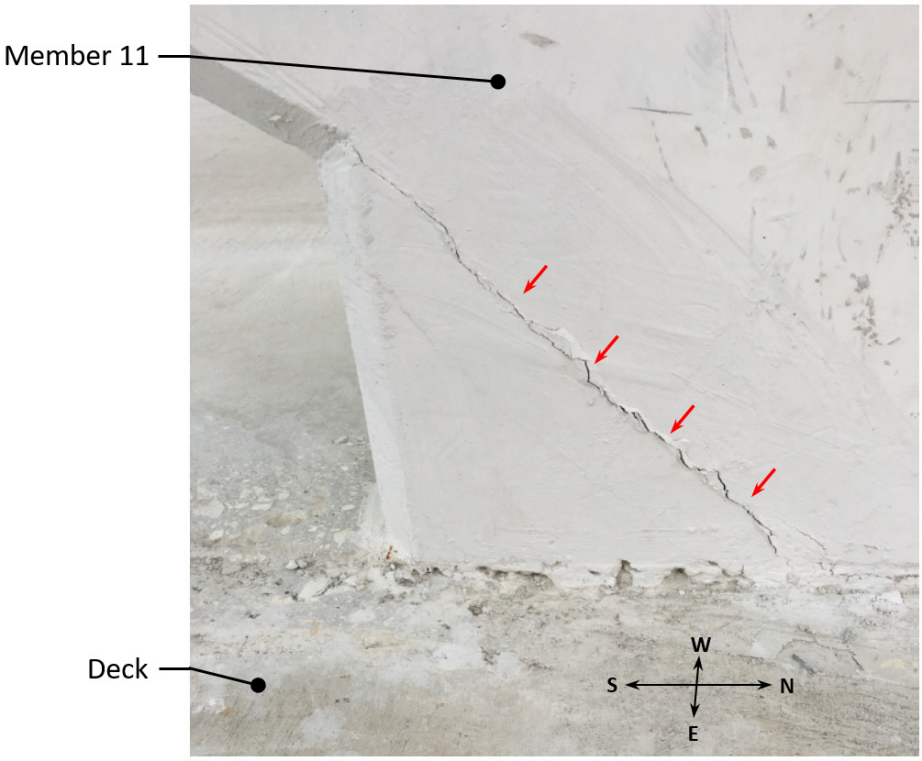

Figure 17. Photograph showing east side of member 11 at the deck after SPMT transport. Captured on March 10, 2018 at 12:29 p.m. Corresponds to Bridge Factors Factual Report Photo "FIGG Bridge Engineers, Inc. Photo Submission FCA-S7".

Figure 18. Photograph showing east side of members 11 and 12 at the deck after SPMT transport. Captured on March 10, 2018. Corresponds to Bridge Factors Factual Report Photo "MCM's Photo Submission MCM-4".

Figure 19. Photograph showing west side of member 12 at the deck after SPMT transport. Captured on March 10, 2018. Corresponds to Bridge Factors Factual Report Photo "MCM's Photo Submission MCM-3".

3.6 POST-TENSIONING FORCE IN MEMBER 11 IS REMOVED

The post-tensioning rods in truss member 11 served multiple purposes during the SPMT transport process. The forces imparted by these rods onto member 11 served to counteract tensile forces in the member while the north end of the bridge was cantilevered beyond the north SPMT support point. The forces from these rods also served to generate both a beneficial vertical clamping force across the horizontal interface shear plane at the base of member 11 and a detrimental horizontal shearing force that was driving the base of truss members 11 and 12 northward relative to the deck. Given that the angle of member 11 relative to the deck is approximately 32 degrees, the magnitude of the detrimental post-tensioning-induced horizontal shearing force was approximately 1.6 times the magnitude of the beneficial vertical clamping force.

Once the SPMT move was complete and the main span was resting on the pier supports, truss member 11 was expected to only carry axial compressive forces within the overall structure. Thus, the construction plan called for removal of the post-tensioning forces in the truss member 11 rods. This removal of post-tensioning forces served to reduce both the clamping force on the horizontal plane under member 11 and also reduce the driving force pushing truss members 11 and 12 northward relative to the deck.

Immediately after the post-tensioning in truss member 11 was removed, the distress previously observed in the member 11 and 12 nodal region grew significantly.[i] The decrease of the clamping force would have resulted in a reduction in the frictional resistance on the shear plane. Thus, since the large dead load induced northward shearing force was still present, a large shear resisting mechanism was still required. At the same time, the centroid of this shear resisting mechanisms would have shifted further toward the north end of the member 11 and 12 nodal region.

The northward movement, or dislocation, of the upper part of the truss member 11 and 12 nodal region relative to the deck is apparent in two specific structural behaviors that were observed. First, cracking was observed on the north face of truss member 12. The northward movement of the base of this member, while the top of the member was restrained from translation and rotation by the canopy, caused the member to bend in double curvature and exhibit flexural cracking. These north face cracks, annotated in Figure 35 and Figure 41, were perpendicular to the flexural tensile extreme fiber of the member and were observed within the lower half of the member. Second, cracking consistent with interface shear along much of the node and punching shear at the northern extent of the node was observed in the deck around the bases of truss members 11 and 12.

It is surmised that the northward dislocation of the nodal region relative to the deck was temporarily resisted by two primary mechanisms: 1) the lower portion of truss member 12

[i] The post-tensioning rods in member 2 served similar purposes to the rods in member 11. Similar distress was observed in the member 1 and 2 nodal region after the post-tensioning force in member 2 was removed. Views of the distress in the member 1 and 2 nodal region are shown in NTSB Bridge Factors Factual Report Photos 85 and 86.

whose bottom end was connected to the diaphragm and whose top end was connected to the canopy, and 2) steel reinforcement that crossed the shearing planes under truss member 11 and beside truss member 12. The steel reinforcement crossing the shear plane under truss member 11 was illustrated in Figure 14 (shown as green bars in this figure). The steel reinforcement crossing the vertical shear plane below the east side of truss member 12 is shown in Figure 20 as the annotated green #4 rebars. The vertical pipe sleeves paralleling this shear plane are also shown. An identical geometrical configuration occurred for the shear plane on the west side of truss member 12. Given the orientations of the shear planes, the amount of translation that had already occurred, and the lack of clamping forces, it is likely that the concrete-to-concrete interface shear resistance along these vertical planes was not offering significant resistance.

The column steel reinforcement in truss member 12 from the level of the drain pipe up to a few feet above the deck level is shown in Figure 21 as red vertical bars. The vertical reinforcement, with lap splices beginning just above the deck level, and the confinement reinforcement combine to create a reinforced concrete column that was able to buttress much of the load being driven northward by truss member 11.

Within truss member 12, there were three #11 bars running vertically along the south face and three #7 bars running vertically along each of the east, north, and west faces. The lower ends of these reinforcements were anchored into the bottom of the north diaphragm and extended above the deck level. These bars were lap spliced with matching bars beginning just above the cold joint at the base of truss member 12. The two exceptions to this lap splice description are the #11 bar on the center of the south face and the #7 bar on the center of the north face. These two bars conflicted with the horizontal drain pipe and thus the lower bar in the lap splice was detailed to hook within the volume of concrete immediately above the drain pipe.

It is important to note that the longitudinal post-tensioning anchorages in the deck were not in a location that could resist a significant portion of the northward thrust applied to the nodal region by truss member 11. As will be discussed in Section 6.3.2 of this report, only horizontal loads applied within the footprint of truss member 11 had an opportunity to flow outward to the longitudinal post-tensioning anchorages. Since the horizontal interface under truss member 11 was cracked and the node was translating northward, it appears that only the northward shear force transferred into the deck via the reinforcing bars traversing the member 11 footprint shear plane would have been reacted by these anchorages. Recall that there were only six #7 bars engaged on this shear plane (see Figure 14).

Figure 22 through Figure 41 provide chronological photographic evidence of the distress observed in the nodal region between the time of truss member 11 detensioning and the afternoon of March 14, 2018. Text messages collected from the contractor indicate that the detensioning operations for truss members 2 and 11 were about to begin at 2 p.m. on March 10, 2018. Similar evidence indicates that the detensioning operations were complete at 6:30 p.m. on March 10, 2018. Photographs captured by a stationary camera situated on a nearby building provide evidence that member 11 was detensioned first and that the detensioning was completed before 3:00 p.m. The detensioning of member 2 was completed later, between 4:30 and 5:30 p.m.

The photographs in Figure 22, Figure 23, Figure 24, Figure 25, and Figure 26 were captured at approximately 3:16 p.m. on March 10, 2018. The photographs in Figure 22 and Figure 24 show the west and east sides, respectively, of truss member 11 at the deck, while the image in Figure 23 shows the south side of member 11 at the deck. The photographs in Figure 25 and Figure 26 show the deck to the east and west sides of truss member 12. Given that these photographs were captured immediately after the detensioning of member 11, and given the significant increase in distress as compared to that shown in Figure 17 through Figure 19 which were captured immediately before detensioning, it is clear that the significant increase in distress can be attributed to the detensioning operation.

The photographs in Figure 27 and Figure 28 were captured after the completion of the detensioning of the post-tensioning rods in members 2 and 11. These photographs were sent via text message on March 10, 2018 at 7:08 p.m. by a construction worker who was assisting in the construction operation. These images further demonstrate how the distress in the deck and diaphragm had significantly worsened in the hours since the image in Figure 19 was captured.

The photographs in Figure 29, Figure 30, and Figure 31 were captured at approximately 10 a.m. on March 12, 2018. They focus on the north face of the north diaphragm, showing significant distress on either side of truss member 12. Specifically, tension cracks parallel the compression struts that would have been carrying the dead load of the bridge through the nodal region and into the shim stacks. The upper end of these cracks also disconnects the truss member 12 nodal concrete from the surrounding deck along the vertical shear planes to the east and west of truss member 12. The Figure 32 photograph, also captured at approximately 10 a.m. on March 12, 2018 shows cracks on the south face of the north diaphragm. This cracking is consistent with the high shear present in this diaphragm caused by the outboard positioning of the shim stacks relative to the centerline of the bridge.

The photographs in Figure 33, Figure 34, Figure 35, and Figure 36 were captured midday on March 13, 2018. The photographs in Figure 37, Figure 38, Figure 39, Figure 40, and Figure 41 were captured at approximately 1:45 p.m. on March 14, 2018. This set of photographs shows how the distress in the nodal region was progressing during the final two days prior to the collapse.

Figure 33 and Figure 38 show the location on the west side of truss members 11 and 12 at the deck where the horizontal shearing plane under member 11 transitions into being a vertical shearing plane along the west side of member 12. Figure 34 and Figure 37 show the distress apparent on the west and east faces, respectively, of truss member 11 where it meets the deck. Figure 36 provides a close-up view of the northward translation that was occurring along the interface under member 11. Figure 35 and Figure 41 show the flexural cracks on the north face of truss member 12. Figure 39 and Figure 40 show the distress observed at the north end of the deck on the east and west side of truss member 12.

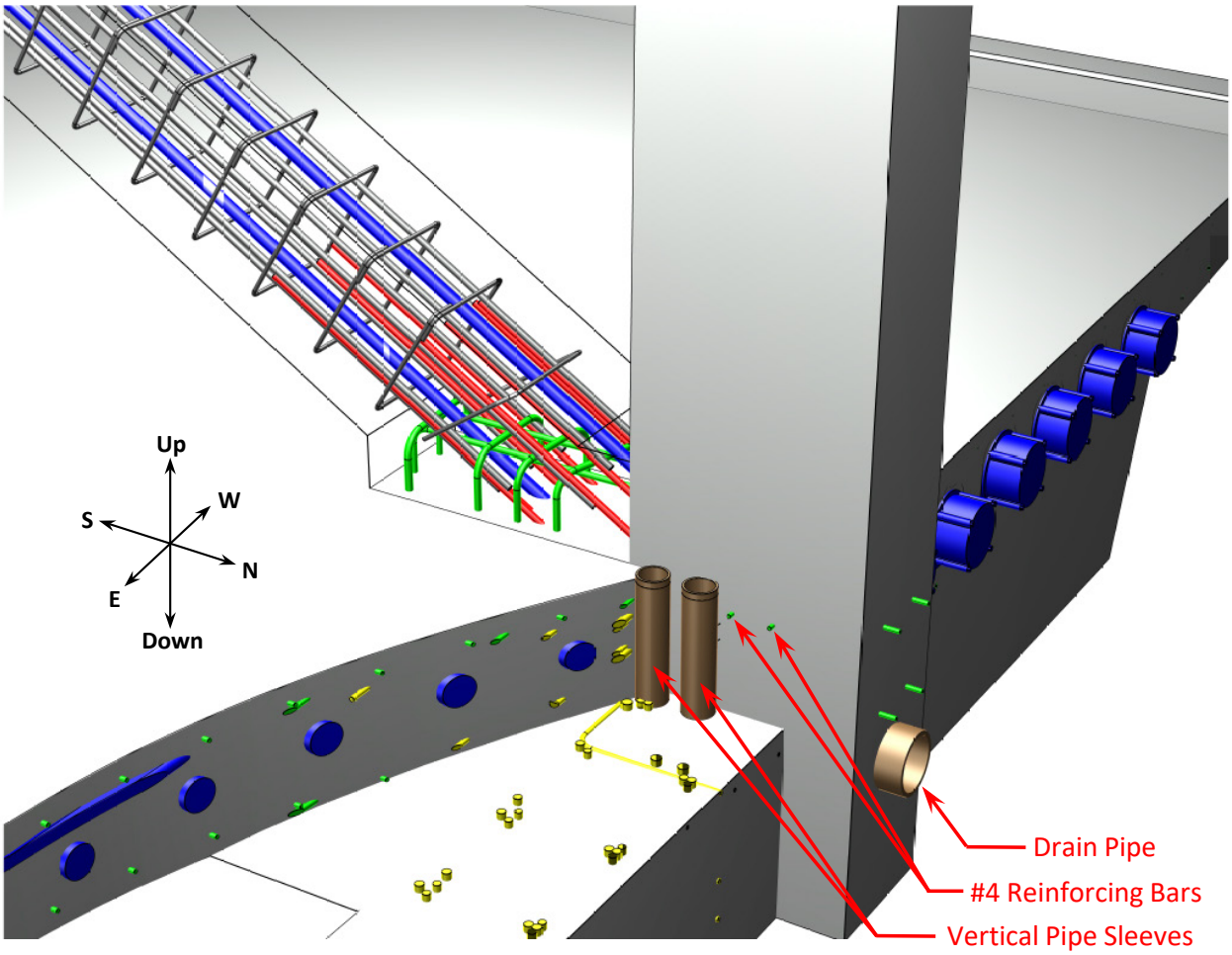

Figure 20. Cutaway illustration showing the reinforcing bars crossing and the conduit paralleling the shear plane below the east face of truss member 12.

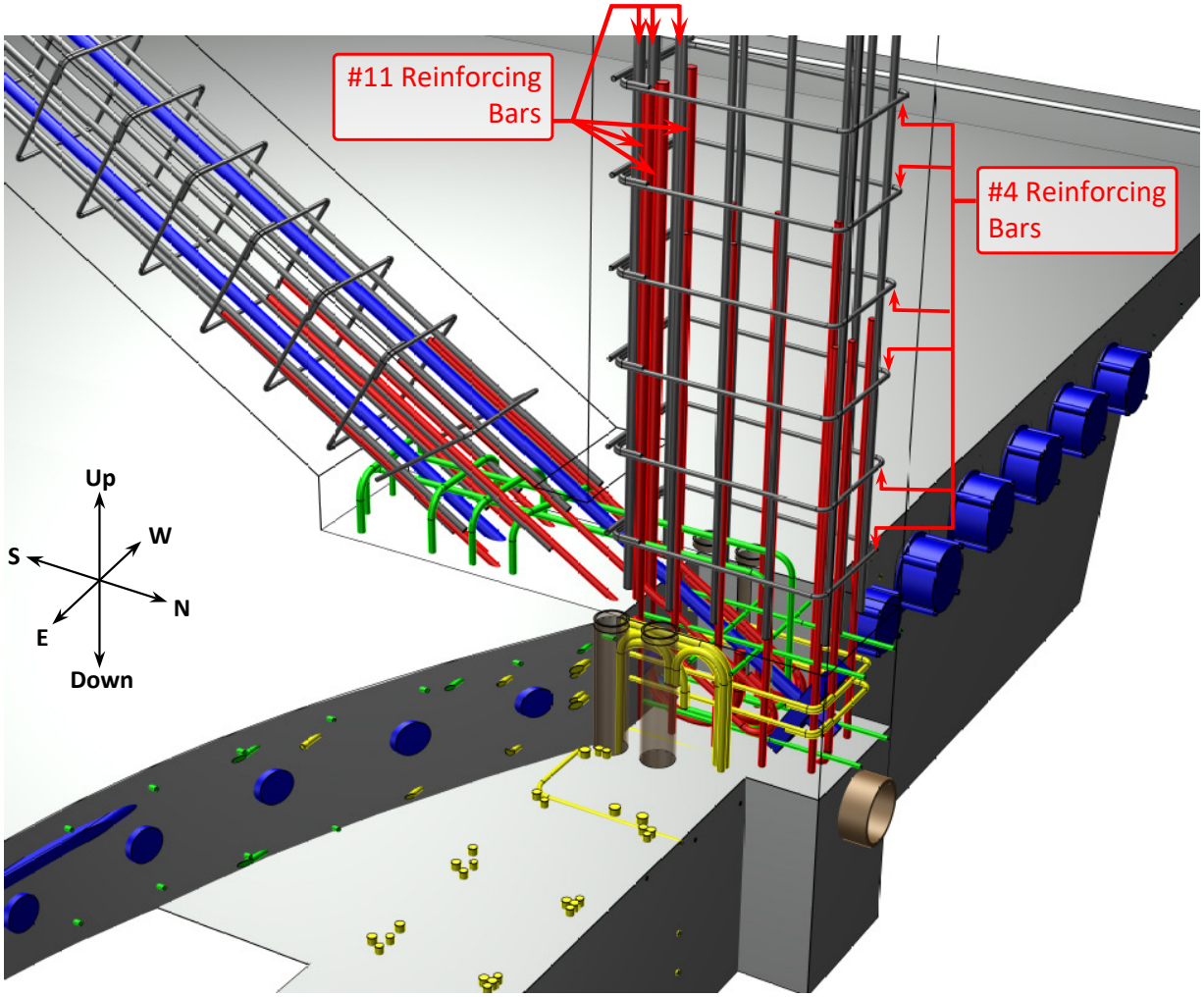

Figure 21. Cutaway illustration showing the reinforcing bars and conduits within and near the base of truss member 12.

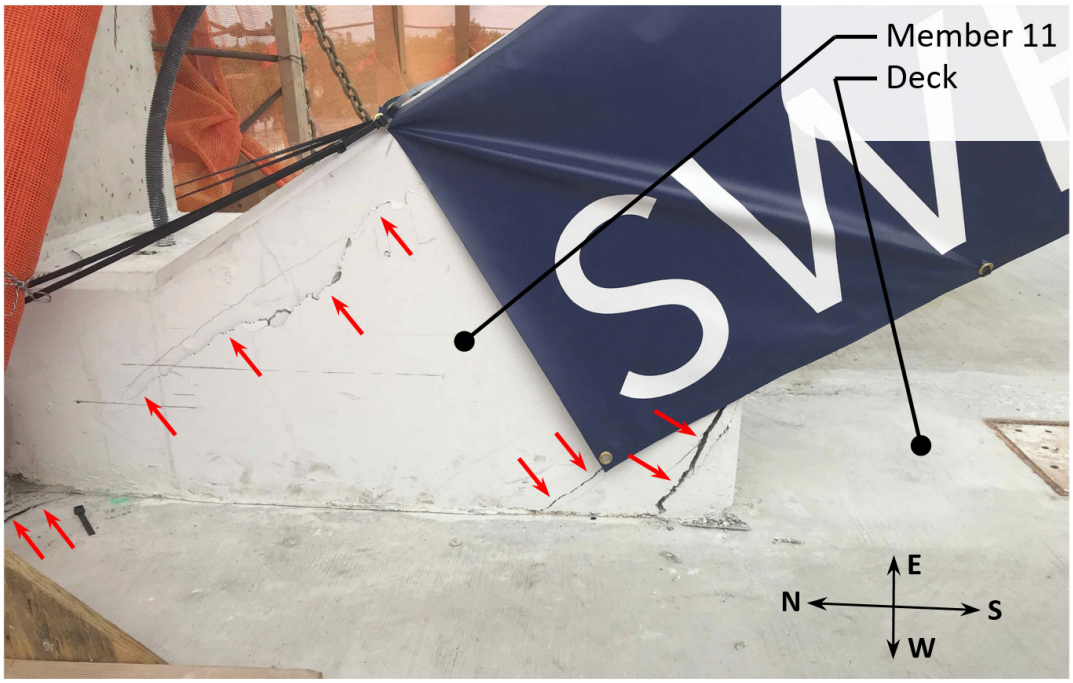

Figure 22. Photograph showing west side of member 11 at the deck after the truss member 11 post-tensioning rod detensioning operation. Captured on March 10, 2018 at 3:16 p.m. Corresponds to Bridge Factors Factual Report Photo 62.

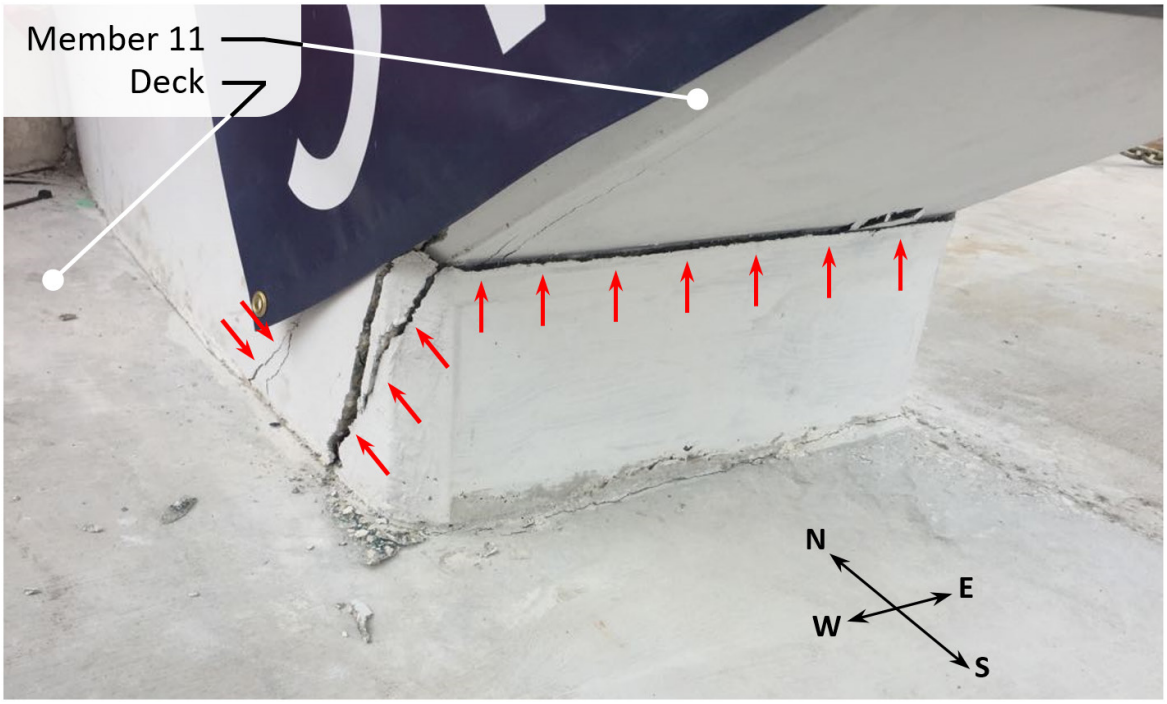

Figure 23. Photograph showing south side of member 11 at the deck after the truss member 11 post-tensioning rod detensioning operation. Captured on March 10, 2018 at 3:16 p.m.

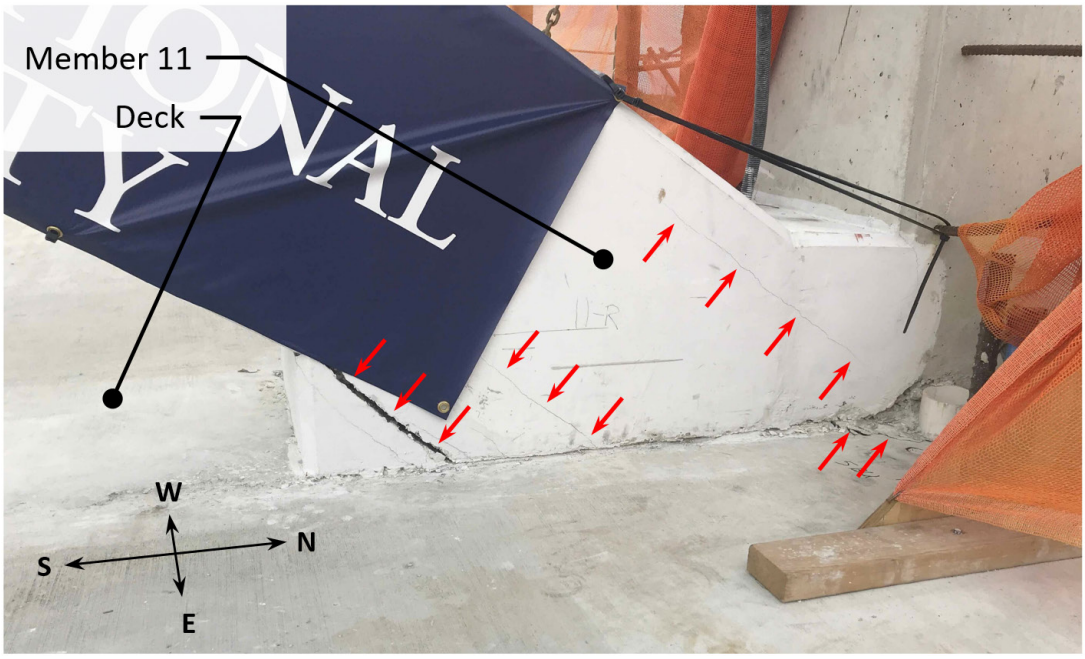

Figure 24. Photograph showing east side of truss member 11 at the deck after the member 11 post-tensioning rod detensioning operation. Captured on March 10, 2018 at 3:17 p.m. Corresponds to Bridge Factors Factual Report Photo 64.

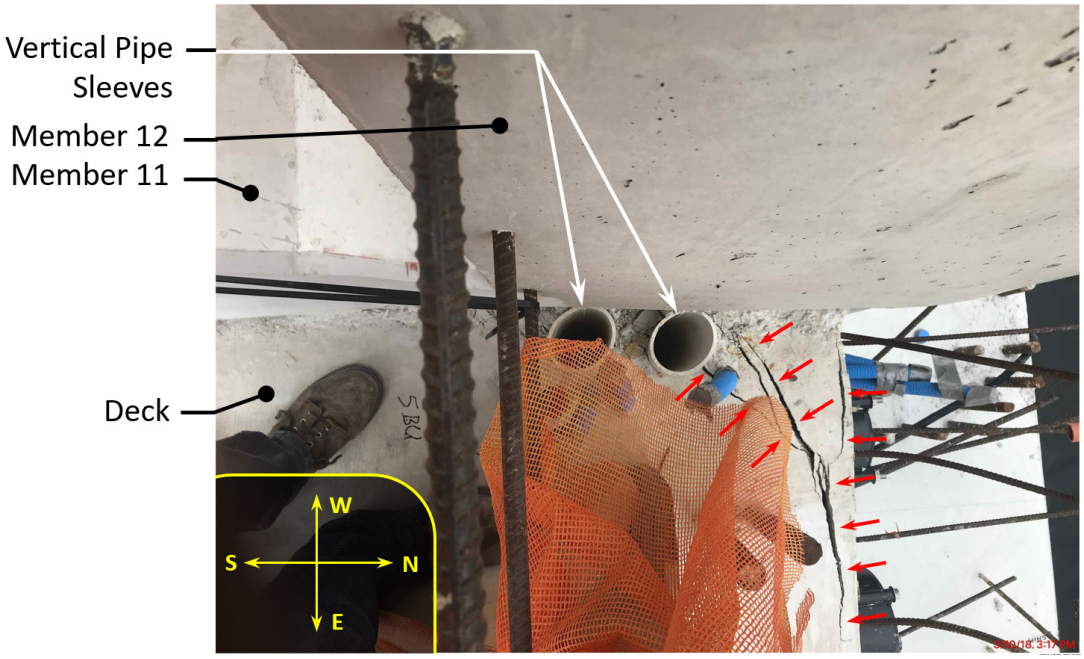

Figure 25. Photograph looking vertically downward along east side of truss member 12 after the truss member 11 post-tensioning rod detensioning operation. Captured on March 10, 2018 at 3:17 p.m. Corresponds to Bridge Factors Factual Report Photo 65.

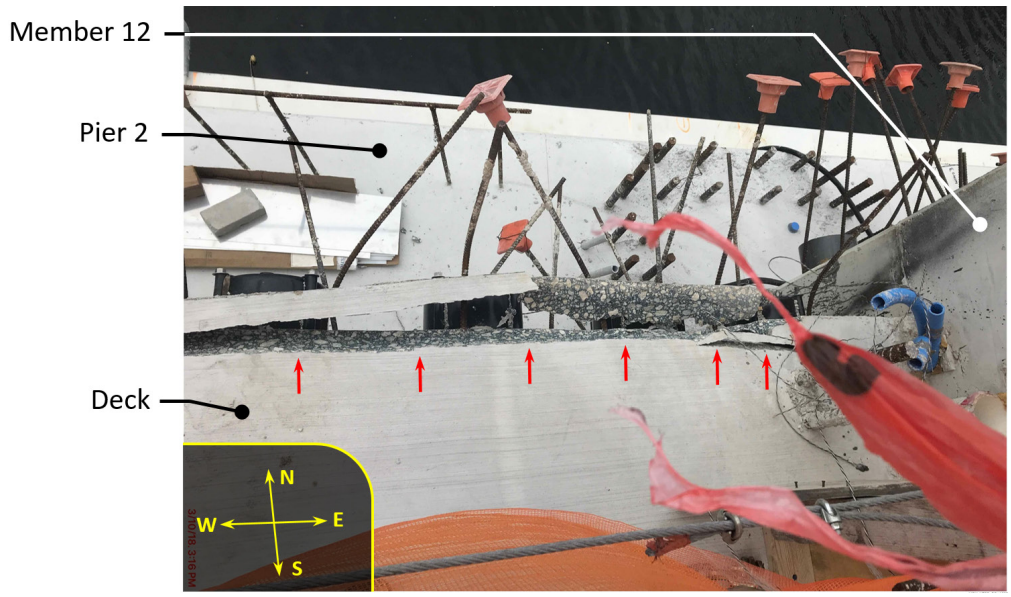

Figure 26. Photograph showing the north end of the bridge deck immediately west of member 12 after the member 11 post-tensioning rod detensioning operation. Captured on March 10, 2018 at 3:16 p.m. Corresponds to Bridge Factors Factual Report Photo 63.

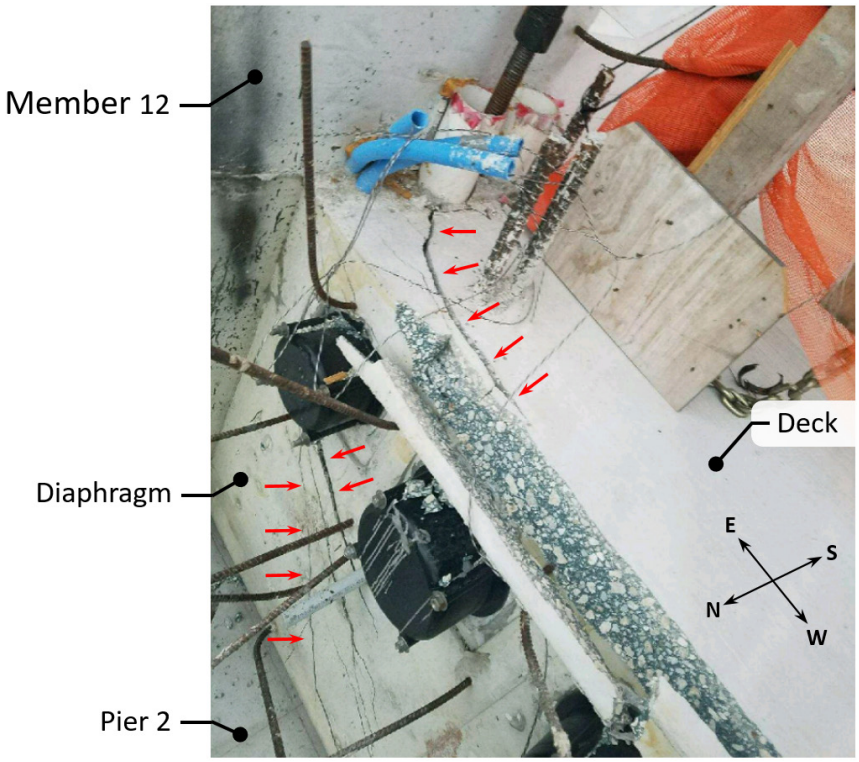

Figure 27. Photograph showing the north end of deck and north face of the north diaphragm immediately west of member 12 after detensioning of members 2 and 11. Source is text message sent by Kevin Hanson on March 10, 2018 at 7:08 p.m.

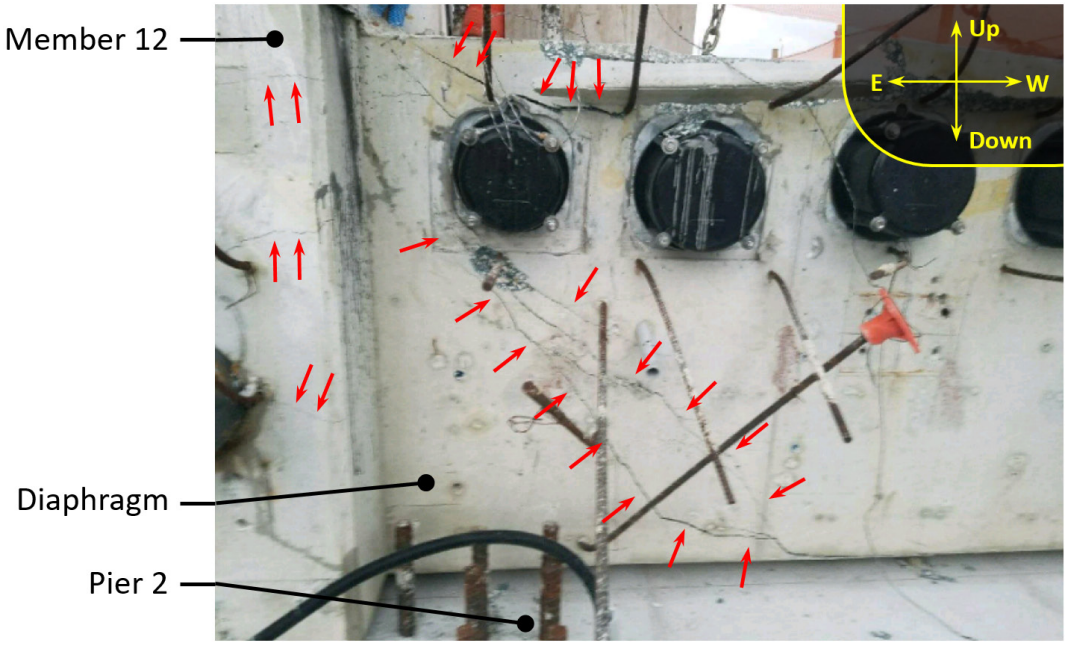

Figure 28. Photograph showing the north face of the north diaphragm immediately west of member 12 after detensioning of members 2 and 11. Source is text message sent by Kevin Hanson on March 10, 2018 at 7:08 p.m.

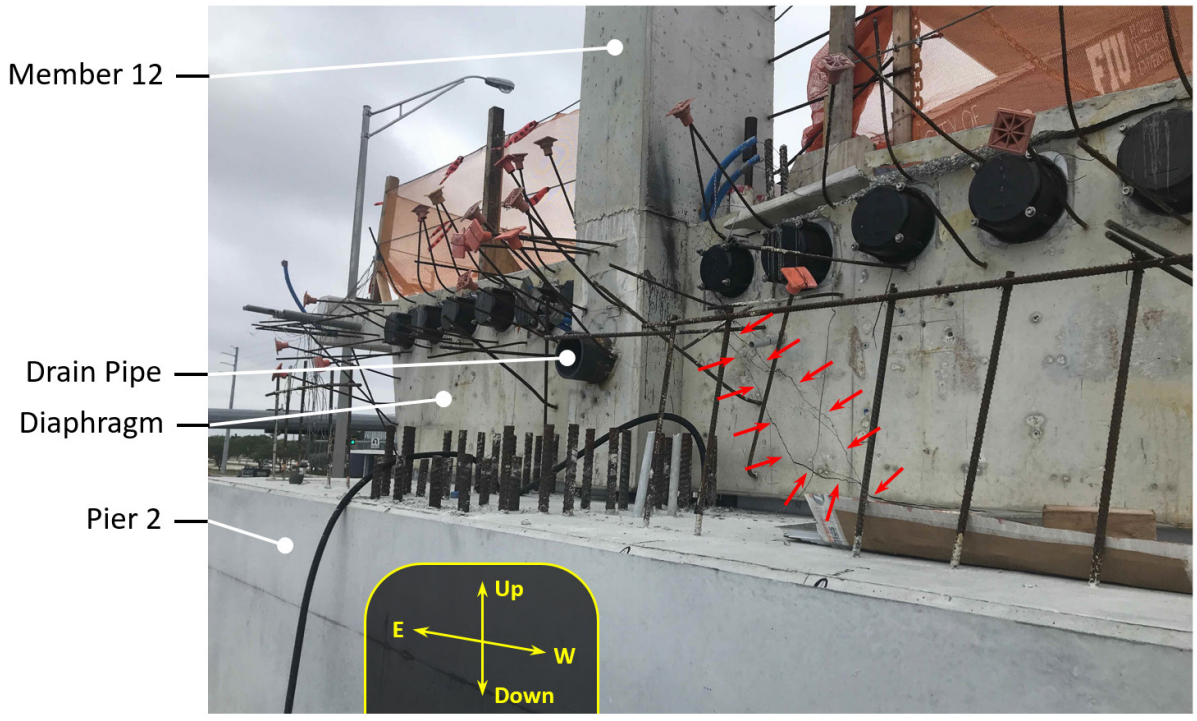

Figure 29. Photograph showing the north face of the north diaphragm on March 12, 2018 at 9:46 a.m. Corresponds to Bridge Factors Factual Report Photo 67.

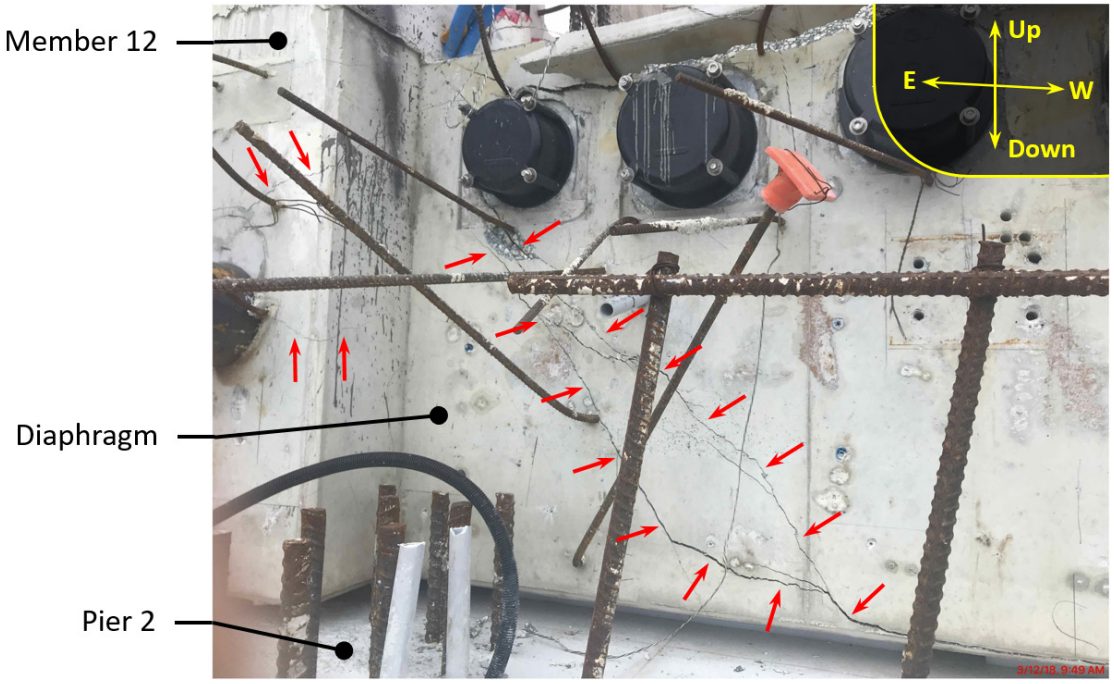

Figure 30. Photograph showing the north face of the north diaphragm immediately west of member 12 on March 12, 2018 at 9:49 a.m. Corresponds to Bridge Factors Factual Report Photo 68.

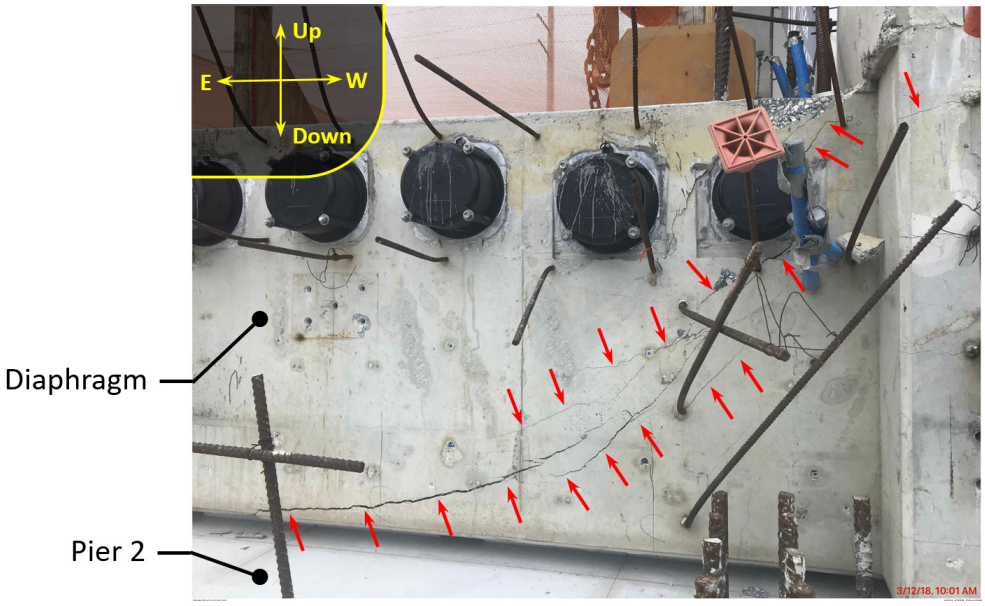

Figure 31. Photograph showing the north face of the north diaphragm immediately east of truss member 12 on March 12, 2018 at 10:01 a.m. Corresponds to Bridge Factors Factual Report Photo 69.

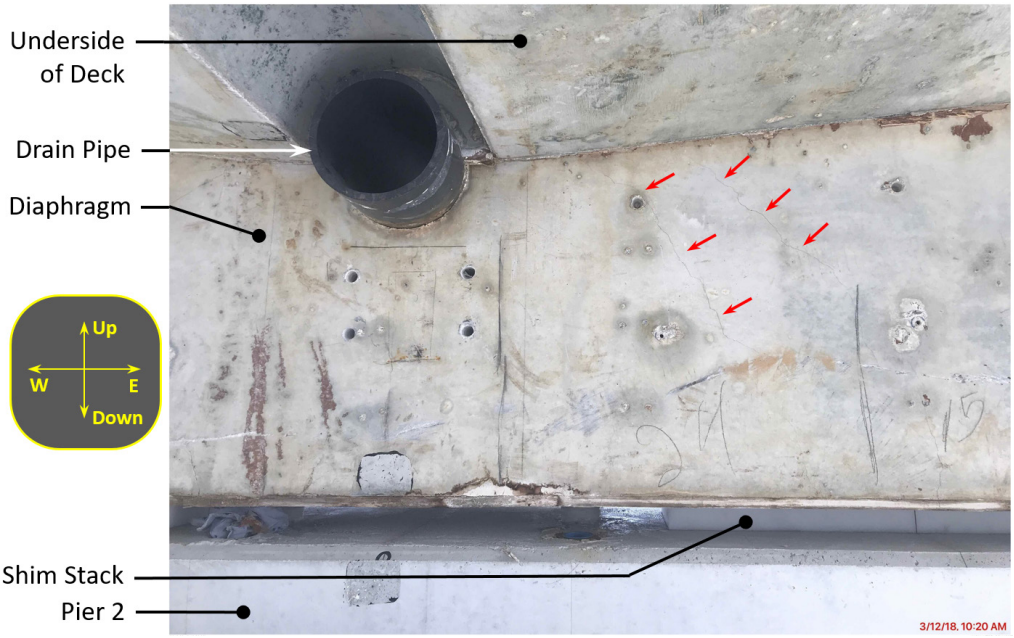

Figure 32. Photograph showing the south face of the north diaphragm between the midline of the bridge and the first bearing pad toward the east on March 12, 2018 at 10:20 a.m. Corresponds to Bridge Factors Factual Report Photo 70.

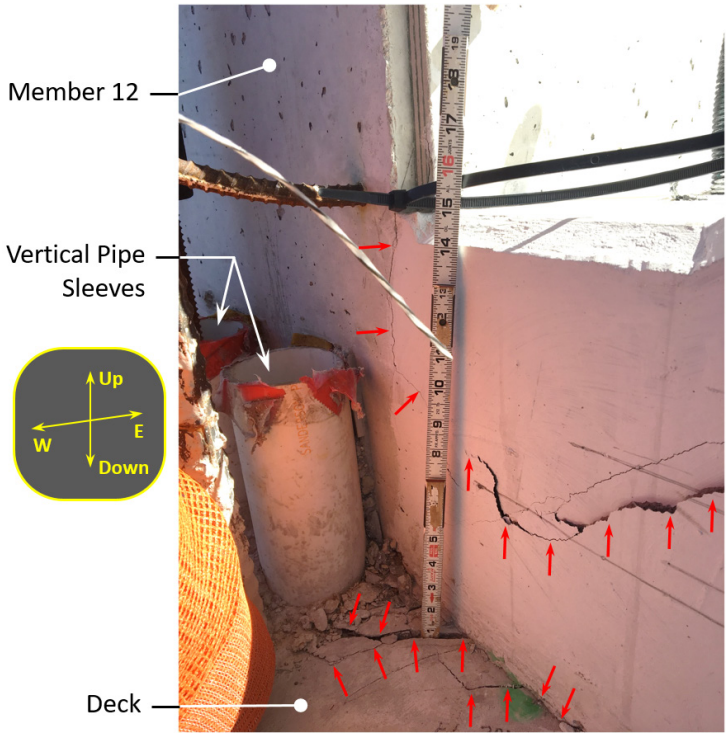

Figure 33. Photograph showing the west face of truss members 11 and 12 where they meet the deck on March 13, 2018 at 11:25 a.m. Corresponds to Bridge Factors Factual Report Photo 79.

Figure 34. Photograph showing the west face of truss member 11 where it meets the deck on March 13, 2018 at 11:17 a.m. Corresponds to Bridge Factors Factual Report Photo 83.

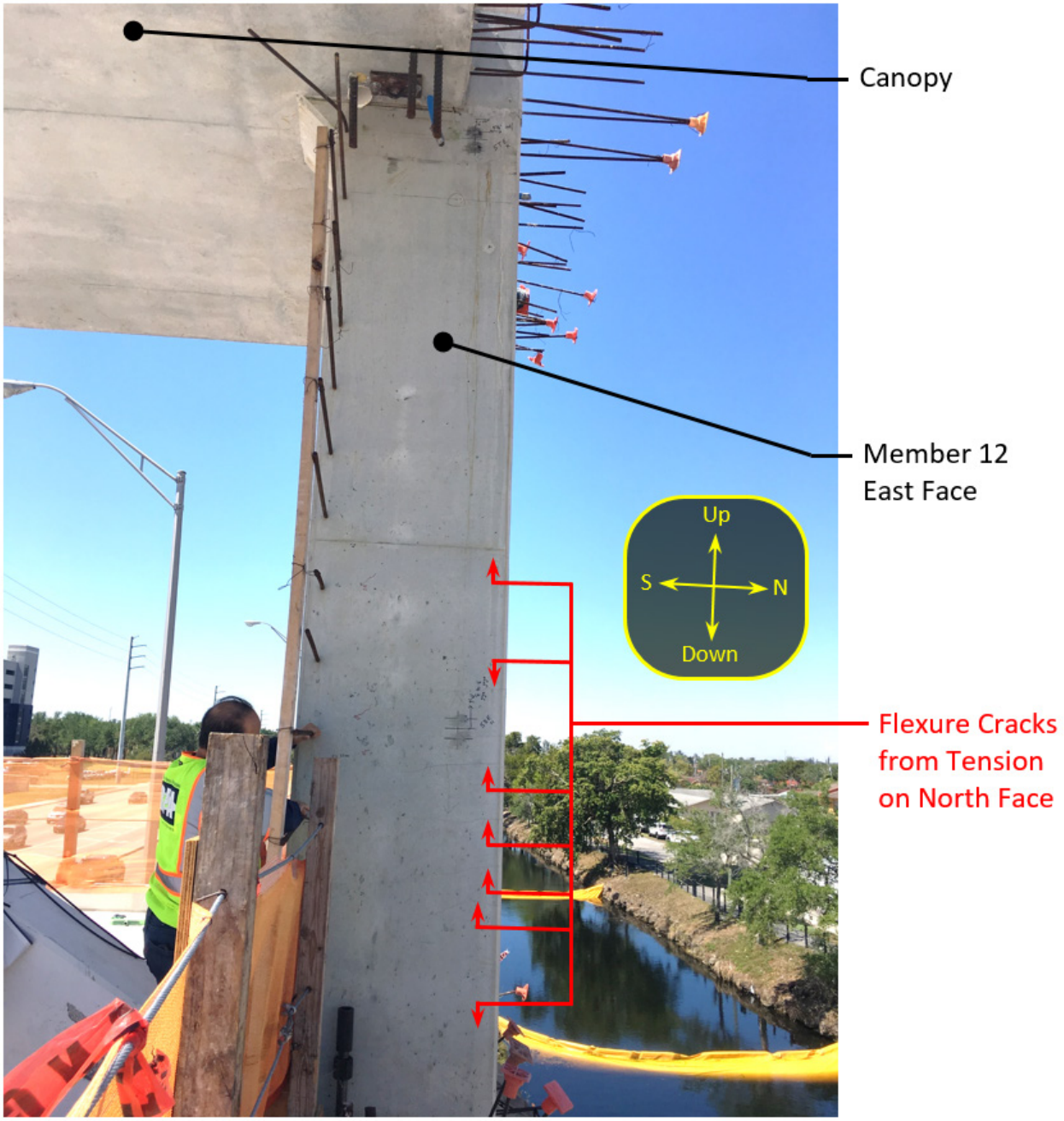

Figure 35. Photograph showing the east face of truss member 12 on March 13, 2018 at 1:21 p.m.

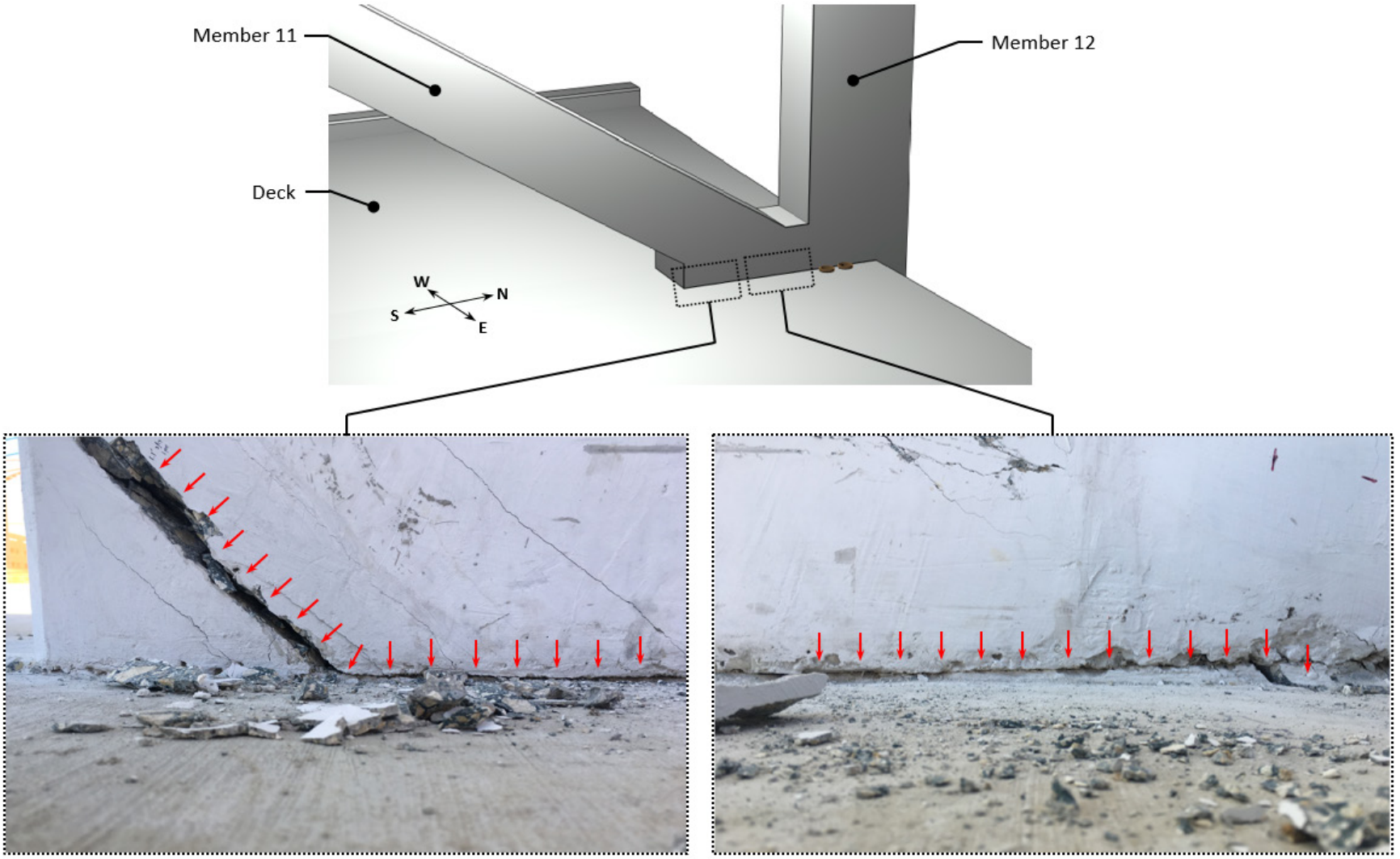

Figure 36. Photographs showing the east interface between of truss member 11 and the deck on March 13, 2018 at 1:29 p.m.

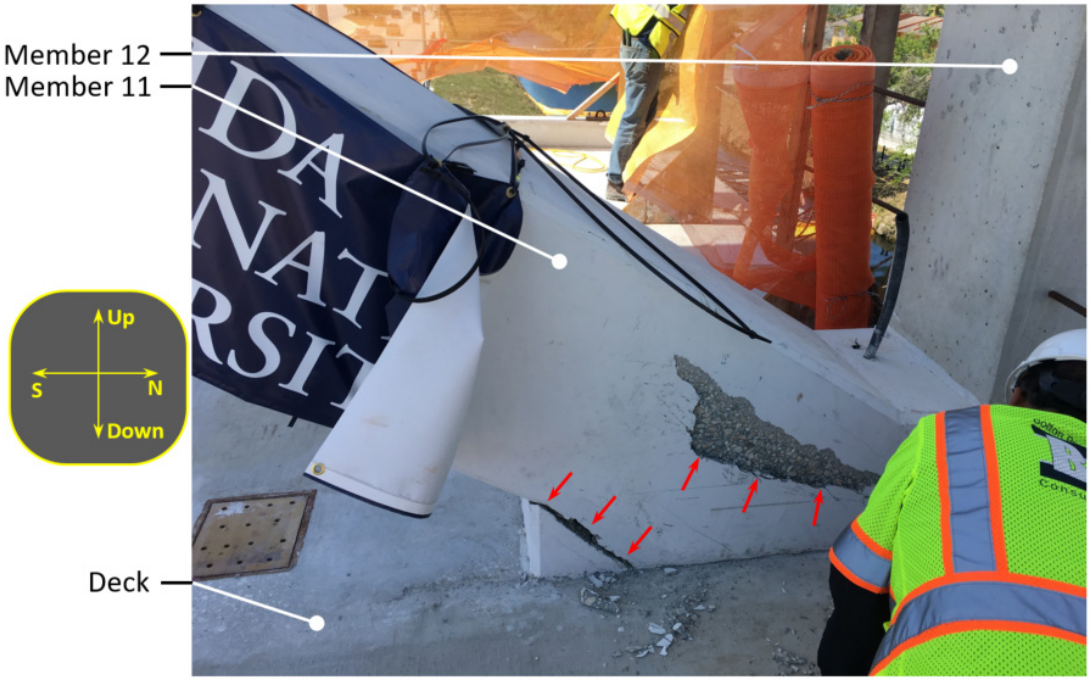

Figure 37. Photograph showing the east face of truss member 11 where it meets the deck on March 14, 2018 at 1:42 p.m. Corresponds to Bridge Factors Factual Report Photo 90.

Figure 38. Photograph showing the west face of truss member 11 where it meets the deck on March 14, 2018 at 1:45 p.m. Corresponds to Bridge Factors Factual Report Photo 92.

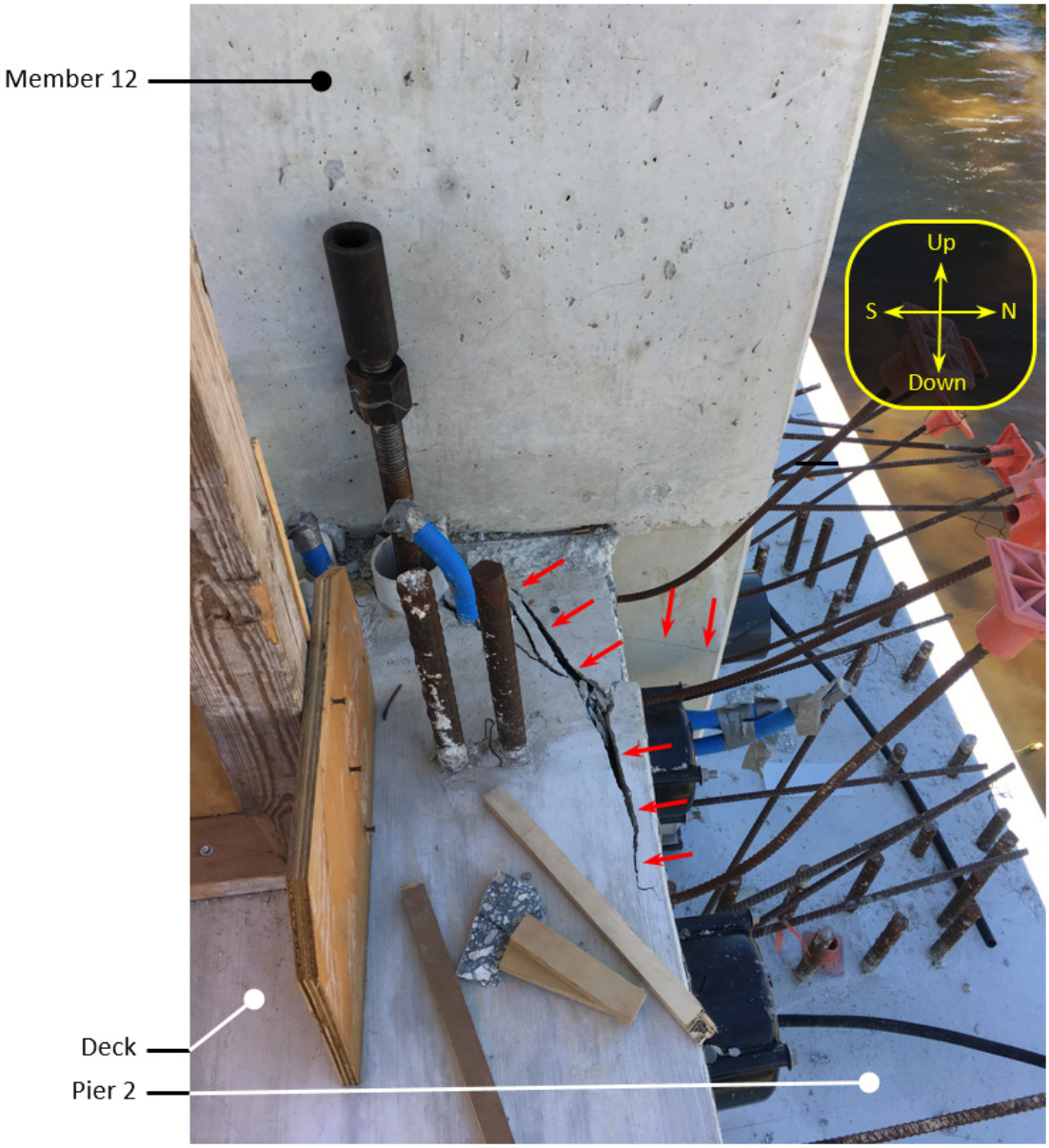

Figure 39. Photograph showing the east face of truss member 12 where it meets the deck on March 14, 2018 at 1:50 p.m. Corresponds to Bridge Factors Factual Report Photo 96.

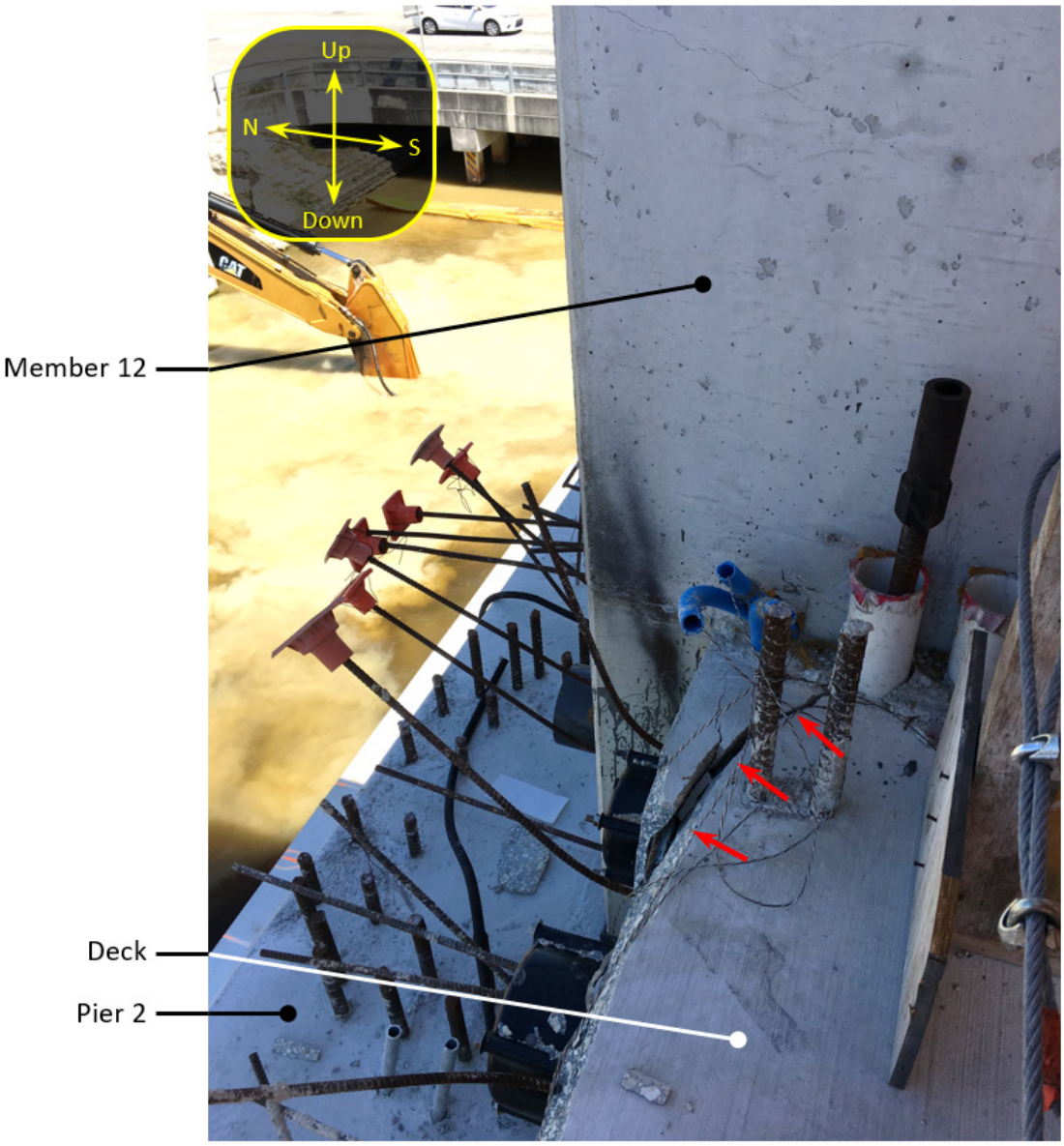

Figure 40. Photograph showing the west face of truss member 12 where it meets the deck on March 14, 2018 at 1:51 p.m. Corresponds to Bridge Factors Factual Report Photo 98.

Figure 41. Photograph showing the west face of truss member 12 on March 14, 2018 at 1:51 p.m. Corresponds to Bridge Factors Factual Report Photo 100.

3.7 SUPPLEMENTAL SHIM INSTALLED

The distress observed in the structure between March 10 and March 13, 2018 prompted FIGG Bridge Engineers to direct the bridge construction contractor to install supplemental support under the north diaphragm. This diaphragm, illustrated in Figure 16, was originally supported on Pier 2 via four shim stacks. Until this time there had been no support along the centerline of the bridge in the area between the vertical pipe sleeves that passed through the diaphragm.

On Tuesday March 13, 2018 at 9:45 a.m. the bridge design firm directed the contractor to immediately place a shim under the diaphragm in the area along the bridge centerline between the existing two innermost shim stacks. The contractor was told that lifting or "jacking" of the bridge was not required; thus, the shim was to be manually inserted in the space between the diaphragm and Pier 2.

Figure 42 and Figure 43 show the new shim after insertion. Both images are of the same shim, with Figure 44 showing a view from the north and Figure 45 showing a view from the south. In Figure 45 one of the original white shim stacks is visible on the right side of the image.

Given that the four existing shim stacks were already supporting the weight of the bridge on Pier 2, the manual insertion of a new shim stack under the diaphragm (i.e., insertion without the lifting of the bridge to rebalance the loads between the five shim stacks) is not anticipated to have permitted any sizeable load to be distributed into the new shim stack. Thus, the new shim would have only carried load in a situation where further distress caused a downward movement of the center of the diaphragm relative to the remainder of the diaphragm.

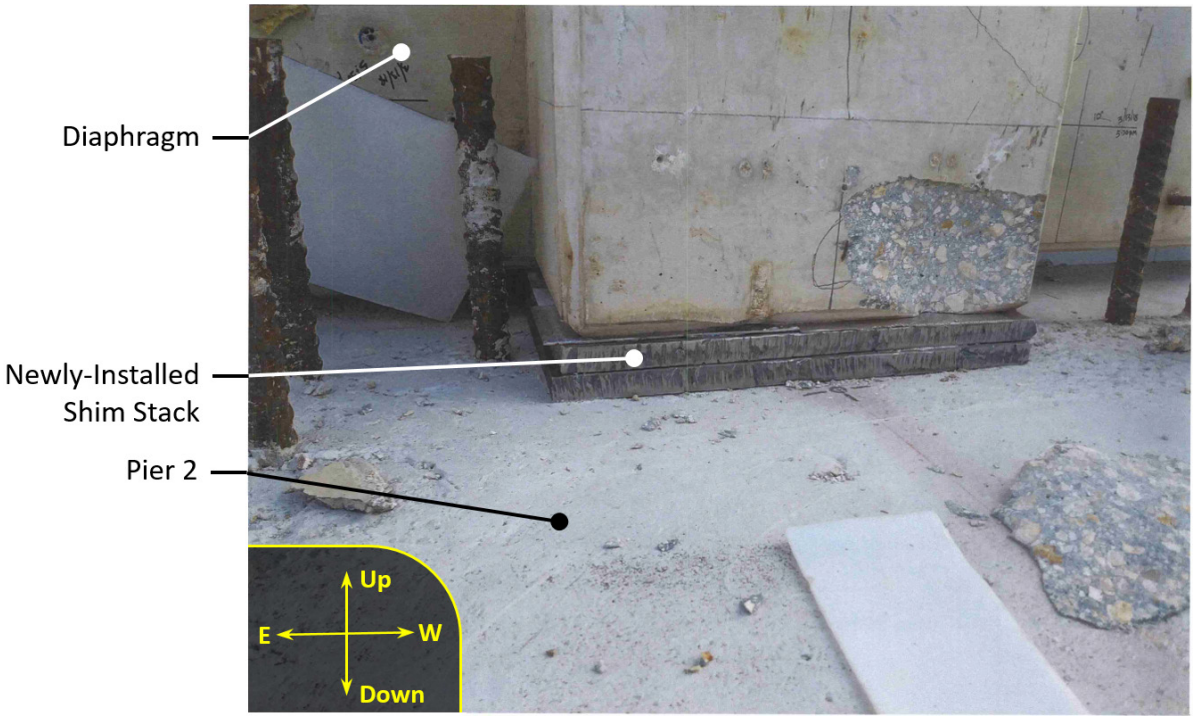

Figure 42. Photograph showing the north side of the north diaphragm after the installation of the new shim and before March 14, 2018 at 1:38 p.m.

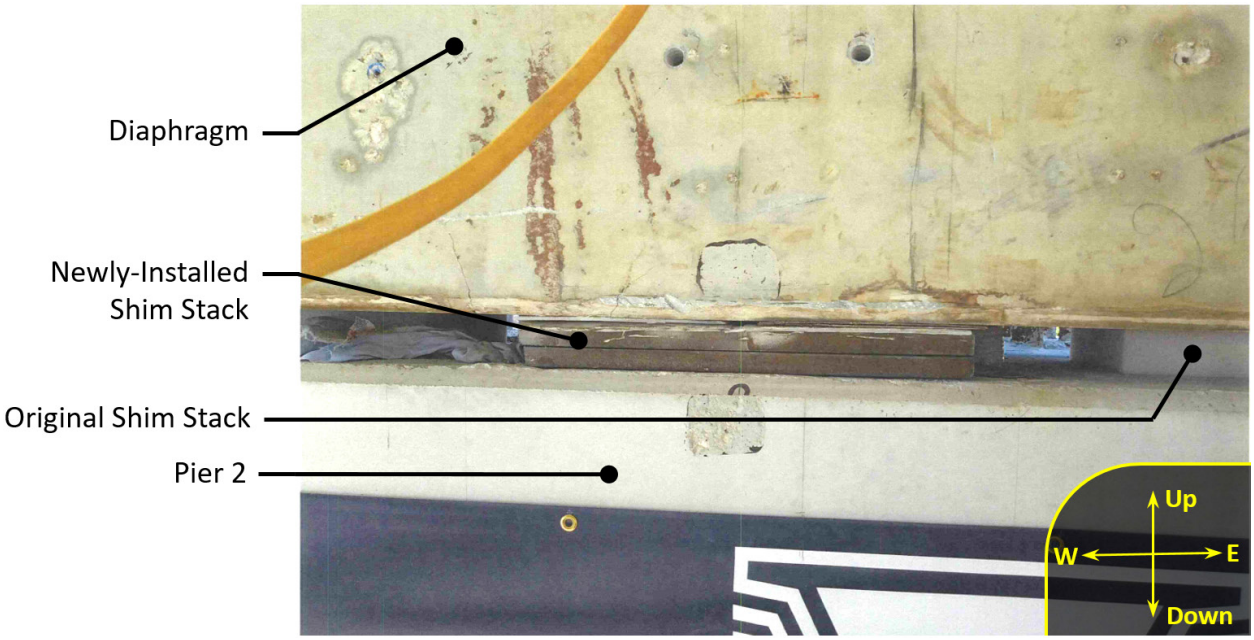

Figure 43. Photograph showing the south side of the north diaphragm after the installation of the new shim and before March 14, 2018 at 1:38 p.m.

3.8 POST-TENSIONING FORCE IN MEMBER 11 IS REAPPLIED

In an attempt to arrest the distress observed in the structure, FIGG Bridge Engineers decided to retension the post-tensioning rods in truss member 11. Although the investigation found no record explicitly describing the intent of this action, presumably the intent was to generate clamping force across the horizontal shear interface under truss member 11. Recall that the angle of action of truss member 11 is such that the magnitude of the detrimental horizontal driving force created by applying axial post-tensioning in truss member 11 is approximately 1.6 times the magnitude of the beneficial vertical clamping force generated across the horizontal shear plane at the top of the deck.

Recognize that retensioning of the post-tensioning rods cannot return the node to the pre-damaged condition and may, as a result of the inelastic nodal region damage[j], generate different effects than were assumed in the original design of the structure. As described in earlier sections of this chapter, the member 11 and 12 nodal region was damaged. The upper portion of the nodal region had already begun to dislocate northward in response to the existing, largely bridge self-weight induced forces carried through member 11. Retensioning the

[j] A structural element that has been inelastically damaged (i.e., damaged through an irreversible action such as cracking of concrete or yielding of steel) cannot be returned to its original, pre-damage state. Once the damage has occurred, the structural material will have permanently changed from its original condition and the resistance that the material and larger structural system offer to subsequent loadings will be different.

member 11 post-tensioning rods increased the force effect on the node and exacerbated the damage.

Figure 44, which provides an illustration showing a north-south oriented vertical slice along the truss member line of the bridge through the truss member 11 and 12 nodal region, shows the location of the rod anchorages within the concrete under truss members 11 and 12. The two post-tensioning rods in member 11, referred to as rod 11S on the south face and rod 11N on the north face, are shown in the figure.[k]

Post-collapse evidence indicates that, of the two post-tensioning rods in truss member 11, the bottom end of rod 11S was well anchored into the deck on the south side of the failure region while the bottom end of rod 11N was anchored into the portion of the nodal region that was severely cracked and that translated northward during the collapse. The contractor executing the post-tensioning operation reported that the retensioning of the rods had just been completed at the time of collapse. Thus, it is assumed that the rods were sufficiently anchored immediately before collapse to generate their intended loads in member 11. However, given the upper rod anchorage location relative to the failure planes, rod 11N is not expected to have been generating significant clamping or shear forces on the interface shear failure planes in the nodal region.

Annotations in Figure 44 identify key locations within the nodal region. An approximation of the east-west oriented failure plane is identified by the solid red line A-B-C-D-E-F. An approximation of the north-south oriented failure planes in the deck is identified by the red crosshatched region bounded by C-D-E-H. There are two red crosshatched planes, one at each of the east and west faces of truss member 12. The drain pipe (dark blue fill) that bounded the bottom of the D-E-F failure plane and the vertical pipe sleeves (light blue fill) that perforated the C-D-E-H failure planes are shown.

The resistance mechanisms afforded by the structure across the identified failure planes can be deduced by comparing the distress observed prior to collapse with the construction plans and the retained portions of the collapsed structure. Wide structural cracks with rigid body translation along the A-B-C plane (see Figure 37, Figure 45, and Figure 46) and continuing along the C-H line (see Figure 40 and Figure 47) indicate that the concrete bounding these failure planes was offering little resistance. Along inclined plane A-B, two #6 reinforcing bars crossed the plane. Along horizontal plane B-C, six #7 reinforcing bars cross and are perpendicular to the plane. Three additional #7 reinforcing bars, these being the axial reinforcement in the south face of truss member 11, also pass through plane B-C and may have offered some resistance to northward translation along the plane. Vertical plane C-D, which would have experienced direct tensile forces that moved the upper part of the node northward relative to the lower part of the node, did not have any reinforcing bars crossing the plane. Additionally, the steel anchorage plate for post-tensioning rod 11S aligned with this plane and thus served as a discontinuity on the plane. The pair of vertical planes C-D-E-H aligning with the east and west

[k] In the FIGG Plans for the bridge, rod 11S is referred to as Bar B within member 11. Rod 11N is referred to as Bar A.

faces of member 12 each contained a pair of 4.5-inch diameter hollow plastic pipe sleeves. These planes were each crossed by two #4 reinforcing bars. Finally, the horizontal plane D-E-F was effectively the base of member 12. It was crossed by two #11 reinforcing bars on the south face, three #7 reinforcing bars on each of the east and west faces, and two #7 reinforcing bars on the north face. Recall that the drain pipe bisected the base of truss member 12 and thus one #11 reinforcing bar and one #7 reinforcing bar that existed higher up in the member 12 column were not anchored in the diaphragm below the drain pipe.

It is apparent that a significant portion of the shear load applied to the region by member 11 was being resisted by the vertically-oriented reinforcing bars at the base of truss member 12. Due to the geometry of the node, these forces would have been resisted through a combination of 1) horizontal shear on the bars at a location just above the drain pipe, and 2) flexure on truss member 12 rotating about the east-west axis and causing tension on the south face and compression on the north face at the base of the column. This resistance mechanism was contingent on the vertical reinforcing bars remaining lap spliced with the bars in the upper portion of the member and also on the entirety of the truss member 12 cross section remaining geometrically stable.

The distress apparent in the structure surrounding the base of truss members 11 and 12 can be seen in Figure 45, Figure 46, and Figure 47. Figure 48, Figure 49, and Figure 50 provide three post-collapse views of the nodal region under member 12, offering a view of the reinforcements, the plastic pipes that were in and surrounding the failure region, and the validation of the failure planes A-B-C-D-E-F and C-D-E-H identified in Figure 44.

Given the damage in the nodal region, and specifically the locations of the failure planes identified in Figure 44, the retensioning of the post-tensioning rods in truss member 11 was not an effective means of strengthening this nodal region. A retensioned rod 11S may have offered some clamping force across the already sliding B-C failure plane (see Figure 36), but more importantly would have further driven the northward dislocation of the upper part of the node relative to the lower part of the node. This northward dislocation would have placed yet more demand on the remaining nodal region shear resistance mechanisms (i.e., the rebar, primarily under truss member 12, that crossed the failure planes).

Finding:

Retensioning truss member 11 increased demand on and corresponding damage to the member 11 and 12 nodal region until the distress became critical.

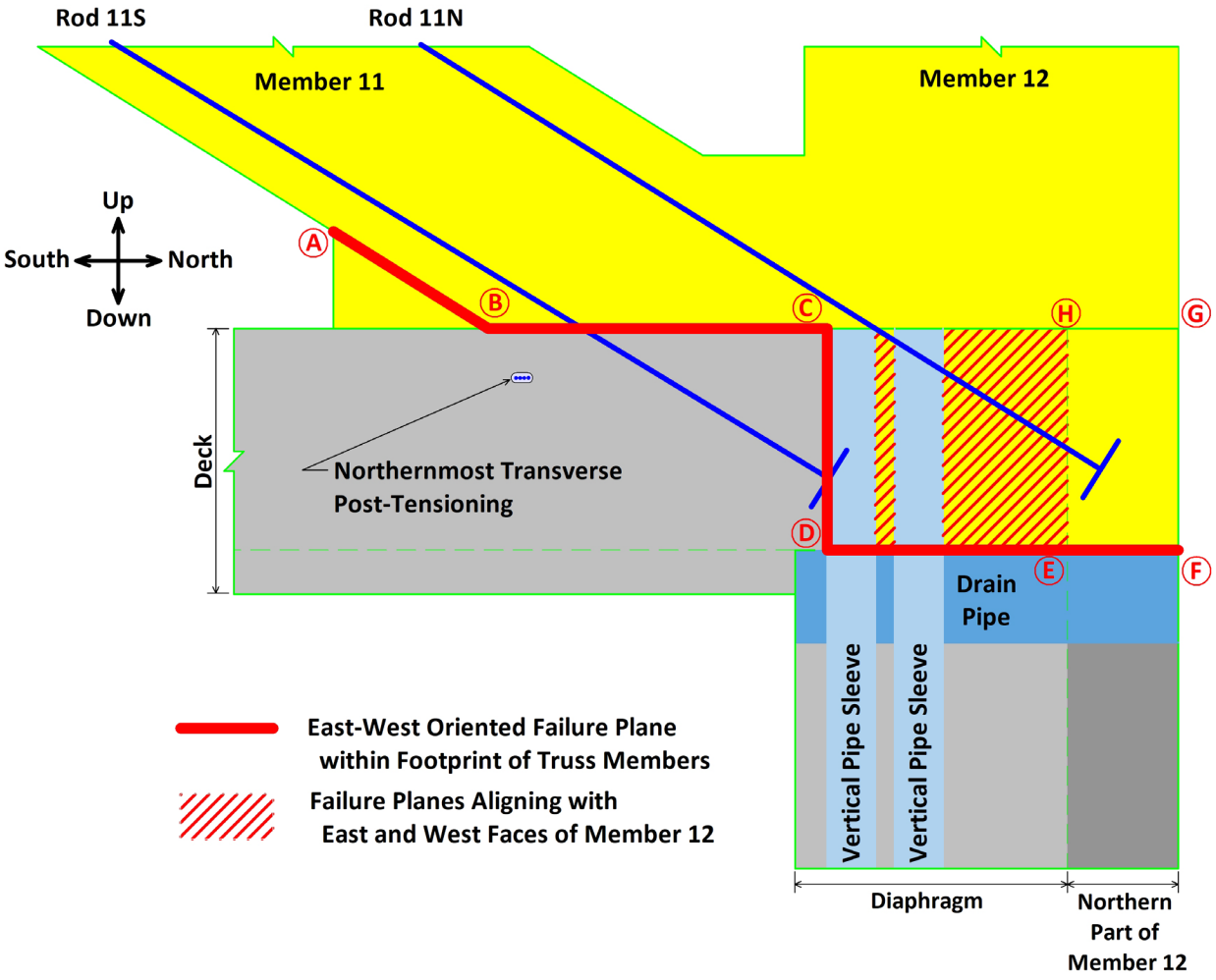

Figure 44. Illustration showing a midline cross section of the truss member 11 and 12 nodal region with annotations indicating resistance mechanisms and distress.

Figure 45. Photograph showing the east face of truss member 11 where it met the deck on March 15, 2018 at 10:53 a.m. Corresponds to Bridge Factors Factual Report Photo 102.

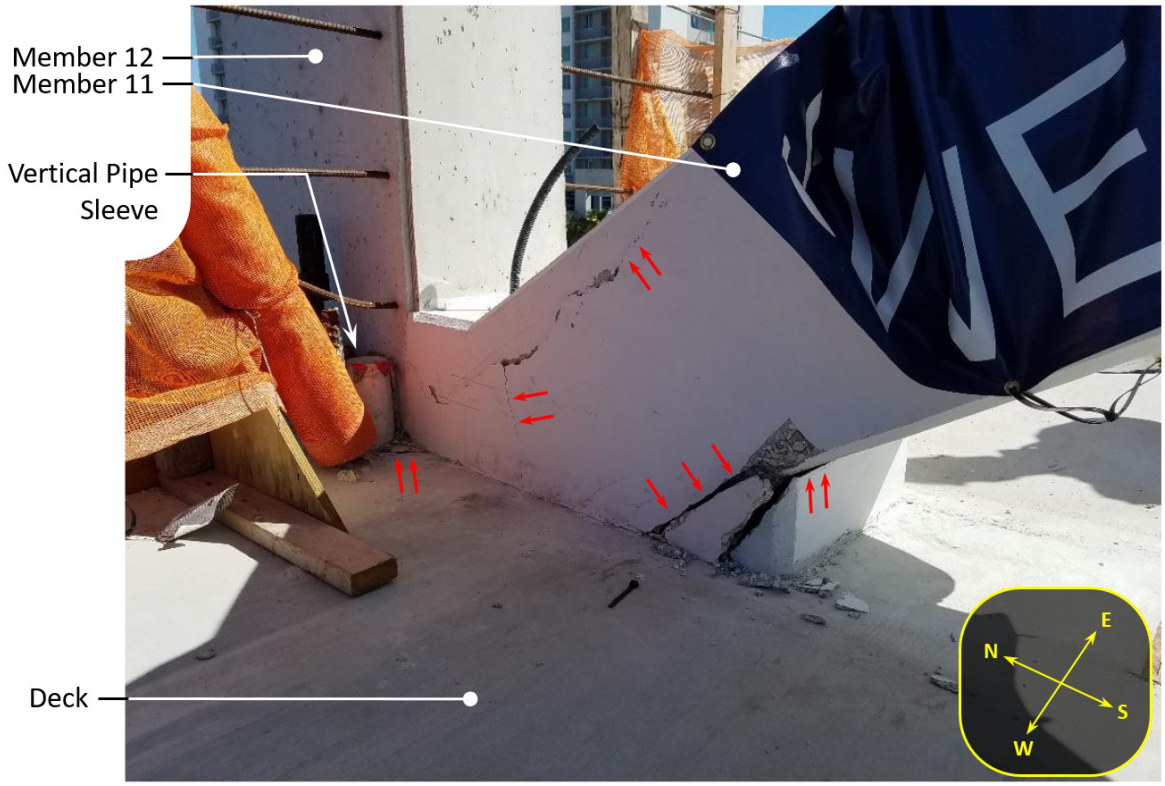

Figure 46. Photograph showing the west face of truss member 11 where it met the deck on March 15, 2018 at 10:55 a.m. Corresponds to Bridge Factors Factual Report Photo 103.

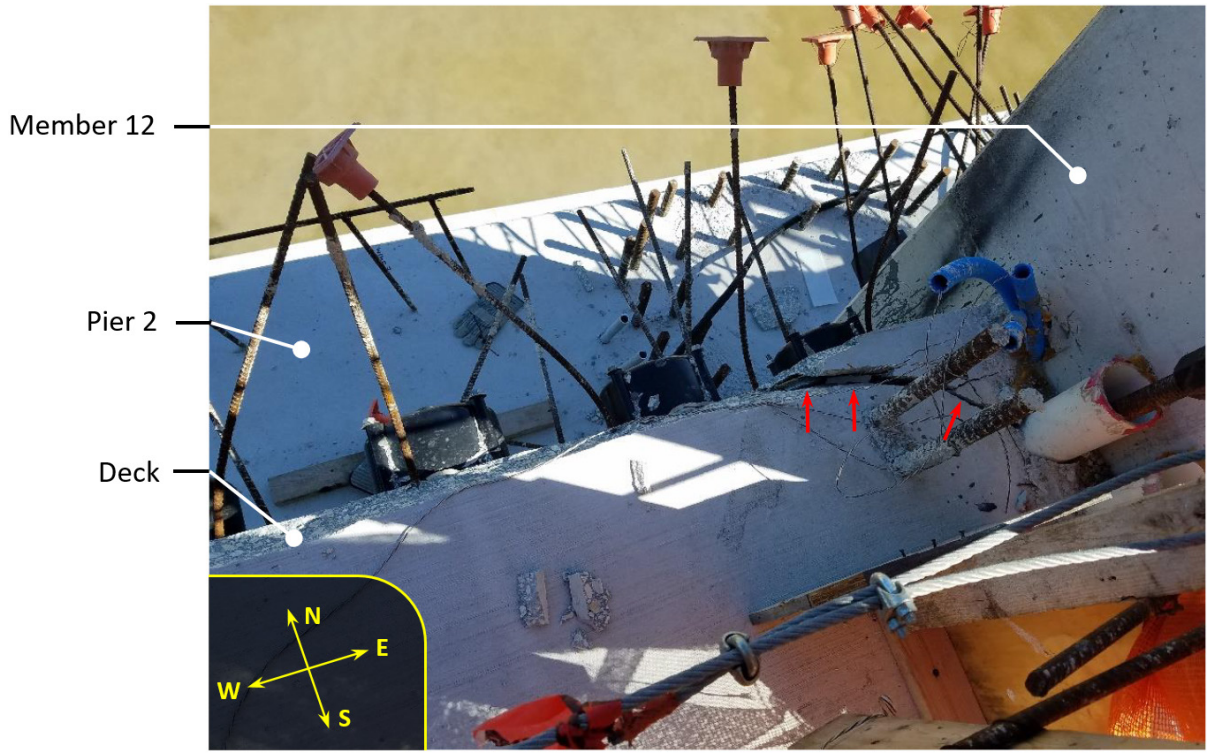

Figure 47. Photograph showing the north end of deck on west side of truss member 12 on March 15, 2018 at 10:55 a.m. Corresponds to Bridge Factors Factual Report Photo 104.

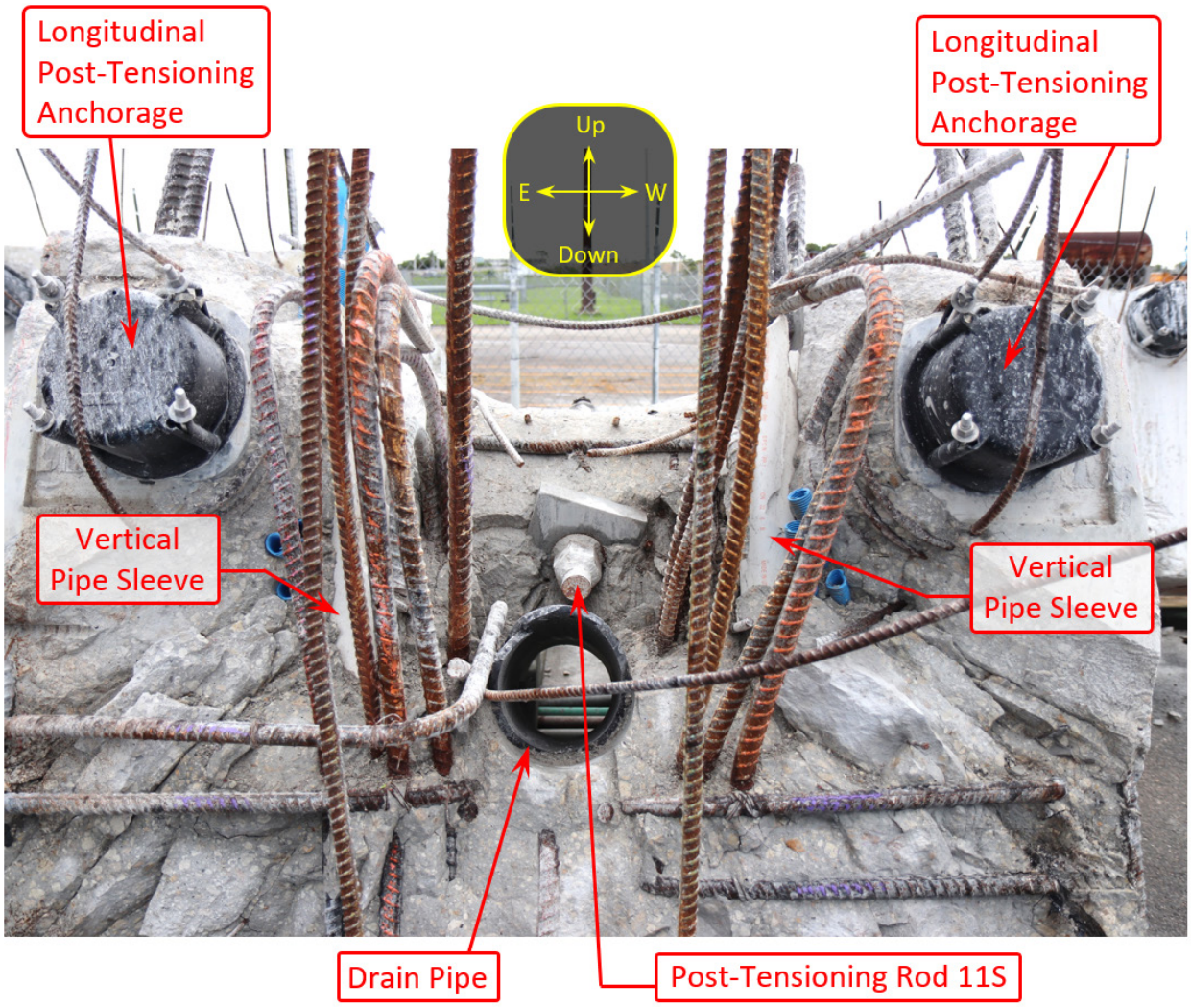

Figure 48. Photograph showing post-collapse condition of deck portion of truss member 11 and 12 nodal region looking from north toward south along bridge centerline.

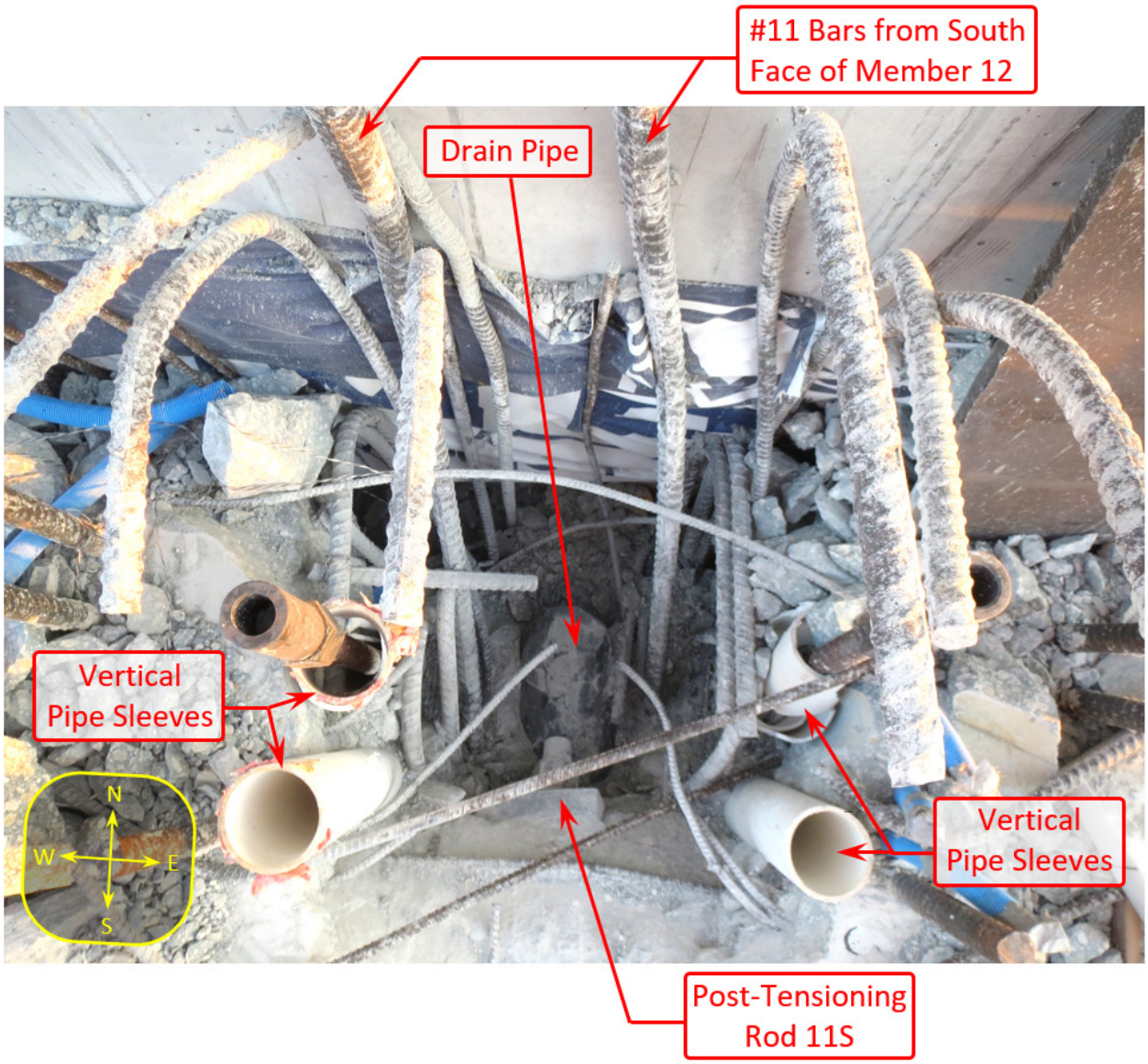

Figure 49. Photograph showing post-rubble removal condition of deck portion of truss member 11 and 12 nodal region looking down with north toward the top of photo.

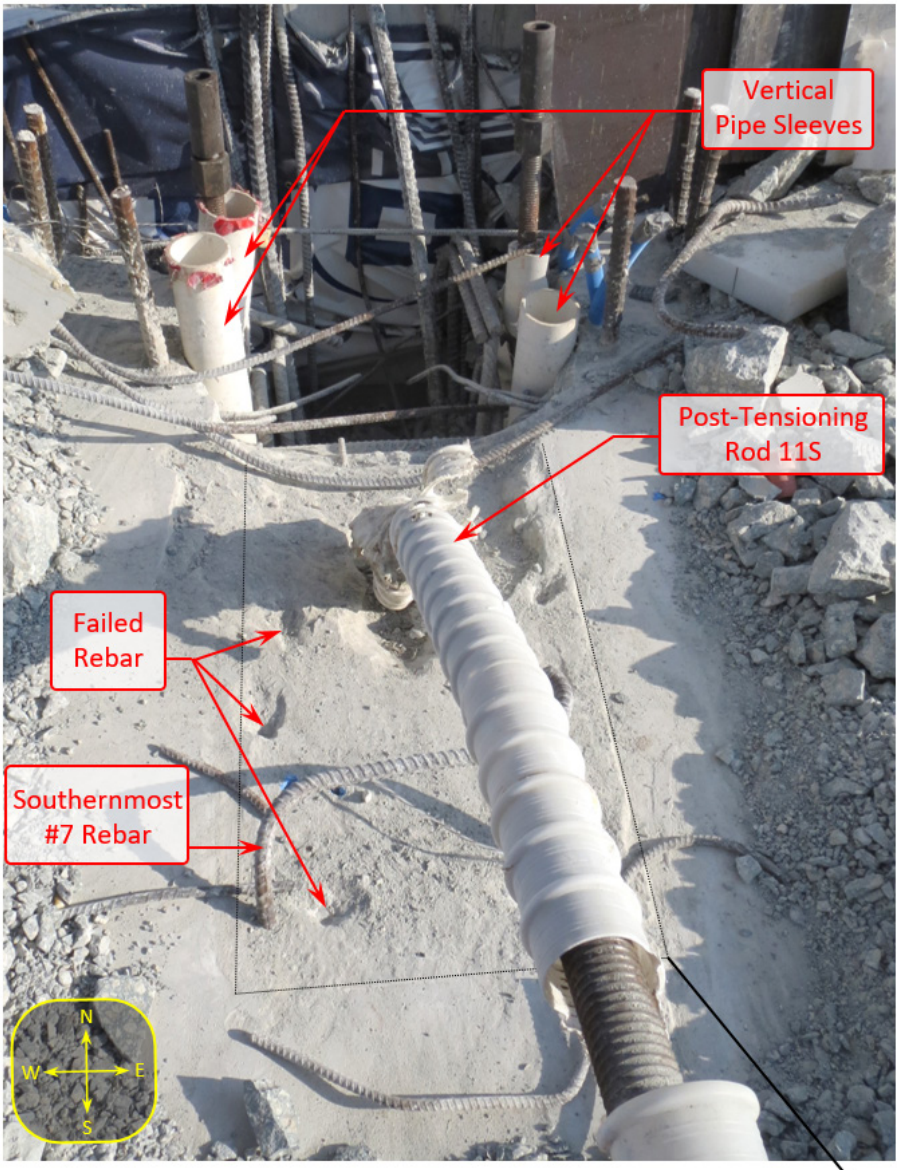

Figure 50. Photograph showing post-rubble removal condition of deck portion of truss member 11 and 12 nodal region looking toward north along bridge centerline. Truss member 11 lower post-tensioning rod is in the foreground.

3.9 BRIDGE COLLAPSE

The bridge collapsed when the demand placed on the truss member 11 and 12 nodal region exceeded the resistance that the structure was able to provide. The base of truss member 12 was being pushed northward by truss member 11, with significant dislocation having occurred prior to collapse. The distressed concrete in the nodal region, with wide concrete cracks and northward rigid body translation of the upper part of the node, leads to the conclusion that the

remaining resistance was largely being provided by the few reinforcing bars that crossed the impending failure planes and the anchorage of the truss member 12 vertical reinforcement into the diaphragm.

The column confinement reinforcement on the south face of truss member 12, #4 bar hoops spaced at 12 inches along the height, served a critical purpose in that they helped maintain the geometric stability of the truss member 12 cross section. These #4 bars, illustrated in Figure 21 and also visible in Figure 51 and Figure 52, ruptured as the #11 vertical reinforcing bars tore out of the south face of truss member 12. The two #11 bars that were anchored below the drain pipe remained anchored into the bottom of the north diaphragm and the three #11 bars from the top portion of the lap splice remained with member 12; however, the upper and lower bars separated at the lap splice location. Thus, working backwards in time, it appears that the #4 reinforcing bar column confinement reinforcement may have been the final force resisting mechanism to be engaged prior to the collapse. As the reinforcing bars crossing the horizontal and vertical shear planes were pushed beyond their limits, the confinement reinforcement in truss member 12 was engaged at the truss member 12 vertical reinforcement lap splice. The confinement reinforcement failed, leading to the unraveling of the connection between member 12 and the deck. Truss members 11 and 12 then translated northward unimpeded as the structural integrity of the bridge was lost.

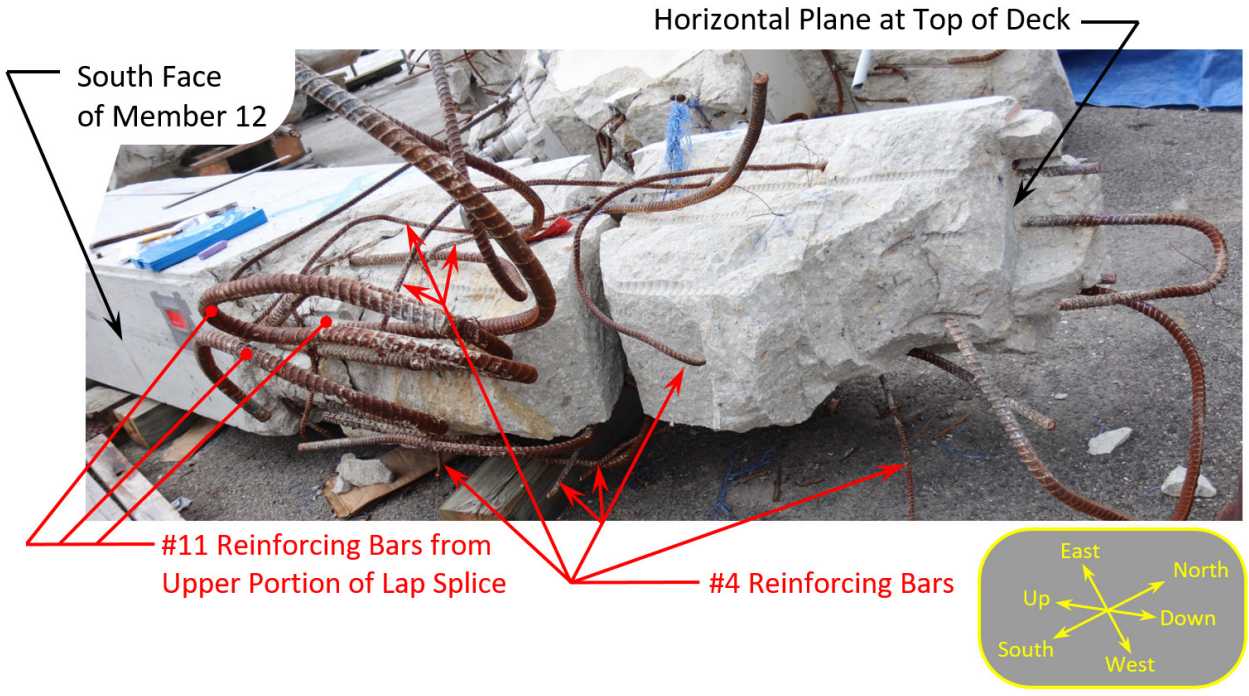

Figure 51. Photograph showing post-collapse condition of the bottom portion of truss member 12. The level of the deck was approximately at the right extent of the member and the east face is on top.

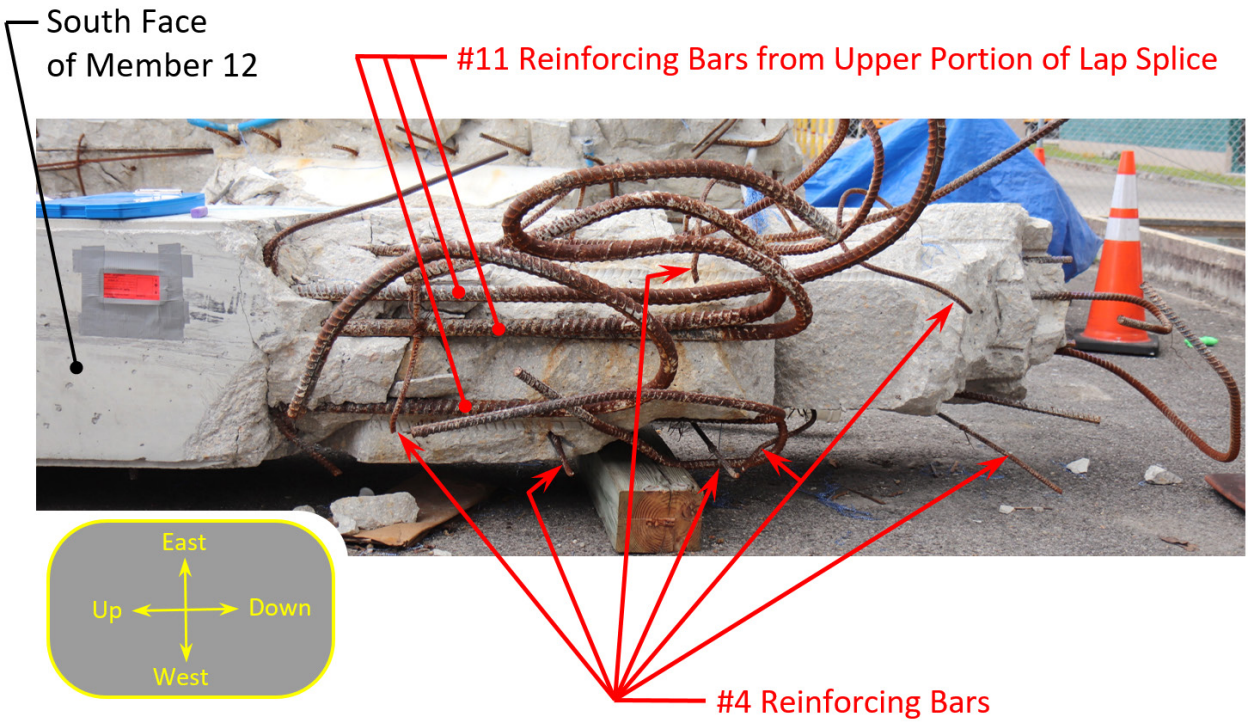

Figure 52. Photograph showing post-collapse condition of the south face of the lower portion of truss member 12. The level of the deck was approximately at the right extent of the member.

4 ASSESSMENT OF COLLECTED PHYSICAL EVIDENCE

Physical evidence was gathered from the structure in the aftermath of the collapse. This evidence provided important insight into the processes that went into the construction of the bridge and the performance of the structure prior to its collapse. This section discusses the assessments of the concrete, the steel reinforcement, the post-tensioning rods, and the hydraulic jack and associated post-tensioning system that was used to retension the bars in member 11. Most of the discussion focuses on the member 11 and 12 nodal region where significant distress was observed prior to the collapse and where the collapse initiated. See Figure 6 for an illustration of the nodal region under discussion.

4.1 CONCRETE COMPETENCY

In any concrete structure, the competency of the concrete is of critical importance to the overall performance of the structure. Concrete competency is a general term that collectively refers to whether the fresh concrete was appropriately consolidated, whether any segregation occurred within the concrete during placement or consolidation, and whether layers of poor quality concrete might have formed, particularly adjacent to formwork. The competency of the concrete in the vicinity of the member 11 and 12 nodal region was assessed through the cutting and sampling of retained portions of the node.

Figure 53 provides a photograph showing the vertical cut that was completed through the retained deck portion of the member 11 and 12 nodal region. The cut is parallel to and approximately 20-inches east of the east face of member 12. The diaphragm at the north end of the bridge is on the right side of the image. Visual examination of this cut face allows for an assessment of the competency of the concrete in this portion of the bridge. The concrete, both here and on the parallel cut approximately 20-inches west of the west face of member 12, was observed to be well consolidated and did not exhibit any segregation. In addition, no honeycombing[l] was identified on either cut face.

Concrete in other nearby portions of the nodal region was also examined. No honeycombing or segregation was observed in the cores extracted from the deck at the east and west extents of the north end of the deck. The concrete in a core extracted from the top deck surface centered under where member 11 met the deck was also judged to be competent. Finally, the fractured surfaces of the lower portions of retained members 11 and 12 were assessed; no competency issues were identified.

[l] Honeycombing is a term that refers to a local volume of poorly consolidated concrete. The voids in a honeycombed volume may or may not connect, and their size ranges from the size of coarse aggregate up to the dimensions of the element cross section. Poor workmanship, overly stiff fresh concrete, and complex formworks can all lead to honeycombing.

Figure 53. Photograph of longitudinal cross section of bridge deck after being cut from retained nodal region deck element. The vertical cut is approximately 20-inches east of the east face of member 12.

4.2 CONCRETE COLD JOINT UNDER MEMBERS 11 AND 12

The construction process for the bridge included multiple concrete placements, with cold joints at specific locations between placements. The cold joint of the most interest occurred at the deck level under members 11 and 12. The concrete for the deck was cast first and was cured. Members 11 and 12 were cast thereafter, with the fresh concrete from the second pour being cast against the hardened concrete from the first pour. The location and properties of this cold joint were extensively studied, and the full details are provided elsewhere in a separate factual report[m]. The cold joint was found to be located on a horizontal plane at the intersection of the deck and members 11 and 12. The hardened surface of the first concrete placement was found to not have an intentionally roughened surface, and a portion of the failure surface under member 11 was found to coincide with this cold joint.

[m] Graybeal and Haber, "NTSB Accident ID: HWY18MH009, Concrete Interface Under Members 11 and 12" Turner-Fairbank Highway Research Center Factual Report, Federal Highway Administration, February 2019.

4.3 STEEL REINFORCEMENT RECONCILIATION

The positioning of the expected steel reinforcement at the expected location within a reinforced concrete structure is a key contributor to the overall performance of the structure. The available evidence, including the FIGG Plans, photographic documentation captured during construction, and post-collapse portions of the structure were examined. The assessment focused on the steel reinforcement and the post-tensioning rods in the member 11 and 12 nodal region.

To assess the reinforcement in the deck near the nodal region, the retained deck component was cut along vertical planes to the east and west of where members 11 and 12 met the deck. The cut faces were compared to the construction plans. Figure 54 provides an illustration showing an example of the process used, here for a longitudinal cut through the cross section of the deck at a location approximately 20-inches east of the east face of member 12. These cut faces were observed to accurately replicate the construction plans for the given location in the bridge.

Reinforcing bars extending from retained pieces of the collapsed bridge into the member 11 and 12 nodal region were also examined. Figure 55 shows a photograph of the member 11 and 12 nodal region that was captured during the installation of the steel reinforcement into the formwork in July 2017. Although some of the reinforcing bars had not yet been installed at the time the photo was captured, the reinforcement shown in the photo is consistent with post-collapse observations of the same reinforcement. Figure 48 through Figure 52 show the reinforcing bars that were accessible for examination after the collapse.

The reinforcement in member 12 was found to closely match the FIGG Plans. The lap lengths of the #11 and #7 reinforcing bars were appropriate. The positions of the #4 confining bars were appropriate.

Two specific deviations from the FIGG Plans were identified through this reinforcement reconciliation process. Both deviations can be observed through comparison of the renderings in Figure 56 and Figure 57. Figure 56 was created based on the FIGG Plans, and Figure 57 is a modified version wherein the identified differences in reinforcement positions have been implemented. Note that all the 3-dimensional renderings in this report are based on the modified model presented in Figure 57 since the reinforcement positions it shows reflect the structure at the time of collapse.

The first deviation from the FIGG Plans pertains to the lower anchorage for post-tensioning rod 11S. Figure 55, Figure 48, and Figure 49 were instrumental in reconciling the as-built location. The reconciliation found that the anchor plate for rod 11S was embedded slightly deeper into the bridge deck than was shown on the FIGG Plans. The line of action of the rod was maintained (i.e., the position of the rod within member 11 and the angle relative to the remainder of the structure was not changed), but the anchor plate and nut were positioned approximately 7 inches farther along the original line of action (i.e., northward and downward) relative to the FIGG Plans.

The second deviation from the FIGG Plans pertains to the interface shear reinforcement crossing from the deck into the base of member 11, shown as the green bars in Figure 14. These

bars were found to be positioned slightly differently than was shown in the FIGG Plans. Based on the post-collapse height of the southernmost bar as shown in Figure 50, and the bar positions that can be observed in the photograph Figure 55, it is determined that these reinforcing bars extended approximately 8 inches above the cold joint at the base of member 11. Also, the interface shear reinforcing bars were distributed slightly differently over the member 11 to deck footprint, with the northernmost #7 bar being moved southward so that it was positioned in the space between rod 11N and 11S. The locations where the bars crossed the failure plane under member 11 were accurately determined based on measurements from the collapsed structure.

These two deviations from the FIGG Plans also necessitate the minor movements of a few other reinforcing bars which would conflict with the new locations of the anchor plate and the interface shear reinforcement. The conflicting bars were moved as little as possible while ensuring that their as-built locations best aligned with the available evidence. These conflicting bars can be identified by comparing the images in Figure 56 and Figure 57.

The two specific deviations described above, namely the member 11-to-deck interface shear reinforcement positions and the rod 11S anchor plate movement, are not considered to be significant deviations from the FIGG Plans and it is not expected that these deviations would have had any noticeable effect on performance. Instead, they are recognized as minor deviations of reinforcement placement associated with the tying of steel reinforcement cages for a reinforced concrete structure. Thus, no significant deviations from the construction plans were identified through this assessment of reinforcing bar sizes and locations. The expectation established on the FIGG Plans, which was consistent with the assumptions made in the FIGG Design, was met by MCM in constructing the nodal region.

Finding:

No significant deviations from the construction plans were identified through the assessment of in-place steel reinforcement sizes and locations.

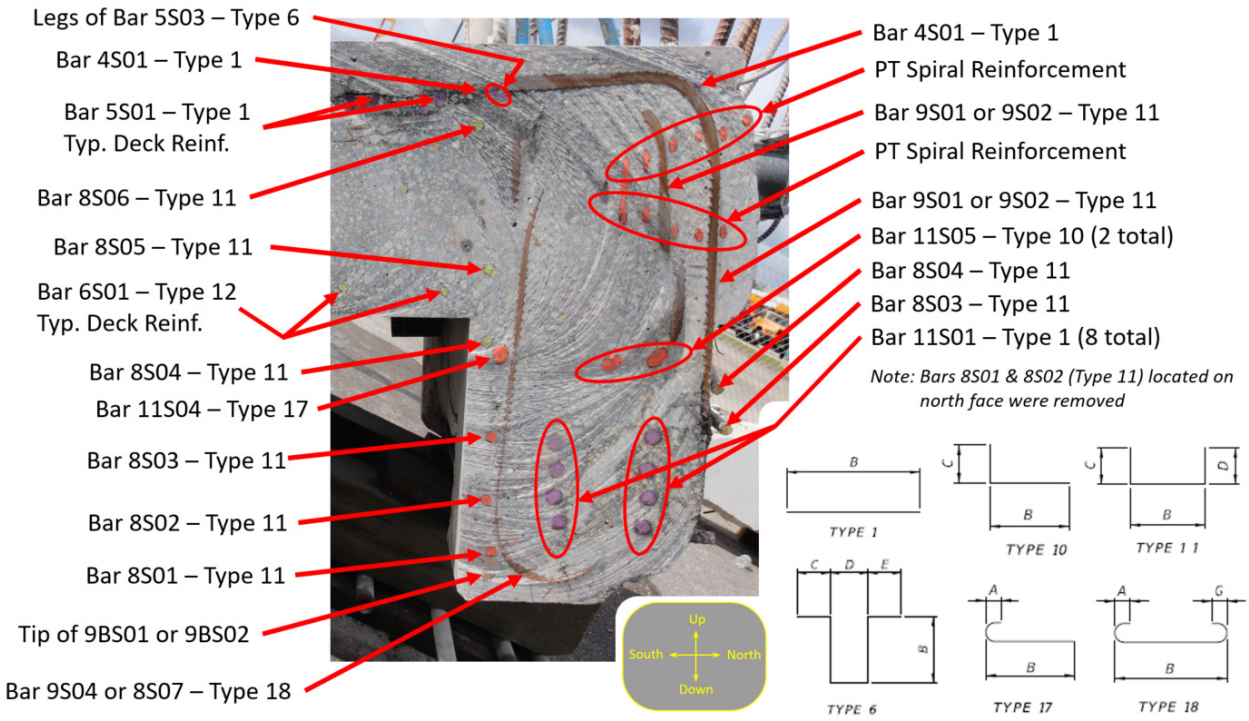

Figure 54. Illustration of reinforcing bar assessment and reconciliation, shown here for a portion of the deck after being cut from the retained nodal region deck element. The vertical cut is approximately 20-inches east of the east face of member 12.

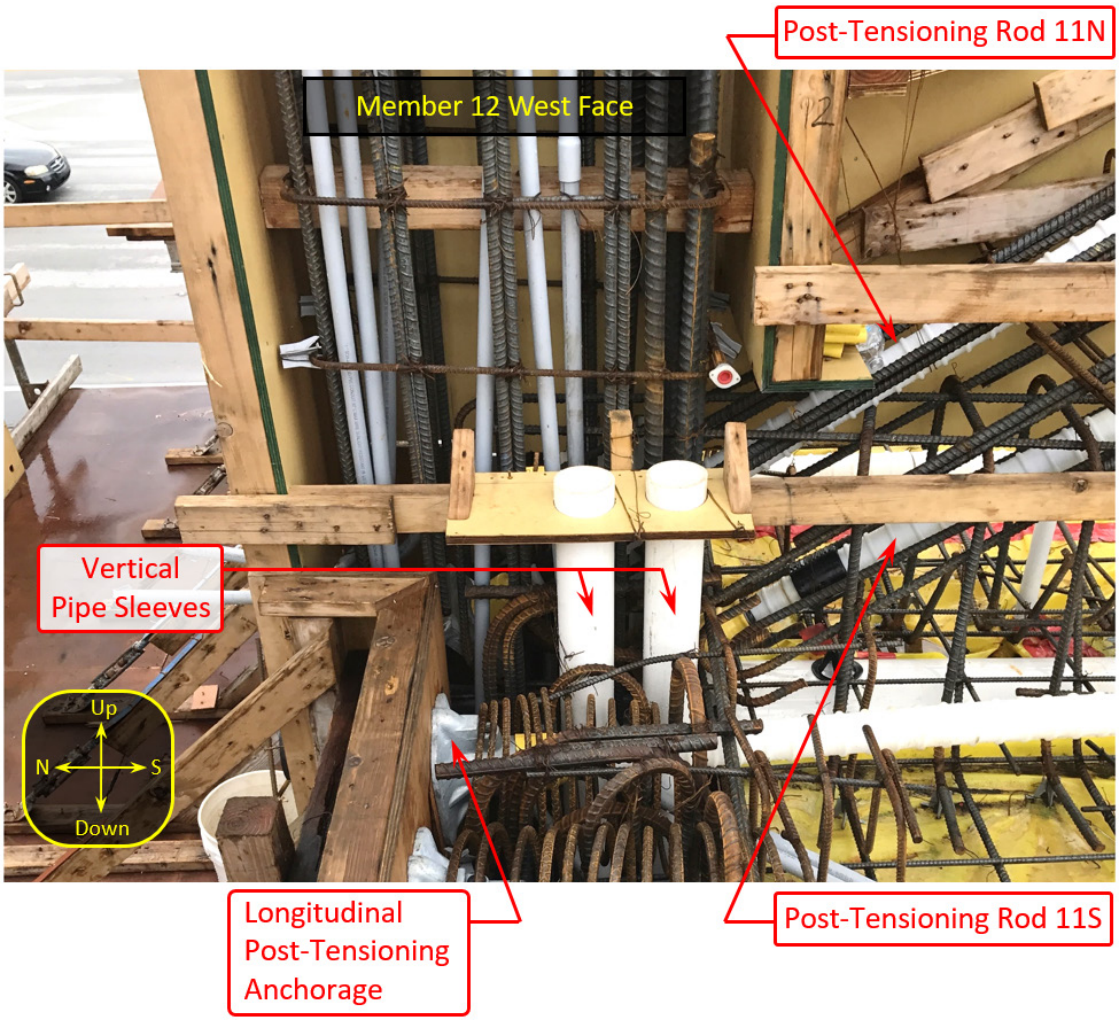

Figure 55. Partially completed installation of conduit and reinforcing bars in the member 11 and 12 nodal region. Corresponds to Bridge Factors Factual Report Photo 8.

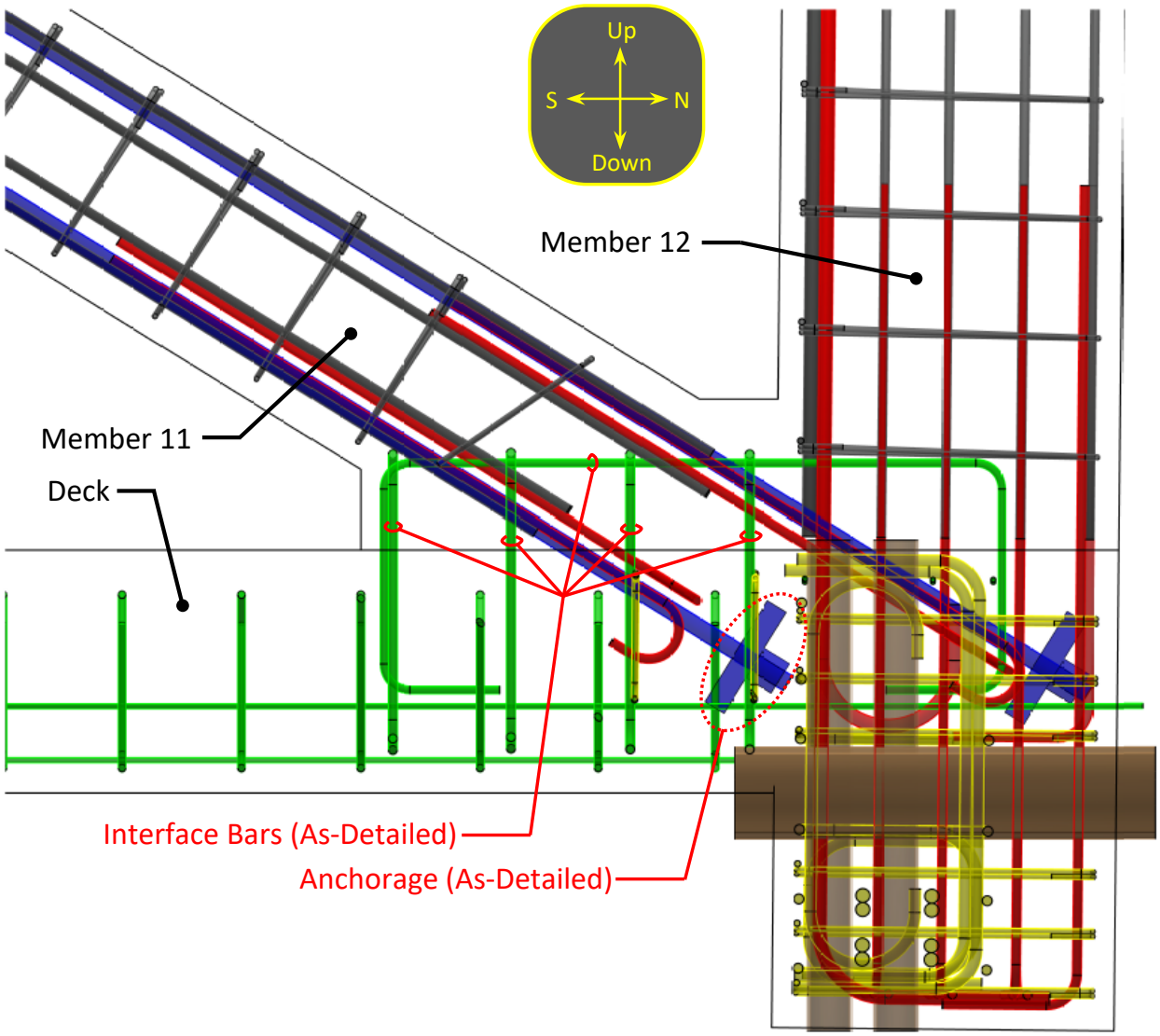

Figure 56. Illustration showing a rendering of the construction plans for the member 11 and 12 nodal region along the truss line of the bridge.

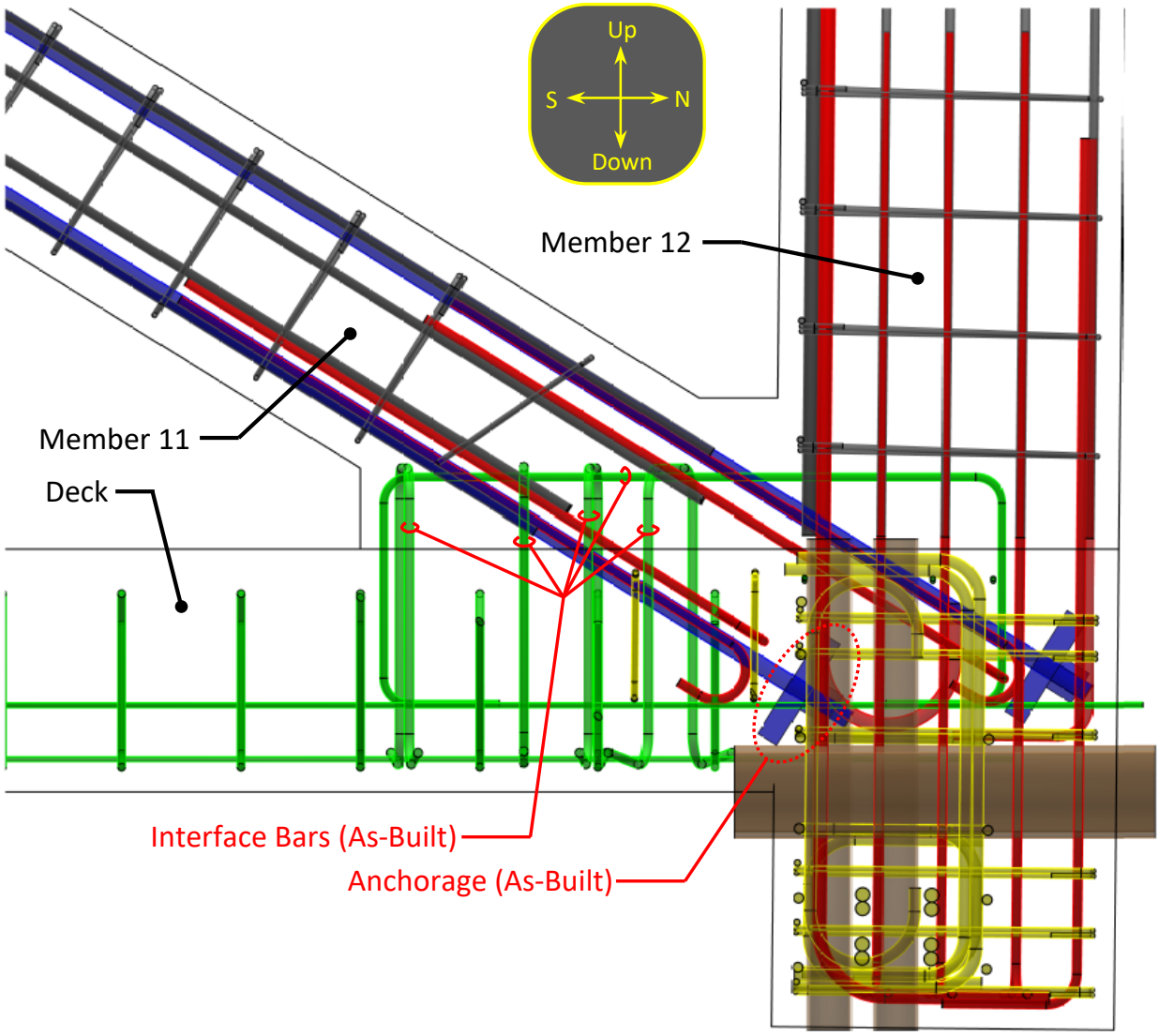

Figure 57. Illustration showing a rendering of the as-built reinforcement geometry the member 11 and 12 nodal region along the truss line of the bridge.

4.4 CONCRETE MATERIAL PROPERTIES

Specific material properties were defined for the concrete used in this bridge construction project. Samples were extracted from the collapsed structure, transported to the FHWA Turner-Fairbank Highway Research Center, then assessed according to standardized test methods. Full documentation of the samples, tests, and results can be found in a separate factual report[n]. The compressive strength and the air content of the concrete met project requirements. The density, tensile strength, modulus of elasticity, and Poisson's ratio were also measured and reported.

Finding:
The concrete material properties relied upon in the FIGG Design were supplied in the construction of the bridge.

4.5 STEEL REINFORCEMENT MECHANICAL PROPERTIES

The construction project specifications defined specific mechanical properties for the steel reinforcement used in this bridge construction project. Steel samples were extracted from the collapsed structure, transported to the FHWA Turner-Fairbank Highway Research Center, then assessed according to standardized test methods. Full documentation of the samples, tests, and results can be found in a separate factual report.[n] The yield strength, tensile strength, and tensile elongation at fracture were measured for sample #5, #8, and #11 reinforcing bars. In all cases, the performance of the samples met or exceeded the required behaviors.

Finding:
The reinforcing steel material properties relied upon in the FIGG Design were supplied in the construction of the bridge.

4.6 STEEL POST-TENSIONING ROD MECHANICAL PROPERTIES

Specific mechanical properties were defined for the post-tensioning rods used in this bridge construction project. A sample was extracted from the collapsed structure, and a second sample was retained from the onsite stockpile of as-yet-unused post-tensioning rods. These rods were transported to the FHWA Turner-Fairbank Highway Research Center then assessed according to standardized test methods. Full documentation of the samples, tests, and results

[n] Ocel, Graybeal and Haber, "NTSB Accident ID: HWY18MH009, Steel and Concrete Materials Testing" Turner-Fairbank Highway Research Center Factual Report, Federal Highway Administration, October 2018.

can be found in a separate factual report.[h] The tensile strength and the elongation at fracture were observed to exceed the minimum specified values.

Finding:
The steel post-tensioning rod mechanical properties relied upon in the FIGG Design were supplied in the construction of the bridge.

4.7 HYDRAULIC JACK PERFORMANCE ASSESSMENT

The construction process for the bridge required the use of hydraulic jacks to apply tensioning forces to rods embedded within the structure. At the time of the bridge collapse, a construction action to post-tension the rods in member 11 had just been completed. The hydraulic jack that was in use was retained as evidence and transported to the FHWA Turner-Fairbank Highway Research Center for performance assessment. Full documentation of the assessment can be found in a separate factual report[o]. The jack and associated equipment were found to operate correctly, including the ability to apply the full range of loads and to do so in accordance with the specified calibration.

Finding:
The hydraulic jack that was used to post-tension the rods in member 11 was performing appropriately at the time of the collapse.

[o] Ocel, Graybeal and Haber, "NTSB Accident ID: HWY18MH009, Post-Tensioning System Performance Testing" Turner-Fairbank Highway Research Center Factual Report, Federal Highway Administration, August 2018.

5 CRACKING PROGRESSION AND DISLOCATION OF THE NODE

Over the three weeks leading up to the collapse of the FIU Pedestrian Bridge, the structure displayed notable cracking of the reinforced concrete. Both the severity and extent of the cracking progressed, with distress at some locations worsening and distress at other new locations becoming apparent. The distress was observed and documented by parties associated with the design, construction, and operation of the bridge. Much of the distress apparent in the structure has been presented within the Chapter 3 discussion of the bridge's response as it progressed to collapse. This chapter focuses specifically on four locations within the bridge that were repeatedly captured in photographs documenting the advancing and worsening distress.

A set of images focused on the east side of member 11 at the deck is presented in Figure 58. The first image, from February 24 and presented previously in Figure 10, shows an approximately 0.04-inch (1-mm) wide crack[p] at the chamfer of member 11. The second image, from March 10 and presented previously in Figure 24, shows that the first crack had grown to approximately 0.5-inch (13 mm) in width and that other cracks had now become visible. The final two images show the cracking on March 14 and 15 as presented previously in Figure 37 and Figure 45, respectively. The initial crack at the chamfer of member 11 was now approximately 0.75-inch (19-mm) wide. Concrete had also begun to spall in this heavily distressed region. Recall also, as was describe in association with Figure 36, a crack had formed along the interface between member 11 and the deck and that the member was translating northward relative to the deck.

A set of images focused on the west side of member 11 at the deck is presented in Figure 59. The first image, from February 26 and presented previously in Figure 12, shows an approximately 0.04-inch (1-mm) wide crack and an approximately 0.08-inch (0.5-mm) wide crack at the chamfer of member 11. The second image, from March 10 and presented previously in Figure 22, shows that the original two cracks had widened to approximate widths of 0.375-inch (10-mm) and 0.12-inch (3-mm), and that additional cracks had also become visible. The final two images show the cracking on March 13 and 15 as presented previously in Figure 34 and Figure 46, respectively. The initial cracks at the chamfer of member 11 had collectively grown to approximately 0.75-inch (19-mm) wide and spalling had begun to occur. Large cracks are also visible farther north on the member, along with some spalling.

A set of images focused on the north end of the deck on the east side of member 12 is presented in Figure 60. The first image, from March 10 after the SPMT move and previously presented in Figure 18, shows an approximately 0.04-inch (1-mm) wide crack extending from the vertical pipe sleeves toward the north end of the deck. The next two images show the more extensive cracking that was visible later on March 10 and then through March 14 as

[p] Crack dimensions were not transmitted to the investigators by those capturing the photographs. The crack dimensions stated in this chapter are based on scaling from nearby objects with known dimension (e.g., thickness of dimensional lumber).

presented previously in Figure 25 and Figure 39. By March 14, these cracks collectively were upwards of 0.5-inch (13-mm) wide.

A set of images focused on the north end of the deck on the west side of member 12 is presented in Figure 61. The first image, from March 8 prior to the SPMT move and previously presented in Figure 13, shows an approximately 0.04-inch (1-mm) wide crack extending from the vertical pipe sleeves toward the north end of the deck. The next two images show the more extensive cracking that was visible on March 10 and then through March 14 as presented previously in Figure 27 and Figure 40. By March 14, the identified crack was upwards of 0.5-inch (13-mm) wide.

These crack progression illustrations demonstrate that the distress in the structure continued to grow during the weeks and days leading up to the collapse. In particular, the cracking became markedly worse immediately after the detensioning of member 11 on March 10, 2018. Cracking and spalling continued to worsen over the following four days, with the upper part of the node further dislocating to the north, until the structure collapsed.

The extensive, large cracks observed in the member 11 and 12 nodal region during the days prior to collapse are abnormal for a reinforced concrete structure. Cracks in concrete occur for a variety of reasons (e.g., restrained shrinkage, thermal effects, structural loading, etc.). Crack widths range from sizes smaller than can be detected by unaided human vision (approximately 0.01 inch or 0.25 mm wide) up to large widths that indicate gross separation of the two opposing portions of the structure. For reference, in a reinforced concrete element cracks up to approximately 0.016 inch (0.4 mm) are often considered generally acceptable with formal acceptance needing to consider the purpose of the structure and the location of the cracks.[q] The structural cracks in this bridge, located in critical regions of a non-redundant single plane truss, were more than forty times larger.

This scale of cracking in this structure was a clear indication that the intended load resisting mechanisms were failing and that inelastic redistribution of loads to unanticipated load paths was occurring. As those unanticipated load paths were pushed beyond their limits, the structure exhibited ever more distress until failure occurred.

Finding:
The distress continued to grow over time.

[q] AASHTO LRFD Bridge Design Specification (2016) speaks about 0.017-inch wide cracks for environmental exposure conditions where cracks can be tolerated due to reduced concerns with appearance and/or corrosion. American Concrete Institute Committee 224 report on Control of Cracking in Concrete Structures (2008) speaks about 0.016-inch wide cracks being reasonable in certain favorable environmental conditions.

Finding:

The structure behaved with sufficient ductility to provide warning before failure through development of significant and visible distress.

Finding:

Detensioning of post-tensioning rods located within truss member 11 significantly increased damage to the member 11 and 12 nodal region.

Finding:

The structural cracking and northward dislocation of the upper part of the member 11 and 12 nodal region as documented in the days leading up to the collapse is strong evidence that the structure was progressing toward failure.

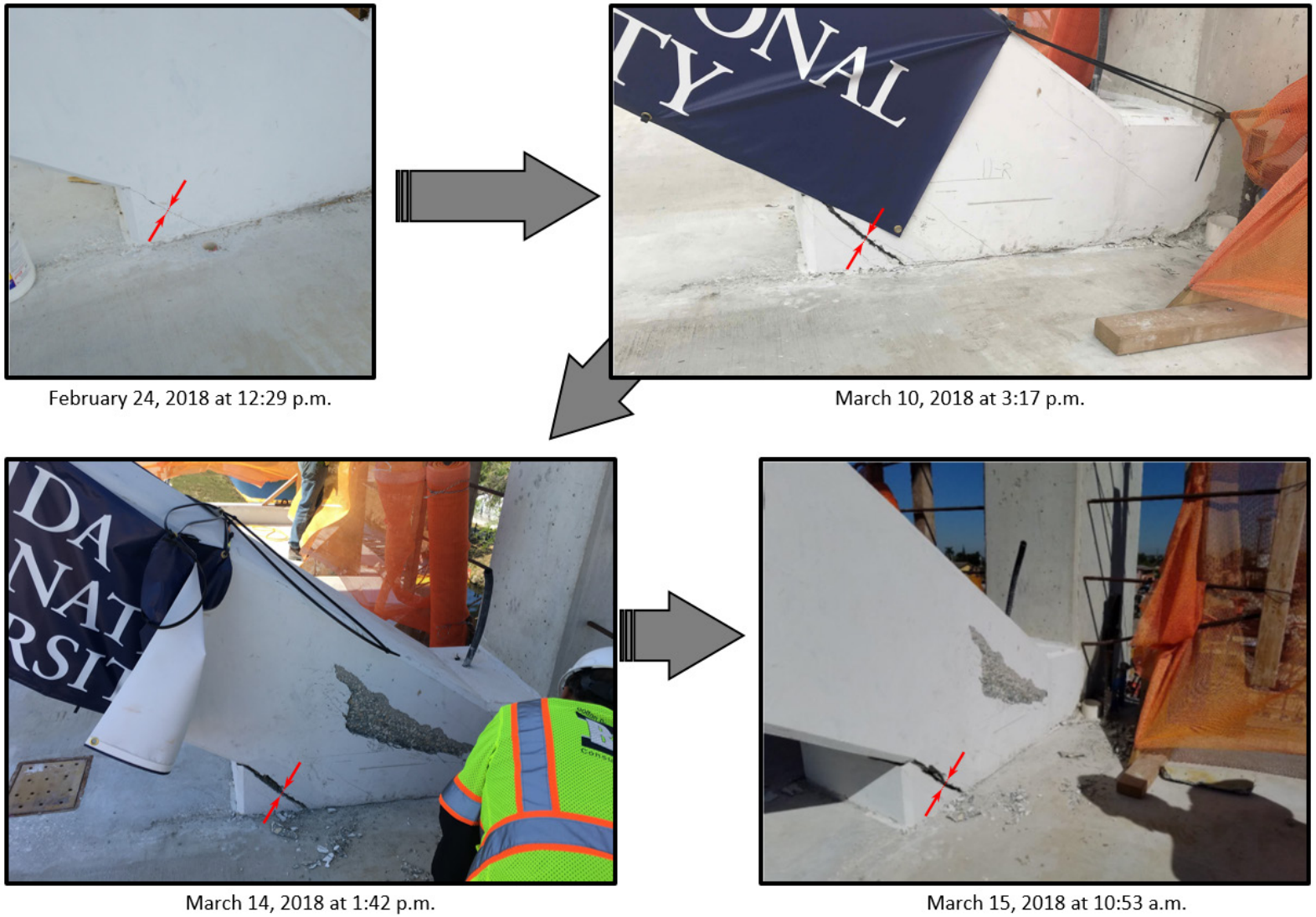

Figure 58. Photographs showing the progression of cracking on the east side of member 11 at the deck.

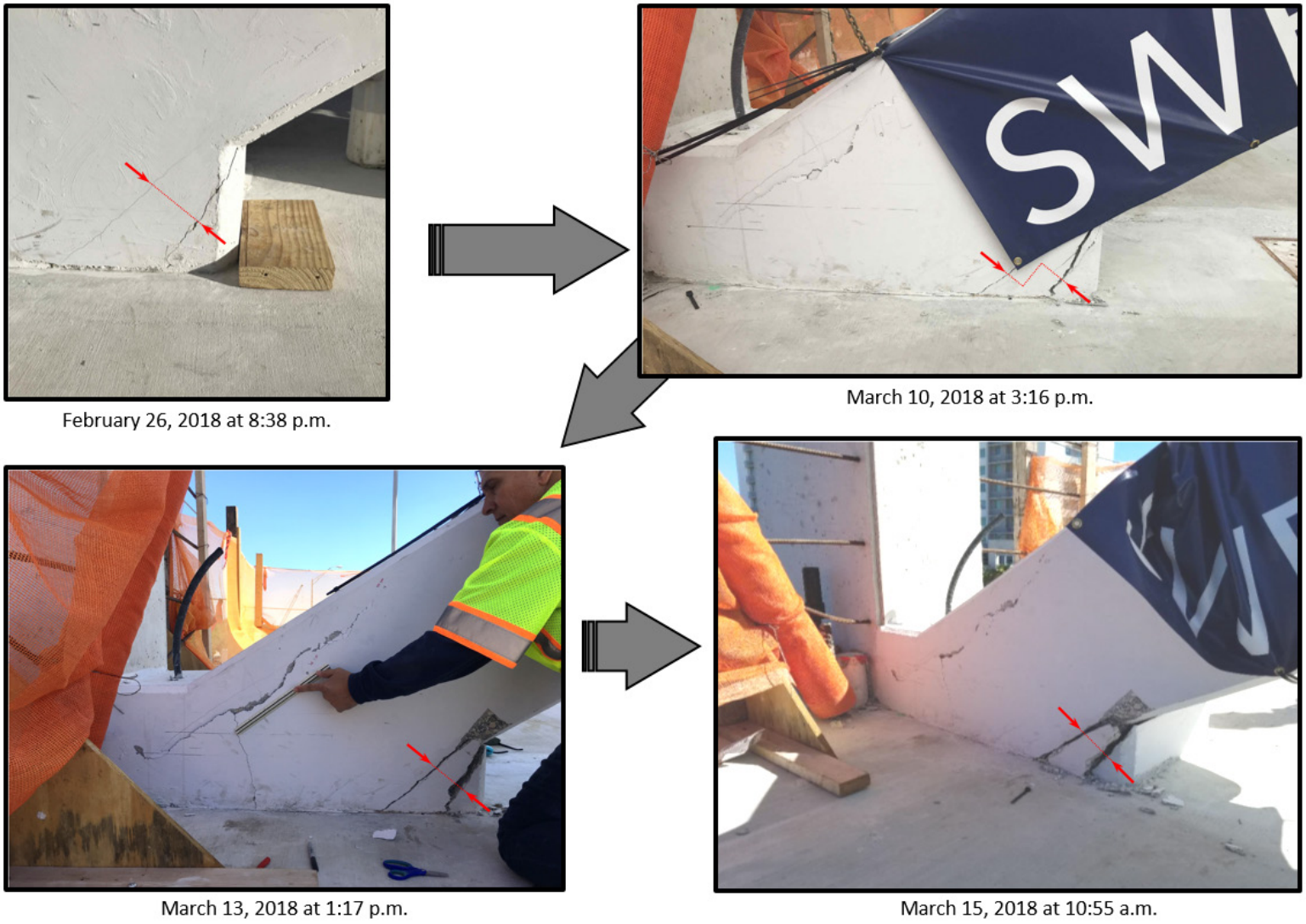

Figure 59. Photographs showing the progression of cracking on the west side of member 11 at the deck.

March 10, 2018 after SPMT Move

March 10, 2018 at 3:17 p.m.

March 14, 2018 at 1:50 p.m.

Figure 60. Photographs showing the progression of cracking on the north end of the deck on the east side of member 12.

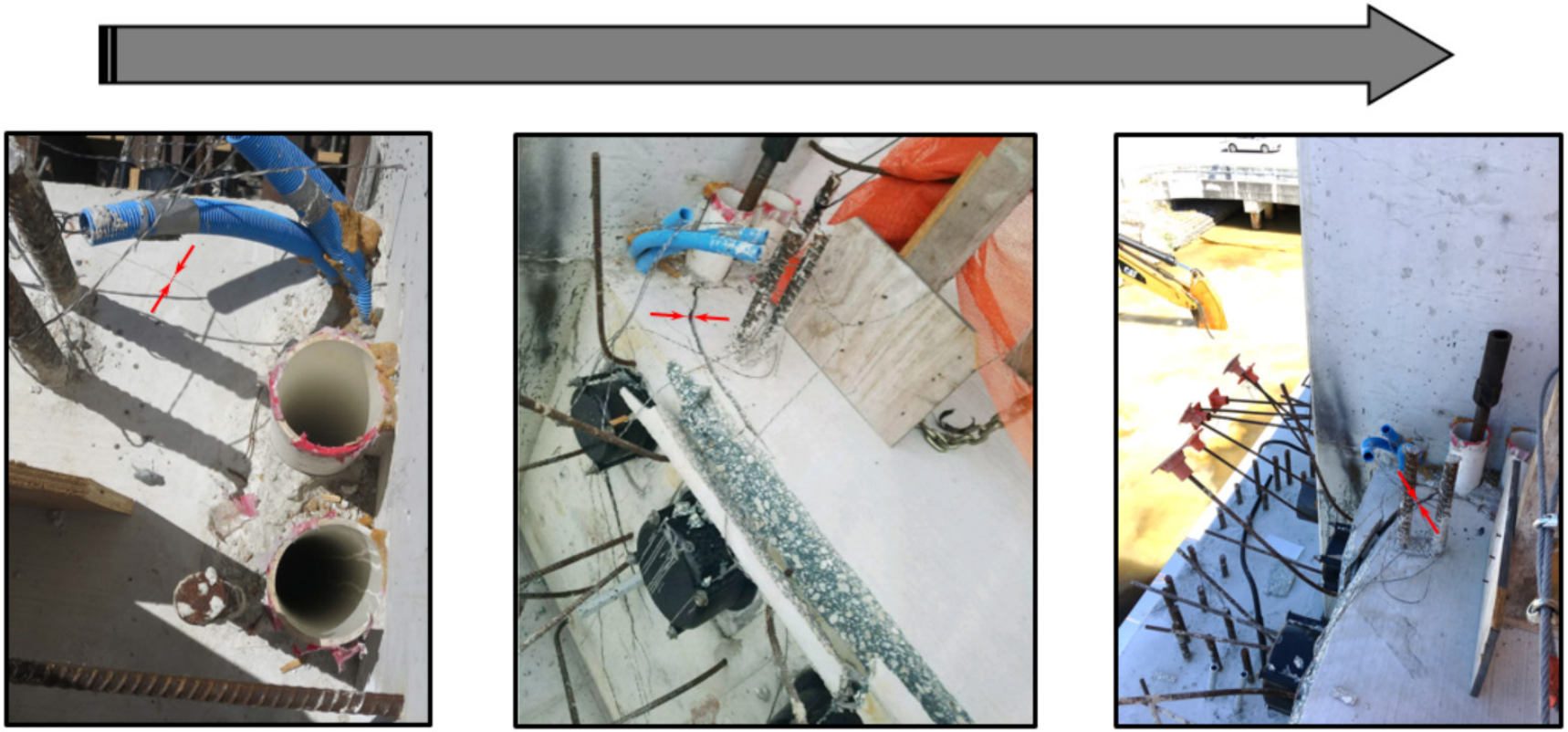

Figure 61. Photographs showing the progression of cracking on the north end of the deck on the west side of member 12.

6 REVIEW OF SUPERSTRUCTURE FINAL DESIGN CALCULATIONS AND RELEASED FOR CONSTRUCTION PLANS

The superstructure final design calculations, referred to herein as the FIGG Design, were signed and checked by Licensed Professional Engineers employed by FIGG Bridge Engineers. The Released for Construction Plans, herein referred to as the FIGG Plans, were sealed and signed by a Professional Engineer with FIGG Bridge Engineers. The FIGG Design was the basis for the FIGG Plans. The FIGG Plans were used by Munilla Construction Management (MCM) to build the bridge. The FIGG Plans were produced to provide MCM the detailed information on the needed materials, components, and procedures to construct the bridge. The project design requirements mandated the use of multiple established bridge design and construction specifications. This section of the report discusses the assessment of the designs and analyses that were performed in the FIGG Design and whether these designs and analyses met the mandated requirements or were adequate for this project. These assessments are referred to herein as the FHWA Check.

6.1 FIGG DESIGN DOCUMENTATION

The FIGG Design included calculations for the three distinct construction stages of the main-span transport, main-span simply-supported over 8th Street and the fully completed two-span structure. The level of detail included in the FIGG Design varied for each construction stage with the fully completed two-span structure having the most thorough documentation. As stated previously, the main-span collapsed while it was simply supported. The level of detail for the calculations of the bridge during this simple-span construction stage was not sufficient for the FHWA Check to thoroughly assess the FIGG Design. More specifically, the calculations for this construction stage provided limited information on the bridge analysis that generated the forces (demands) on the bridge members. This lack of information resulted in the FHWA Check being unable to definitively identify sources of calculated demand errors.

Finding:
The FIGG Design did not provide sufficient documentation of design approach, analysis methodology, and key assumptions for all the critical construction stages.

6.2 BRIDGE DESIGN REQUIREMENTS

The primary specification mandated for the design of the bridge structure was the American Association of State Highway and Transportation Officials Load and Resistance Factor Design Bridge Design Specifications, Seventh Edition with 2015 Interims. In this report, these specifications are referred to as “AASHTO LRFD”.

The FHWA Check focuses on the analysis and design of the nodal regions of the FIU pedestrian bridge. The nodal regions are located at any part of the bridge in which truss members are

connected to either the bridge canopy or deck. Informed by the physical evidence presented in earlier sections, this section will focus on the design of the nodal regions where truss members 2 and 11 meet the deck.

The AASHTO LRFD groups multiple types of individual loadings into load combinations or limit states. Individual loads included in these load combinations are then factored (either increased or decreased) to produce the most demanding singular total factored force effect for the element being designed. These load combinations and factors are prescribed in the AASHTO LRFD and are referred as limit states. The FIGG Design for interface shear appropriately used the AASHTO LRFD "Strength I" limit state to generate the applied force effects (demand) on the truss member nodal regions. The FIGG Design used the following AASHTO LRFD Strength I loadings and load factors:

- Dead load of structural components and nonstructural attachments (DC) = 1.25
- Pedestrian live load (PL) = 1.75
- Primary post-tensioning force (PT) = 1.0
- Force effect due to uniform temperature (TU) = 0.5

AASHTO LRFD Article 1.3.2.1 addresses bridge redundancy by applying a redundancy factor to the computed force effects for all limit states. The redundancy factor, η_R, varies between 1.05 for non-redundant members and 0.95 for bridges with an exceptional amount of redundancy. Structures with conventional levels of redundancy have η_R equal to 1.0. Therefore, the redundancy factor can either increase or decrease the demand on a bridge structure due to the structure's redundancy characteristics. The forces computed in the FIGG Design calculations use a redundancy factor equal to 1.0 (conventional levels of redundancy). A η_R equal to or greater than 1.05 would be appropriate and strongly recommended by the FHWA for the FIU pedestrian bridge structure due to the singular load path provided by the single-line truss. This increased redundancy factor was not used in the FHWA Check in order to provide a clear comparison to the FIGG Design.

Finding:
FIGG Design used a redundancy factor of 1.0, consistent with that commonly used for structures with redundant load paths, even though this single-line truss structure only provided a singular load path.

When a concrete element is cast onto an existing concrete element, the surface (interface) between the elements is referred to as a cold joint. The transfer of forces across a cold joint can be achieved through the mechanics of interface shear. Interface shear is generated through multiple resistance mechanisms. For the case of a cold joint, resistance is provided by the roughness (i.e., friction) and associated cohesion (i.e., chemical bond) across the contact area of the two concrete elements (i.e., interface surface), and by the magnitude of the force compressing (i.e., clamping) the two surfaces together. This compressive force is related to

both the amount of reinforcing steel crossing the interface surface and the amount of permanent loading whose line of action is perpendicular to the interface. Occasionally supplemental compressive forces supplied through other means (e.g. post-tensioning forces) might be included.

The main span superstructure of the FIU pedestrian bridge was built off-site in three concrete casting phases. First, the entire deck/walkway was cast and allowed to harden. Second, truss members 1 through 12 were cast atop the deck and allowed to harden. Third, the canopy concrete was cast atop the truss members. This phased concrete placement process resulted in cold joints at each end of every truss member; one located at the bottom of the truss members (i.e., deck to truss member interface) and the other at the top of the truss member (i.e., truss member to canopy interface). Both interface surfaces of each truss member were designed to transfer forces through interface shear.

The AASHTO LRFD design provisions in Article 5.8.4 titled *Interface Shear Transfer – Shear Friction* were used for the FIGG Design of the connection of the truss members to the bridge deck and bridge canopy. The governing equation in Article 5.8.4 to determine connection capacity, referred to as nominal capacity, is AASHTO LRFD Equation 5.8.4.1-3 shown below.

$$V_{ni} = cA_{cv} + \mu\left(A_{vf}f_y + P_c\right) \qquad \text{(LRFD 5.8.4.1-3)}$$

with: V_{ni} = nominal interface shear resistance (kip)
c = cohesion factor specified in Article 5.8.4.3 (ksi)
A_{cv} = area of concrete considered to be engaged in interface shear transfer (in^2)
μ = friction factor specified in Article 5.8.4.3 (dimensionless)
A_{vf} = area of interface shear reinforcement crossing the shear plane within the area A_{cv} (in^2)
f_y = yield stress of reinforcement but design value not to exceed 60 (ksi)
P_c = permanent net compressive force normal to the shear plane; if force is tensile, P_c = 0.0 (kip)

The permanent net compression, P_c, generates interface shear capacity. The AASHTO LRFD in Article 3.4.1 states:

> "*Where the permanent load increases the stability or load-carrying capacity of a component or bridge, the minimum value of the load factor for that permanent load shall also be investigated…both extreme combinations may need to be investigated by applying either the high or the low load factor as appropriate*"

AASHTO LRFD defines the load factor on DC (dead load of structural components and non-structural attachments) can be taken as either 1.25 (to generate a maximum) or 0.90 (to generate a minimum). FIGG Design used a load factor on DC of 1.25 in their P_c calculation.

Based on the above AASHTO LRFD provisions, FHWA concludes that since P_c increases the load-carrying capacity, the minimum extreme combination should have been investigated.

Investigating only the maximum extreme combination and neglecting the minimum extreme combination will result in an overestimation of P_c and thus an overestimation of the interface shear capacity. Even though the AASHTO LRFD provision in Article 3.4.1 is not explicitly required when calculating interface shear capacity, it would be appropriate and strongly recommended by the FHWA to use the 0.90 factor on dead load when determining P_c so as to obtain a minimized interface shear capacity value for the purposes of design.

Note that the FHWA Check, fully described later in this document, used a load factor on DC of 1.0 when determining P_c. Using his value, instead of 0.9, obviates the concern that the FHWA Check was overly strict when interpreting the AASHTO provisions related to P_c.

Finding:
FIGG Design did not use the lower bound load factor for determination of the governing permanent net compression, P_c, in the interface shear designs, resulting in an overestimation of capacity.

The AASHTO LRFD sets upper limits on the capacity that is generated from Equation 5.8.4.1-3. The nominal interface shear resistance, V_{ni}, calculated using equation 5.8.4.1-3 cannot exceed values determined from AASHTO LRFD Equations 5.8.4.1-4 and 5.8.4.1-5 shown below. The least of these three nominal capacity determinations is the controlling nominal interface shear resistance.

$$V_{ni} \leq K_1 f'_c A_{cv} \qquad \text{(LRFD 5.8.4.1-4)}$$

$$V_{ni} \leq K_2 A_{cv} \qquad \text{(LRFD 5.8.4.1-5)}$$

in which:

$$A_{cv} = b_{vi} L_{vi} \qquad \text{(LRFD 5.8.4.1-6)}$$

with: f_c' = specified 28-day compressive strength of the weaker concrete on either side of the interface (ksi)
K_1 = fraction of concrete strength available to resist interface shear, as specified in article 5.8.4.3
K_2 = limiting interface shear resistance specified in Article 5.8.4.3 (ksi)
b_{vi} = interface width considered to be engaged in shear transfer (in.)
L_{vi} = interface length considered to be engaged in shear transfer (in.)

The AASHTO LRFD provisions require the nominal resistance calculated from the equations above be further reduced by multiplying them by a resistance factor, φ, which is always equal to or less than 1.0. For the types of construction materials used in the FIU pedestrian bridge, the AASHTO LRFD requires φ equal to 0.90 for interface shear. This reduced capacity value is called the "factored interface shear resistance" and designated as V_{ri}. AASHTO LRFD Article 5.8.4.1-2,

replicated below, requires this factored interface shear resistance (capacity) to be greater than the total factored force effect (demand) generated from the governing AASHTO LRFD limit state (Strength I for this design). This total factored load force effect is designated as V_{ui}.

$$V_{ri} = \varphi V_{ni} \geq V_{ui} \qquad \text{(LRFD 5.8.4.1-2)}$$

with: V_{ni} = nominal interface shear resistance (kip)
V_{ui} = factored interface shear force due to total load based on applicable strength load combination (kip)
φ = resistance factor. For normal weight concrete value is 0.90.

6.2.1 BRIDGE MODELING AND ANALYSIS USED IN FIGG DESIGN

As previously described, the FIU pedestrian bridge was constructed in multiple stages. Each of these construction stages generated unique forces on the bridge structure. The structure needed to be designed to withstand the forces generated from each of these stages.

The FIGG Design utilized four analytical models for the design of the FIU pedestrian bridge. These analytical models were used to evaluate three critical construction stages. These stages were: 1) main span transport during Stage 2, 2) main span in simply-supported condition occurring at the conclusion of Stage 2, and 3) the completed bridge occurring at the conclusion of Stage 4.

The following are descriptions of each model used in the FIGG Design:

- Main Span Erection Model – A two-dimensional model of the main span during its transport, described within Stage 2 in Section 2.2 above.
- Simple Support Model – A three-dimensional solids model of the main span when it was simply supported between the End Bent 1 and Pier 2, described within Stage 2 in Section 2.2 above.
- Longitudinal Model – A two-dimensional model of the fully completed, two-span, continuous structure, described within Stage 4 in Section 2.2 above. Every significant structural bridge component was included in this model.
- Fixed Pylon Model – A three-dimensional solids model of the main span that was adjusted to replicate the main span performance in its completed condition (i.e., at the conclusion of Stage 4 in Section 2.2 above). This was done by modeling the main span as a propped cantilever that was simply supported at End Bent 1 and fixed to eliminate all rotations at Pier 2.

It should be noted that two of the models, the Longitudinal Model and Fixed Pylon Model, were used to generate the forces used for the FIGG Design of the completed two-span bridge. However, the structural components included in these two models were different. The

Longitudinal Model was used to generate forces for every component in the bridge superstructure while the Fixed Pylon Model was used to generate forces only for components located in the main span.

Each analytical model generated multiple force effects for every structural component included. For the design of the truss member connections, the truss member axial forces were extracted from these analyses and used in the design of each truss member connection. The axial force in the truss member was subsequently resolved into vertical and horizontal components. This resolution of forces is illustrated in figure 62 for the 11-12 nodal region, where the large arrow represents the axial force in Member 11 from the analytical model, and the two smaller arrows represent this axial force resolved into two orthogonal components acting on the interface shear surface. The vertical component is the compressive or clamping force that contributes to interface shear resistance. The horizontal component is the shearing force on the interface shear surface or the interface shear demand. Axial forces in the truss members due to dead load (self-weight) of the structural components and non-structural attachments (DC), pedestrian live loading (PL), forces induced in the structure from post-tensioning (PT), and forces induced in the structure due to temperature (TU) were extracted from the analytical models and used in the FIGG Design of the force transfer across the shear interface surface in the nodal regions.

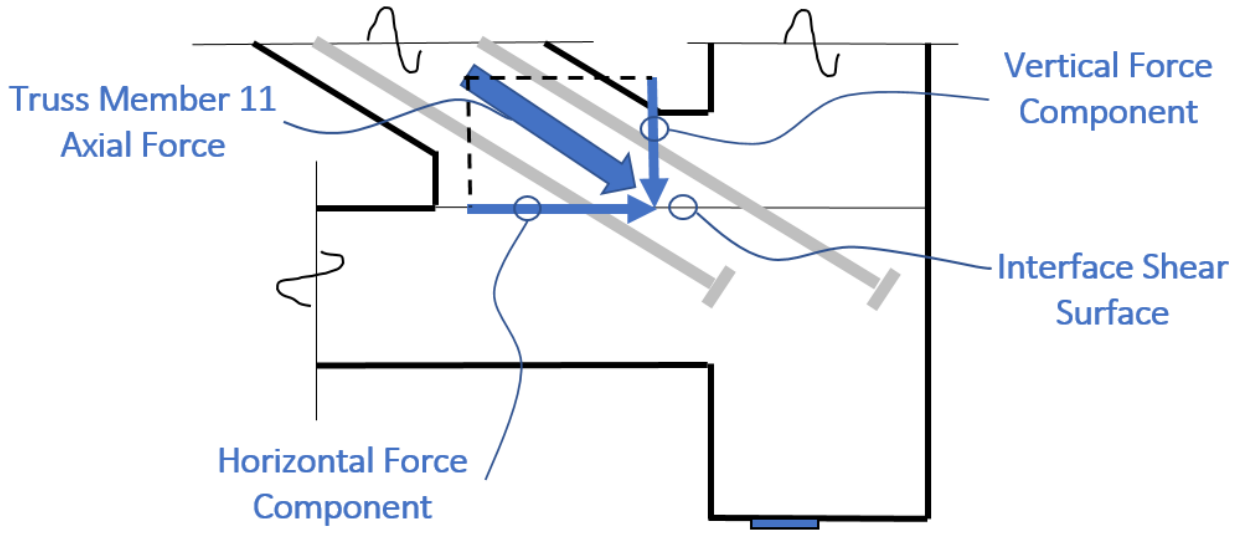

Figure 62. Force from truss member 11 on the nodal region shear interface surface.

Figure 63 shows the interface (horizontal) shear demand results for each main span truss nodal region generated from the four models used in the FIGG Design. With regard to the results from the Simple Support Model and Fixed Pylon Model, the FIGG Design only included the forces identified by the designer as most critical between these two models. Therefore, the results shown in figure 63 only reflect the identified maximums between these two analytical models. The Simple Support Model generated the governing interface shear force effects for every nodal region except for nodal regions 7-8 and 11-12. The governing interface shear force effects for nodal regions 7-8 and 11-12 were generated from the Fixed Pylon Model. The FIGG

Design did not include the results from the Main Span Erection Model or the Longitudinal Model when they were comparing interface shear demands in order to determine the maximum force effects. The interface shear forces shown in figure 63 are generated from the load combination and load factors prescribed in the AASHTO LRFD Strength I limit state. This limit state was used for the interface shear design of all truss cold joints in the nodal regions. The two numbers shown on the horizontal axis of the figure 63 chart identify each nodal region by the two truss member identification numbers (refer to figure 4) that connect into that region.

As discussed earlier, truss members 2 and 11 were tensioned for the main span transport (during Stage 2) and for a short duration after the main was placed on End Bent 1 and Pier 2 (end of Stage 2). The results shown below for nodal regions 1-2 and 11-12 include the effects of the temporary post-tensioning in truss members 2 and 11 for the Main Span Erection Model and did not include these effects in the Longitudinal Model. The inclusion of temporary post-tensioning in truss members 2 and 11 for the Simple Support and Fixed Pylon Models could not be verified. Analysis results from the Simple Support and Fixed Pylon Models for nodal regions 4-5, 6-7 and 8-9 were not included in the FIGG Design and therefore could not be included in figure 63. The magnitude without direction (i.e., absolute value) of the interface shear demand is shown in figure 63.

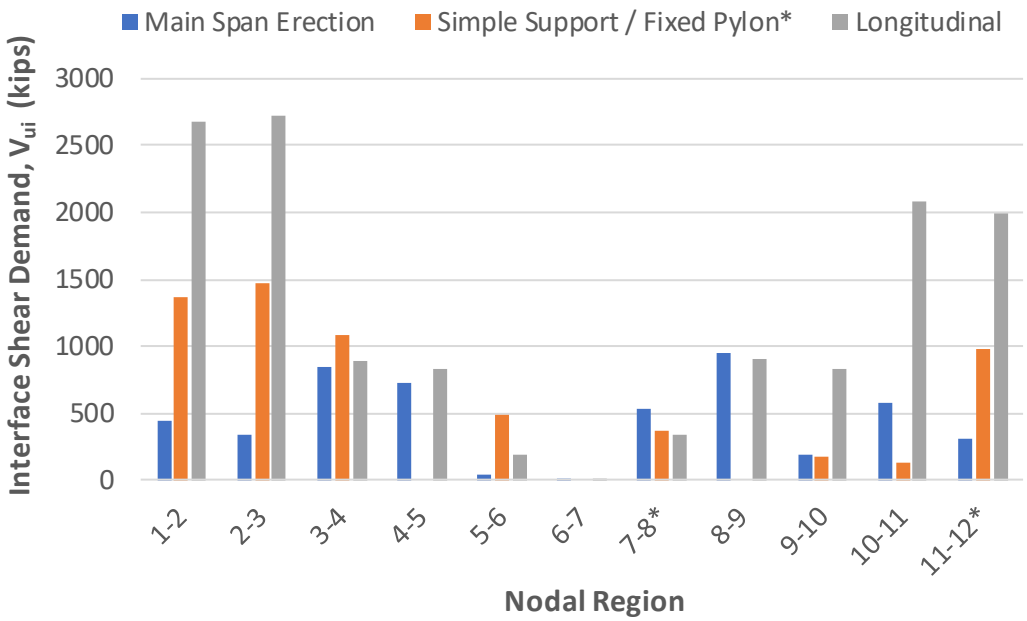

Figure 63. Nodal zone interface shear demand results generated for the FIGG Design.

The chart in figure 63 shows that the interface shear demand generated for each construction stage can vary significantly. Both the magnitude of the interface shear demand and concurrent permanent net compression force, *Pc*, need to be considered for each construction stage in determining the governing load case for each nodal region. Therefore, the largest interface

shear demand does not always coincide with the governing load case. Using the results included in the FIGG Design the following governing construction stages for each nodal zone were identified:

- Main-span Erection (Stage 2 during transport) – Governed for nodal zones 4-5, 6-7, 7-8 and 8-9.
- Simple Support (Stage 2 for simple-span placement) – Governed for nodal zones 3-4 and 5-6.
- Fixed Pylon (Stage 4) – Did not govern for any nodal zones.
- Longitudinal Model (Stage 4)– Governed for nodal zones 1-2, 2-3, 9-10, 10-11 and 11-12.

Figure 63 also shows that the forces generated from the Longitudinal Model (for the completed bridge structure) generated the largest forces for the nodal regions at the north and south ends of the main span. *It should be noted that the FIGG Design exclusively used the results from the Simple Support / Fixed Pylon modeling combination for the design of every main span nodal region*.

Finding:
FIGG Design did not consider loadings from all critical construction stages in determining the governing interface shear demands.

6.2.2 FIGG DESIGN OF NODAL REGIONS FOR INTERFACE SHEAR CAPACITY

The FIGG Design for the FIU pedestrian bridge contained design calculations for the interface shear transfer across the cold joints in the nodal regions between the bridge truss members to the bridge deck and canopy. These calculations followed the AASHTO LRFD interface shear provisions described in Section 6.2 above.

Listed below are the values for the parameters used for the interface shear capacity determination in the FIGG Design. The values for μ, K_1, and K_2 align with the situation described in the AASHTO LRFD Article 5.8.4.3 as "normal-weight concrete placed against a clean concrete surface, free of laitance, with surface intentionally roughened to an amplitude of 0.25 in."

- **c = 0.0 ksi.** This value indicates that the FIGG Design conservatively ignored the effects of cohesion on the interface shear resistance.
- **μ = 1.0.**
- **K_1 = 0.25.**
- **K_2 = 1.5 ksi.**
- **ϕ = 0.90.** Resistance factor for shear; per AASHTO LRFD Article 5.5.4.2.1.

- f_y **= 60 ksi.** This value indicated the designer's use of ASTM A615 Grade 60 steel reinforcement.
- f'_c **= 8.5 ksi.** This value indicates the weakest concrete compressive strength on either side of the interface as specified by the designer.

Table 1 summarizes the interface shear design parameters and the corresponding interface shear capacities, V_{ri}, calculated for each main span cold joint nodal region in the FIGG Design. It should be noted that the FIGG Design assumed a cohesion factor equal to 0.0 ksi and therefore did not consider interface shear capacity due to cohesion. The AASHTO LRFD permits relying on cohesion in the interface shear capacity determination.

Table 1 shows the interface shear capacity determined for the shear interface surface, typically the cold joint footprint area, in each nodal region using the FIGG Design assumptions. The limiting interface shear capacity factors in AASHTO LRFD Articles 5.8.4.1-4 and 5.8.4.1-5, K_1 and K_2, did not control for any of the main span nodal zone designs. Interface shear capacity calculations were not generated for nodal regions 4-5, 6-7, and 8-9 in the FIGG Design. The information in the table is based on the reinforcement identified in the FIGG Design. The FIGG Plans called out slightly different reinforcement details at nodal regions 1-2, 2-3 and 10-11.

Table 1. Nodal Region Interface Shear Capacity Calculation Summary (FIGG Design)

Nodal Region	**$A_{cv} = b_{vi} \times L_{vi}$** ($in^2$)	**A_{vf}** (in^2)	**P_c** (kips)	**Interface Shear Capacity [$V_{ri} = \varphi V_{ni}$] with c = 0.0 ksi** (kips)
1-2	21" x 57.6" = 1210 in^2	8 - #7 = 4.80 in^2	1275	1407
2-3	21" x 58.0" = 1218 in^2	14 - #6 = 6.16 in^2	1298	1501
3-4	21" x 85.6" = 1798 in^2	18 - #7 = 10.80	579	1104
4-5	Design for this nodal region not included in FIGG Design			
5-6	21" x 79.3" = 1664 in^2	12 - #7 = 7.20 in^2	230	596
6-7	Design for this nodal region not included in FIGG Design			
7-8	21" x 68" = 1428 in^2	12 - #7 = 7.20 in^2	449	793
8-9	Design for this nodal region not included in FIGG Design			
9-10	21" x 67.0" = 1407 in^2	12 - #7 = 7.2 in^2	703	1021
10-11	21" x 58.0" = 1218 in^2	6 - #6 = 2.64 in^2	1210	1232
11-12	21" x 42.0" = 882 in^2	8 - #7 = 4.80 in^2	1233	1369

The FHWA Check identified two consistent errors in the interface shear computations included in the FIGG Design. AASHTO LRFD Article 5.8.4.1 states that the value for P_c used in the capacity calculation shall only consider "permanent net compressive force normal to the shear

plane". The value for P_c used in the FIGG Design included both the compressive forces from permanent loading such as the dead load of the structure and from non-permanent (transient) loadings, such as pedestrian live load. In addition, the compressive forces from loading were inappropriately amplified by the Strength 1 maximum load factors.

Finding:
The FIGG Design incorrectly increased and amplified the effects of the clamping force across the interface shear surface resulting in a significant overestimation of capacity.

Finding:
FIGG Design conservatively did not rely on the cohesion contribution of the interface shear capacity calculation.

6.3 FHWA Evaluation of the FIGG Design (FHWA Check)

6.3.1 Bridge Modeling and Analysis of Interface Shear Demand

FHWA completed four separate structural analyses of the bridge, each one developed by a different person using a different software package. These analyses focus on the FIU pedestrian bridge in the construction stage at the time of collapse (i.e., end of Stage 2, the same stage as was assessed in the FIGG Simple Support Model). Three of these models were two-dimensional, the fourth was a three-dimensional model. 2-D Models #1 and #2 are grid analysis models comprised of beam elements with post-tensioning and non-linear time dependent material effects considered. 2-D Model #3 is a grid analysis model comprised of truss elements in which the post-tensioning effects are superimposed. The 3-D Model is a finite element model comprised of solid elements with the post-tensioning sequence considered. The results generated from the four independent analytical models were compared to each other and found to have very good agreement producing similar results. Table 2 shows the interface shear demand results (magnitude only) for each of the four FHWA analyses. The results included in the table are for the construction stage in which the bridge is simply supported on the piers and truss members 2 and 11 remain post-tensioned. The table presents results for the AASHTO LRFD Strength I Limit State load combination of 1.25DC + 1.0PT.

Figure 64 shows the interface shear at each truss nodal zone generated from FHWA Check 2-D Model #1 with directionality on the cut through the truss member side of the nodes. As they are consistent with the results from the remaining three FHWA Check models, the interface shears generated from this model will be used for the FHWA Check in the remainder of this report. The interface shears for nodes 1-2, 3-4, 10-11 and 11-12 included results for cases in which truss members 2 and 11 are both tensioned and detensioned. The detensioning of truss members 2 and 11 had minimal effect on the other nodal regions and therefore these results are not presented.

Table 2. FHWA Check Interface Shear Demand Results

Nodal Region	2-D Model #1 (kips)	2-D Model #2 (kips)	2-D Model #3 (kips)	3-D Model (kips)
1-2	2,481	2,476	2,549	2,544
2-3	2,575	2,570	2,589	2,660
3-4	1,090	1,081	1,124	1,061
4-5	977	960	963	940
5-6	628	625	586	624
6-7	519	515	506	515
7-8	338	331	337	381
8-9	19	12	37	61
9-10	80	82	89	34
10-11	1,491	1,504	1,421	1,254
11-12	1,835	1,846	1,806	1,816

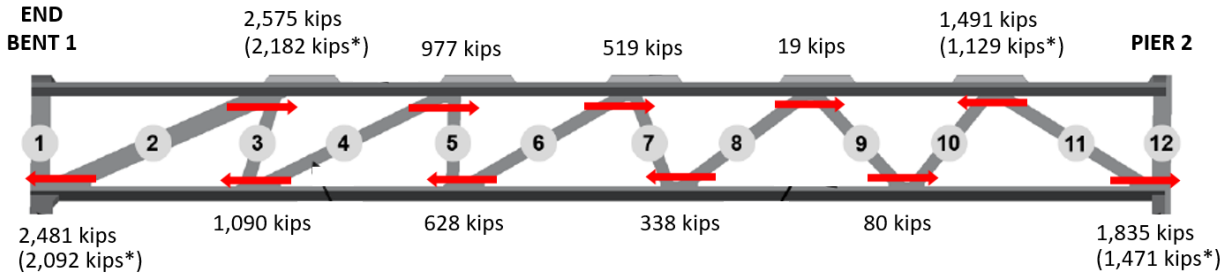

* De-tension of Truss Members 2 and 11 PT Bars

Figure 64. Interface shear demands from FHWA independent analysis.

Figure 65 shows a comparison of the interface shear demands generated by the analytical model used by the FIGG Design and those generated from the FHWA Check analysis. The AASHTO Strength I Limit Strength was used to generate the interface shear demands for both the FIGG Design and FHWA Check. The results for the FIGG Design came from the Simple Support and Fixed Pylon Models. For clarity, the results are only shown for the nodal zones that were included in the FIGG Design. Nodal regions 4-5, 6-7 and 8-9 were not included in the FIGG Design. Truss members 2 and 11 carried the highest force levels in the main span and failure of nodal region 11-12 initiated the collapse.

The FHWA Check generated significantly higher interface shear demand for the nodal regions at the ends of truss member 2 (nodal regions 1-2 & 2-3) and truss member 11 (nodal regions 10-11 & 11-12) when compared to the results used for the FIGG Design. The Simple Support and Fixed Pylon Model results which were used exclusively in the FIGG Design resulted in the underestimation of interface shear demand compared to the FHWA Check as highlighted here:

- Nodal Region 1-2 – The force effect selected by the FIGG Design of this nodal region underestimated the maximum force effect by approximately 1,100 kips (49%)
- Nodal Region 2-3 – The force effect selected by the FIGG Design of this nodal region underestimated the maximum force effect by approximately 1,100 kips (43%).
- Nodal Region 10-11 – The force effect selected by the FIGG Design of this nodal region underestimated the maximum force effect by approximately 1,360 kips (91%).
- Nodal Region 11-12 – The force effect selected by the FIGG Design of this nodal region underestimated the maximum force effect by approximately 850 kips (46%).

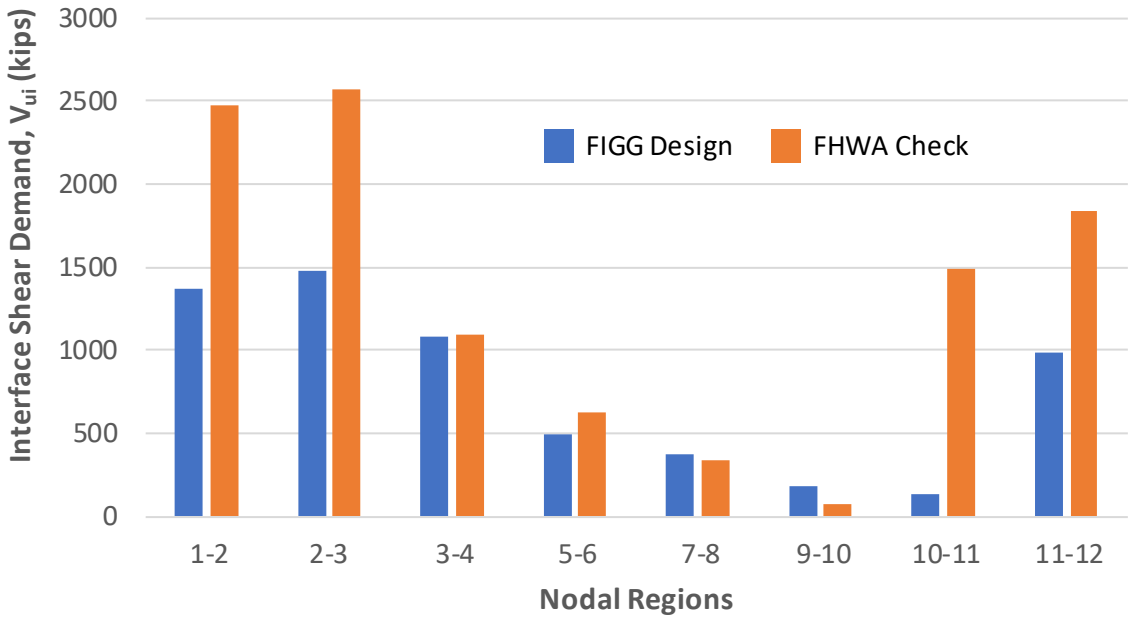

Figure 65. Nodal zone horizontal shear modeling results comparison between FIGG Design and FHWA Check.

Finding:

The analytical modeling relied upon by the FIGG Design was inadequate or misinterpreted, resulting in a significant underestimation of demand at critical and highly loaded nodal regions.

The interface shear demands generated from the FHWA Check were less than the interface shear demands generated from the FIGG Longitudinal Model for the highly loaded nodal regions connecting truss members 2 and 11 to the deck and canopy. Refer to Figure 63 for FIGG Longitudinal Model results. Although the FHWA Check did not assess the accuracy of the FIGG Longitudinal Model results, it is clear that the FIGG Design had access to nodal region demands that exceeded the demands acting upon the bridge at the time of collapse as generated in the FHWA Check. For reasons that remain unknown, the FIGG Design relied on inadequate or misinterpreted results leading to a consistent underestimation of the interface shear demand across many of the main span truss member nodal region cold joints.

Finding:

In some instances, the FIGG Design did produce reasonable estimations for interface shear demand; however, these reasonable interface shear demand values were often not used in the process of sizing of members to resist demands.

6.3.2 Interface Shear Design of Truss Nodal Regions

The FHWA Check assessed the design of the main span truss nodal regions that were produced by the FIGG Design and described in the FIGG Plans. As stated previously, the designs of the nodal regions followed the provisions outlined in the AASHTO LRFD in Article 5.8.4 titled *Interface Shear Transfer – Shear Friction*. As also stated previously the FIGG Design did not include the effects of cohesion in their capacity calculation.

Table 3 compiles the results from the FHWA Check. This check used the results from the FHWA independent analysis using 2-D Model #1, to determine the permanent net compressive force, P_c. The remaining details needed to calculate the interface shear capacity were taken from the FIGG Plans. One detail that was not consistently indicated on the bridge plans dealt with the surface preparation for the cold joint. Multiple drawings in the FIGG Plans deliberately noted when cold joints needed to be roughened to a 0.25-inch amplitude to be consistent with the assumptions made in the FIGG Design; however, the FIGG Plan drawings for the truss nodal regions did not include a note to roughen the surface or any other note pertaining to the surface preparation of interfaces in the nodal regions, which was inconsistent with the assumptions made in the FIGG Design. Despite this FIGG Plan omission, the capacities shown in Table 3 include the effects of an interface shear surface roughened to a 0.25-inch amplitude as assumed in the FIGG Design. As stated previously, the interface shear transfer area, A_{cv}, and the reinforcing steel area crossing the interface surface, A_{vf}, were taken from information included in the FIGG Plans. It should be noted that the A_{vf} values vary slightly from what was assumed in the FIGG Design for nodal regions 1-2, 2-3 and 10-11. Slightly more reinforcing was provided at nodal regions 1-2 and 10-11 and slightly less reinforcing was provided at nodal region 2-3.

Finding:

The FIGG Plans inconsistently identified when intentionally roughen surfaces were needed to fulfill the assumptions of the FIGG Design; otherwise, the FIGG Plans reasonably reflect the expectations established in the FIGG Design.

The interface shear transfer area, A_{cv}, is the area of concrete considered to be engaged and providing interface shear capacity. The computation of this area typically encompasses the entire footprint between the connecting elements. However, A_{cv} needs to consider how interface shear transfer area is affected when located along an edge and/or includes discontinuities. Nodal regions 1-2 and 11-12 are both located at an edge of the bridge deck. The interface areas located within the nodal region footprint and close to deck edge have limited capacity to transfer loads to the body of the deck. The longitudinal post-tensioning, located within the deck, provides the primary mechanism to resist the longitudinal forces delivered by the truss members to the deck. The position of the applied forces from the truss members relative to the post-tensioning location is important. The post-tensioning tendons can only resist applied forces within their region of influence. Forces outside this area cannot be resisted by the post-tensioning.

Table 3. Interface Shear Capacity Results from FHWA Check

Nodal Region	**$A_{cv} = b_{vi} \times L_{vi}$** ($in^2$)	**A_{vf}** (in^2)	**P_c** (kips)	**Interface Shear Capacity [$V_{ri} = \varphi V_{ni}$] with c = 0.0 ksi** (kips)
1-2	21” x 75.25” = 1580	10-#7 = 6.0	925	1156
2-3	21” x 69.0” = 1449	12 - #6 = 5.28	1388	1534
3-4	21” x 85.6” = 1798	18 - #7 = 10.80	865	1361
4-5	21” x 55” = 1155	10 - #6 = 4.4	411	607
5-6	21” x 79.3” = 1664	12 - #7 = 7.20	373	725
6-7	21” x 52” = 1092	10 - #6 = 4.4	617	792
7-8	21” x 68” = 1428	12 - #7 = 7.20	678	999
8-9	21” x 54” = 1134	10 - #6 = 4.4	759	921
9-10	21” x 67.0” = 1407	12 - #7 = 7.20	952	1246
10-11	21” x 58.0” = 1218	10 - #6 = 4.4	1540	1,623
11-12	21” x 42.0” = 882	8 - #7 = 4.80	967	1,130

Figure 66 shows a plan view of the nodal region 11-12 footprint from the FIGG Plans (plan view shown on left) as well as from a post-collapse laser scan of the same region (image shown on

right). On the plan view of this figure, the limits of the area of influence for the longitudinal post-tensioning in the deck are shown with a dotted line projecting 45 degrees from the center of the inner-most post-tension tendon anchorage. The area within the nodal region identified as Zone 3 on this detail falls outside the longitudinal post-tensioning influence area, due to shear lag, and therefore does not have the ability to transfer interface shear force to the adjacent longitudinal post-tensioning. Consequently, the interface shear transfer area located within Zone 3 does not have a load path to properly connect to the bridge deck and should not be used in the interface shear capacity calculation.

A unique detail that occurs at nodal region 11-12 is the presence of two vertical pipe sleeves that flank both faces of the 11-12 nodal region (4 pipes total). These vertical pipes penetrate the full depth of the bridge deck and essentially isolate or "wall-off" the area bounded by these pipes. Consequently, the area identified as Zone 2 in Figure 66 is also isolated from the deck and therefore should not be used in the interface shear capacity calculation for the 11-12 nodal region.

The interface shear designs included in the FIGG Design only used the interface shear transfer areas under truss member 2 for the 1-2 nodal region design and interface shear transfer area under truss member 11 in the 11-12 nodal zone for the nodal region designs. Although the designer's intent cannot be deduced, the FHWA Check determined that the FIGG Design correctly chose to exclude Zone 2 and Zone 3 in determining the area engaged in interface shear transfer.

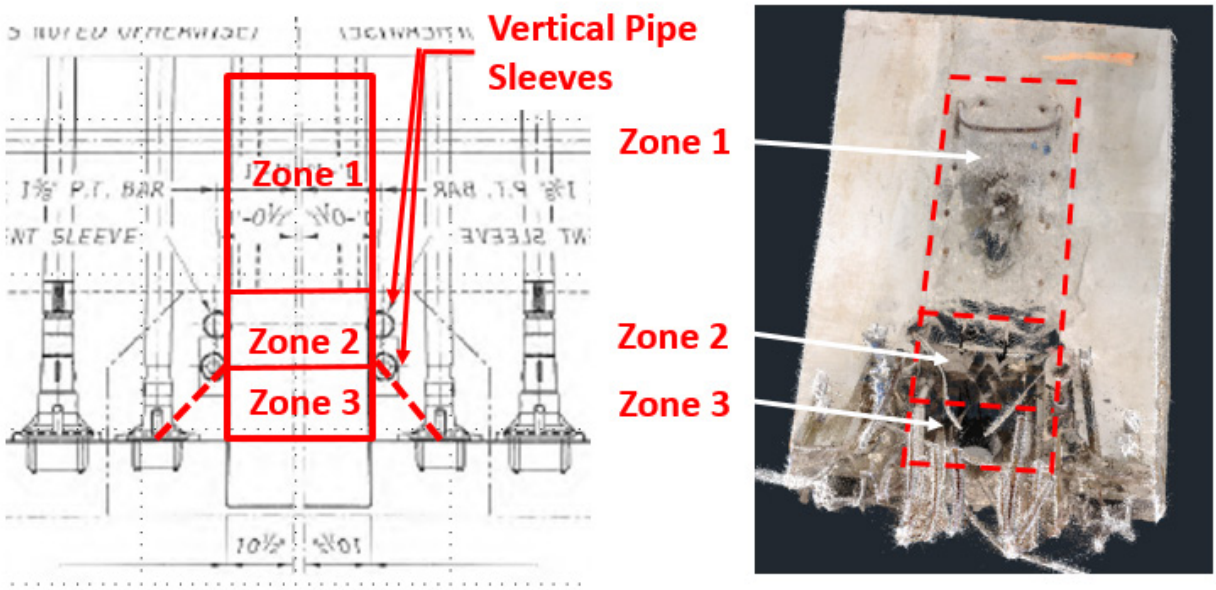

Figure 66. Interface surface zones 1, 2, and 3.

6.3.3 INTERFACE SHEAR CAPACITY COMPARISON

As described previously, interface shear capacity is generated through multiple resistance mechanisms. Resistance is provided by cohesion across the contact area of the two concrete elements (i.e., interface surfaces) and the roughness (i.e., friction) between the surfaces. The normal force coinciding with the roughness comes from two components; the amount of reinforcing steel crossing the interface surface and the amount of permanent compressive loading perpendicular to the interface. Occasionally supplemental compressive forces supplied through other means (e.g. post-tensioning force) are included in the determination of the permanent compressive force.

The capacities shown in the bar graph in Figure 67 are broken down into the two capacity-supplying mechanisms. These are identified as capacity from compressive force (P_c) and capacity from reinforcing steel (A_{vf} x f_y). The interface shear capacity values calculated in the FIGG Design are shown. The FHWA calculated capacity values based on the FIGG Plans with appropriate interpretation of the AASHTO LRFD are also shown.

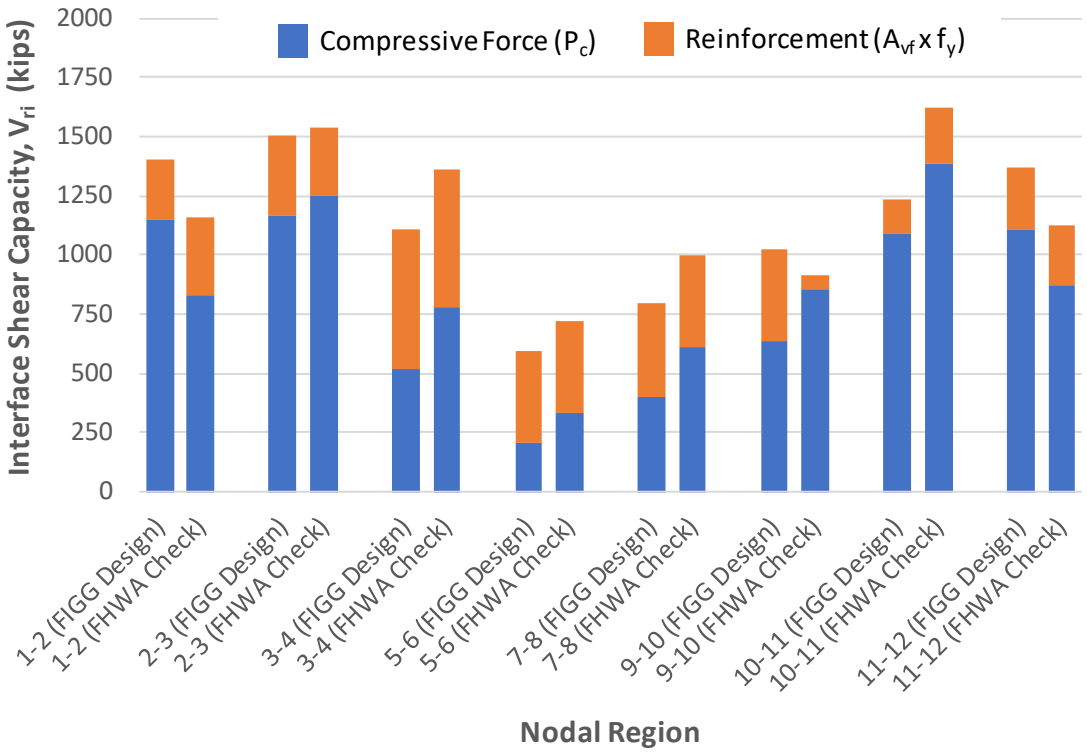

Figure 67. Interface shear capacity breakdown.

This figure shows that, for the highly loaded nodal regions of 1-2 and 11-12, the interface shear capacity is highly dependent on the compressive force (P_c) that was assumed to act on the interface. The high dependence on a capacity from a compressive force that was significantly and inappropriately overestimated resulted in a significantly under-reinforced connection. Had

the FIGG Design used a more appropriate clamping force, the amount of reinforcing at the 1-2 and 11-12 nodal regions would have approximately doubled. However, even the doubling of this reinforcing would have only provided the needed capacity to satisfy the significantly underestimated calculated demand. Comparisons for nodal regions 4-5, 6-7 and 8-9 are not made since capacity calculations for these nodal regions were not included in the FIGG Design.

6.3.4 Demand to Capacity (D/C) Ratios for Bridge at Stage 2 (Time of Collapse)

Figure 68 below displays ratios in which the maximum interface shear demands (forces) acting upon a nodal region is divided by the capacity provided by the nodal region. This produces a ratio commonly referred to as the demand to capacity ratio (D/C). A demand to capacity ratio less than or equal to 1.0 represents an assessment that the capacity provided by the nodal region can adequately carry the applied loading (as prescribed by the design requirements). The lower the value the more conservative the design. A demand to capacity value above 1.0 represents an assessment that the capacity provided by the nodal region is not sufficient to carry the applied loading (as prescribed by the design requirements). The higher the value, the more under-designed the connection. Figure 68 includes D/C ratios for every nodal region in the main span at the time of collapse.

The maximum demands used to compute the D/C ratios in figure 68 were based on the FHWA Check load case for Stage 2 (from Table 2). The capacity was calculated using the interface shear transfer area, A_{cv}, and the reinforcing steel area crossing the interface plane, A_{vf}, as shown on the FIGG Plans (from Table 3). Cohesion was not included in these capacity calculations. In addition, the compressive force, P_c, acting on each interface surface is the concurrent load generated by the FHWA Check for Stage 2. The compressive force used for nodal regions 1-2 and 11-12 includes the temporary post-tensioning in truss members 2 and 11.

Four of the main span nodal regions have D/C ratios above 1.0. The graph below shows that nodal region 1-2 had the highest demand to capacity ratio indicating that this nodal region was the least sufficient to carry the applied load. However, the bridge failed at nodal region 11-12. Comparing these two nodal regions reveals that truss member 2 was 36-inches deep as opposed to the thinner truss member 11 which was 24-inches deep. In addition, nodal zone 1-2 framed into a 42-inch wide deck diaphragm while nodal zone 11-12 framed into a thinner 24-inch diaphragm that was also penetrated by four vertical pipe sleeves that isolated a portion of the nodal region. Therefore, a likely reason for the favorable performance of nodal region 1-2 as opposed to nodal region 11-12 was the unintended capacity from the more substantial elements available at the 1-2 nodal region.

Finding:

The distress observed in nodal regions 1-2 and 11-12 is consistent with the underestimation of demand and the overestimation of capacity identified in these nodal regions.

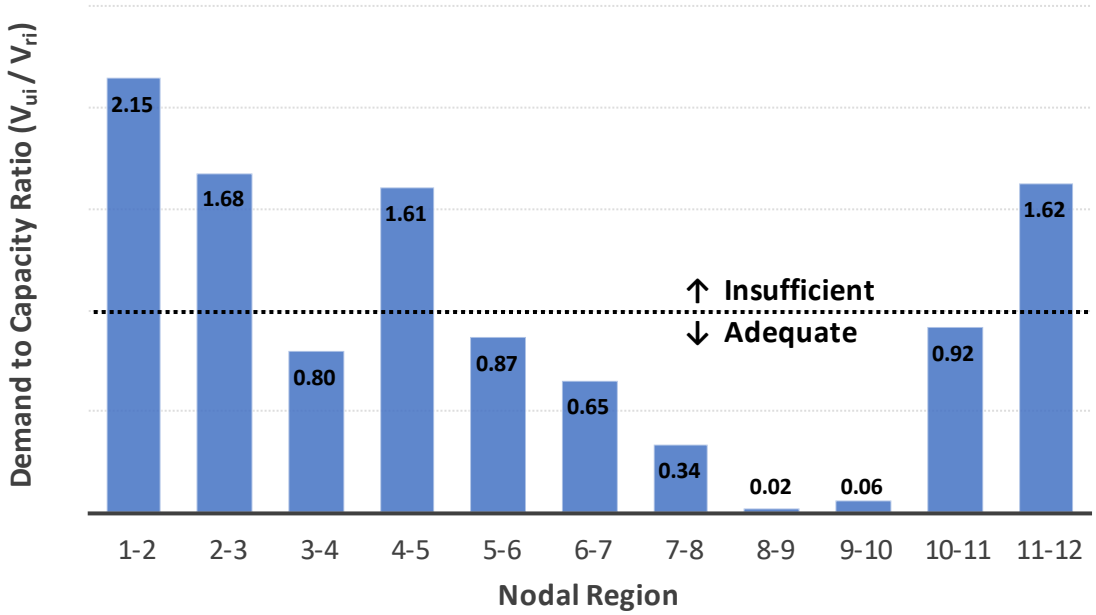

Figure 68. Demand to capacity ratios for main span nodal regions.

7 FINDINGS

After an extensive assessment of the FIGG Design, FIGG Plans, and the physical evidence and documentation collected through the investigation, FHWA has made the following findings.

The distress observed before the collapse, the evidence collected after the collapse, and the assessment of the FIGG Design and FIGG Plans lead to the conclusion that the root cause of the collapse was an inability of the structure to resist interface shear demands in the critical nodal region at the north end of the bridge. Key findings supporting this conclusion include:

- The distress observed in nodal regions 1-2 and 11-12 is consistent with the underestimation of demand and the overestimation of capacity identified in these nodal regions. [Section 6.3.4]
- The analytical modeling relied upon by the FIGG Design was inadequate or misinterpreted, resulting in a significant underestimation of demand at critical and highly loaded nodal regions. [Section 6.3.1]
- The FIGG Design incorrectly increased and amplified the effects of the clamping force across the interface shear surface resulting in a significant overestimation of capacity. [Section 6.2.2]

The FHWA assessment developed the following findings in relation to the performance of the bridge in the days and weeks immediately preceding the collapse.

- The structure behaved with sufficient ductility to provide warning before failure through development of significant and visible distress. [Chapter 5]
- The distress continued to grow over time. [Chapter 5]
- The structural cracking and northward dislocation of the upper part of the member 11 and 12 nodal region as documented in the days leading up to the collapse is strong evidence that the structure was progressing toward failure. [Chapter 5]
- Detensioning of post-tensioning rods located within truss member 11 significantly increased damage to the member 11 and 12 nodal region. [Chapter 5]
- Retensioning truss member 11 increased demand on and corresponding damage to the member 11 and 12 nodal region until the distress became critical. [Section 3.8]

The FHWA assessment developed the following additional findings in relation to specific aspects of the FIGG Design.

- The FIGG Design did not consider loadings from all the critical construction stages in determining the governing interface shear demands. [Section 6.2.10]
- FIGG Design used a redundancy factor of 1.0, consistent with that commonly used for structures with redundant load paths, even though this single-line truss structure only provided a singular load path. [Section 6.2]
- FIGG Design did not use the lower bound load factor for determination of the governing permanent net compression, P_c, in the interface shear designs, resulting in overestimation of capacity. [Section 6.2]
- The FIGG Design did not provide sufficient documentation of design approach, analysis methodology, and key assumptions for all the critical construction stages. [Section 6.1]

- The FIGG Design conservatively did not rely on the cohesion contribution of the interface shear capacity calculation. [Section 6.2.2]
- In some instances, the FIGG Design did produce reasonable estimations for interface shear demand; however, these reasonable interface shear demand values were often not used in the process of sizing of members to resist demands. [Section 6.3.1]

The FHWA assessment developed the following findings related to specific deficiencies in the plans by which this bridge was constructed.

- The FIGG Plans inconsistently identified when intentionally roughen surfaces were needed to fulfill the assumptions of the FIGG Design; otherwise, the FIGG Plans reasonably reflect the expectations established in the FIGG Design. [Section 6.3.2]
- The FIGG Plans called for a detailing scheme wherein the southernmost two reinforcing bars were not anchored on both sides of the critical horizontal shear plan at the base of member 11. This detailing scheme resulted in less reinforcement steel than expected participating in resisting the critical interface shear demand. [Section 3.3]

The FHWA assessment developed the following findings in relation to the materials used in the bridge and the construction activities through which the bridge was built.

- The hydraulic jack that was used to post-tension the rods in member 11 was performing appropriately at the time of collapse. [Section 4.7]
- No significant deviation from the construction plans were identified through the assessment of in-place steel reinforcement sizes and locations. [Section 4.3]
- The concrete material properties relied upon in the FIGG Design were supplied in the construction of the bridge. [Section 4.4]
- The steel material properties relied upon by the FIGG Design were supplied in the construction of the bridge. [Section 4.5]
- The steel post-tensioning rod mechanical properties relied upon in the FIGG Design were supplied in the construction of the bridge. [Section 4.6]

The AASHTO LRFD Bridge Specification states that bridges shall be designed to achieve the objectives of safety, constructability, and serviceability. These objectives are met through the theory of reliability based on current statistical knowledge of loads and structural performance. In LRFD design, the anticipated loads on the bridge are conservatively estimated and the structural system is proportioned to reliably resist those loads. The designer of the FIU Pedestrian Bridge made significant errors in the determination of loads, leading to a severe underestimation of the demands that would be placed on critical portions of the bridge. The designer also significantly overestimated the capacity of a critical portion of the structure. Moreover, when the designer was engaged to assess the worsening performance of the structure, the designer neither recognized that the singular load path in this non-redundant bridge had been compromised nor took appropriate action to mitigate the risk of failure. The tragic end result was the collapse of the bridge.